

Published By

Sivas Cumhuriyet University

<http://cumfad.cumhuriyet.edu.tr>

1(1):2023

Sivas Cumhuriyet University Journal of Engineering Faculty

Sivas Cumhuriyet University Journal of Engineering Faculty (CUMFAD) is the official publication of Cumhuriyet University Faculty of Engineering. CUMFAD is an international journal dedicated to the latest advancement of engineering. The aim of this journal is to provide a platform for scientists and academicians all over the world to promote, share, and discuss various new issues and developments in different areas of engineering. Sivas Cumhuriyet University Journal of Engineering Faculty publishes original research papers, reviews, and letters to the editor within all fields of Science, Technology, Engineering and Architecture. The journal is a scientific and peer-reviewed journal and is published online twice a year, in June and December.

**Sivas Cumhuriyet University Journal of Engineering
Faculty-CUJEF**

**Sivas Cumhuriyet Üniversitesi Mühendislik Fakültesi
Dergisi-CUMFAD**

**Volume / Cilt 1 | Issue / Sayı 1
Pages / Sayfa: 1-47**

August/Ağustos 2023

<https://dergipark.org.tr/tr/pub/cumfad>

Sivas Cumhuriyet University Journal of Engineering Faculty-CUJEF

Sivas Cumhuriyet Üniversitesi Mühendislik Fakültesi Dergisi-CUMFAD

Publisher/Yayıncı

Sivas Cumhuriyet University, Faculty of Engineering
Sivas Cumhuriyet Üniversitesi, Mühendislik Fakültesi
Prof. Dr. Nevzat ASLAN

Editor-in-Chief

Assoc. Prof. Dr. Serdar KOÇKANAT

Editör

Doç. Dr. Serdar KOÇKANAT

Co-Editors

Assoc. Prof. Dr. Fatih KABURCUK
Assoc. Prof. Dr. Mustafa ŞEKER
Asst. Prof. Dr. Abdülkadir ŞEKER

Eş Editörler

Doç. Dr. Fatih KABURCUK
Doç. Dr. Mustafa ŞEKER
Dr. Öğr. Üyesi Abdülkadir ŞEKER

Technical Editor

Asst. Prof. Dr. Mikail PÜRLÜ

Teknik Editör

Dr. Öğr. Üyesi Mikail PÜRLÜ

Technical Check and Layout Assistants

Sivas Cumhuriyet University Electronic
Journal Office

Teknik Kontrol ve Mizanpaj Sorumluları

Sivas Cumhuriyet Üniversitesi Elektronik
Dergi Ofisi

Editorial Board/ Editör Kurulu

- Prof. Dr. Nevzat ASLAN – Sivas Cumhuriyet Üniversitesi/Mühendislik Fakültesi
Prof. Dr. Tarık TÜRK – Sivas Cumhuriyet Üniversitesi/Mühendislik Fakültesi
Prof. Dr. Ali UÇURUM – Sivas Cumhuriyet Üniversitesi/Mühendislik Fakültesi
Prof. Dr. Fuat ÖZYONAR – Sivas Cumhuriyet Üniversitesi/Mühendislik Fakültesi
Prof. Dr. Mehmet ŞİMŞİR – Sivas Cumhuriyet Üniversitesi/Mühendislik Fakültesi
Doç. Dr. Mehmet KONAR – Erciyes Üniversitesi/Havacılık ve Uzay Bilimleri Fakültesi
Doç. Dr. Nuri KAPUCU – Hitit Üniversitesi/Mühendislik Fakültesi
Doç. Dr. Yunis TORUN – Sivas Cumhuriyet Üniversitesi/Mühendislik Fakültesi
Doç. Dr. Hülya DOĞAN – Sivas Cumhuriyet Üniversitesi/Mühendislik Fakültesi
Doç. Dr. İlkey DEMİR – Sivas Cumhuriyet Üniversitesi/Mühendislik Fakültesi
Doç. Dr. Neşe KEKLİKÇİOĞLU ÇAKMAK – Sivas Cumhuriyet Üniversitesi/Mühendislik Fakültesi
Doç. Dr. Murat BOSTANCIOĞLU – Sivas Cumhuriyet Üniversitesi/Mühendislik Fakültesi
Doç. Dr. Hidayet TAKCI – Sivas Cumhuriyet Üniversitesi/Mühendislik Fakültesi
Doç. Dr. Ferhat KILINÇ – Sivas Cumhuriyet Üniversitesi/Mühendislik Fakültesi
Dr. Öğr. Üyesi Türker KOZA – Bozok Üniversitesi/ Yozgat Meslek Yüksekokulu
Dr. Öğr. Üyesi Halil ARSLAN – Sivas Cumhuriyet Üniversitesi/Mühendislik Fakültesi
Dr. Öğr. Üyesi Vekil SARI – Sivas Cumhuriyet Üniversitesi/Mühendislik Fakültesi
Dr. Öğr. Üyesi Pınar BORA – Sivas Cumhuriyet Üniversitesi/Mühendislik Fakültesi
Dr. Öğr. Üyesi Yavuz TÜRKAY – Sivas Cumhuriyet Üniversitesi/Mühendislik Fakültesi
Öğr. Gör. Dr. Sinan KOŞAROĞLU – Sivas Cumhuriyet Üniversitesi/Mühendislik Fakültesi

Publication Board/ Yayın Kurulu

Prof. Dr. Nevzat ASLAN – Sivas Cumhuriyet Üniversitesi/Mühendislik Fakültesi

Prof. Dr. Ali UÇURUM – Sivas Cumhuriyet Üniversitesi/Mühendislik Fakültesi

Prof. Dr. Mehmet ŞİMŞİR – Sivas Cumhuriyet Üniversitesi/Mühendislik Fakültesi

Prof. Dr. Ayten ATEŞ – Sivas Cumhuriyet Üniversitesi/Mühendislik Fakültesi

Prof. Dr. Halil İbrahim ACAR – Sivas Cumhuriyet Üniversitesi/Mühendislik Fakültesi

Prof. Dr. Tarık TÜRK – Sivas Cumhuriyet Üniversitesi/Mühendislik Fakültesi

Prof. Dr. Özcan BEKTAŞ – Sivas Cumhuriyet Üniversitesi/Mühendislik Fakültesi

Prof. Dr. Meltem SARIOĞLU CEBECİ – Sivas Cumhuriyet Üniversitesi/Mühendislik Fakültesi

Prof. Dr. Fazlı SÖZMEN – Sivas Cumhuriyet Üniversitesi/Mühendislik Fakültesi

Doç. Dr. Serdar KOÇKANAT – Sivas Cumhuriyet Üniversitesi/Mühendislik Fakültesi

Doç. Dr. Murat BOSTANCIOĞLU – Sivas Cumhuriyet Üniversitesi/Mühendislik Fakültesi

Doç. Dr. Hidayet TAKCI – Sivas Cumhuriyet Üniversitesi/Mühendislik Fakültesi

Contents / İçindekiler

Editorial

VI

Editörden

VII

Analysis of Flight Based Airport Passenger Arrival Patterns
Uçuş Bazlı Havalimanı Yolcu Geliş Örüntüleri Analizi

Merve Gözde SAYIN, Mustafa BOLAT

1-10

Categorical and Binary Brain Tumor Classification Using Transfer Learning Techniques
Transfer Öğrenme Teknikleri Kullanılarak Kategorik ve İkili Beyin Tümörü Sınıflandırması

Ayşe Gül EKER, Gamze Korkmaz ERDEM, Nevcihan DURU

11-16

Fast And High Preciously Estimator Design with Differential Evolution Algorithm For Shaking Table
Sarsma Tablası İçin Diferansiyel Gelişim Algoritması İle Hızlı Ve Yüksek Hassasiyetli Kestirici Tasarımı

Serdar KOÇKANAT

17-29

Investigation of Liquefaction Behavior of Geyve County of Sakarya Province Soils with GIS
Sakarya İli Geyve İlçesi Topraklarının Sıvılaşma Davranışının GIS ile İncelenmesi

Ayşe Eda ÖZDİN, İsa VURAL

30-37

Recognition and Performance Evaluation of Handwritten Numbers Using a New Segmentation Method
Yeni Bir Dilimleme Yöntemi Kullanılarak El Yazısı Rakamlarının Tanınması ve Performans Değerlendirmesi

Sultan Murat YILMAZ, Serap ÇAKAR

38-47

Editorial

Dear Readers, Dear Researchers,

VI

Cumhuriyet University Journal of Engineering Faculty (CUMFAD) is an international, scientific, peer-reviewed and electronically accessible journal published twice a year by Sivas Cumhuriyet University Engineering Faculty. CUMFAD aims to deliver qualified studies in all engineering branches to its readers with an objective point of view. As the editorial board, we are happy to present the first issue of our magazine to our readers. We would like to express our deepest gratitude to our authors, reviewers and everyone who contributed to this issue of our journal, especially to our advisory board, co-editors, field editors, language editors, and staff responsible for review and typesetting. In addition, we are grateful to all our authors who have been patiently waiting for us, despite the negative impact of the earthquake disaster in our country and the disruptions due to the editorial office change process. Also, we would also like to thank everyone who has contributed and supported our magazine so far. Our next issue will hopefully be published in December 2023.

In this issue, there are 5 research articles that have undergone a strict blind review and editorial process. Studies published in our journal go through three important stages: preliminary review, blind peer-review process and editorial process. During the peer-review process, each article was reviewed by at least two referees. In addition, every article that enters the review process is screened for plagiarism with the help of iThenticate software. We recommend our authors who want to submit their works to our journal for our upcoming issues, to pass their work through a plagiarism software before sending them to us.

For our new issues, you can upload your works to <https://dergipark.org.tr/tr/pub/cumfad>. In addition, our journal aims to expand the academic advisory board and the referee pool. In this context, valuable researchers who want to be on the advisory board of our journal or who want to contribute to our journal as a referee can send their CVs to skockanat@cumhuriyet.edu.tr via e-mail. Referee certification processes are carried out through Dergipark. For this reason, our referees who want to obtain a referee certificate should apply through Dergipark.

See you in the next issue with qualified and original works...

Assoc. Prof. Dr. Serdar KOÇKANAT
Editor
August, 2023

Editör'den

Değerli okuyucular, kıymetli araştırmacılar,

VII

Cumhuriyet Üniversitesi Mühendislik Fakültesi Dergisi (CUMFAD) Sivas Cumhuriyet Üniversitesi Mühendislik Fakültesi tarafından yılda iki defa çıkarılan uluslararası, bilimsel, hakemli ve elektronik ortamda okuyucuların erişimine açık bir dergidir. CUMFAD, tüm mühendislik dallarında nitelikli çalışmalarını nesnel bir bakış açısı ile okuyucusuna ulaştırmayı hedeflemektedir. Yayın kurulu olarak dergimizin ilk sayısını okuyucularımızla buluşturmanın mutluluğu içerisindeyiz. Özellikle danışma kurulumuza, eş editörlerimize, alan editörlerimize, dil editörlerimize ve ön inceleme ve dizgiden sorumlu çalışanlarımıza olmak üzere, yazarlarımıza, hakemlerimize ve dergimizin bu sayısına katkıda bulunan herkese verdikleri emekten ötürü en derin şükranlarımızı sunarız. Ayrıca ülkemizde meydana gelen deprem felaketinin tüm süreçleri olumsuz etkilemesine ve editöryal ofis değişim süreci nedeniyle yaşanan aksamalara rağmen bizleri sabırla bekleyen tüm yazarlarımıza minnettarız. Bununla birlikte şimdiye kadar dergimize katkıda bulunan ve destek sağlayan herkese teşekkür ediyoruz. Bir sonraki sayımızı Aralık 2023'de yayımlanacaktır.

Bu sayımızda sıkı bir kör hakemlik ve editörlük sürecinden geçmiş 5 araştırma makalesi bulunmaktadır. Dergimizde yayımlanmakta olan çalışmalar ön inceleme, kör hakemlik süreci ve editöryal süreç olmak üzere üç önemli aşamadan geçmektedir. Hakemlik sürecinde her makale en az iki hakem tarafından incelenmiştir. Ayrıca, inceleme sürecine giren her makale iThenticate yazılımı yardımıyla intihal taramasından geçmektedir. Önümüzdeki sayılarımız için çalışmalarını dergimize göndermek isteyen yazarlarımıza çalışmalarını bize göndermeden önce mutlaka intihal yazılımından geçirmelerini öneriyoruz.

Yeni sayılarımız için çalışmalarınızı <https://dergipark.org.tr/tr/pub/cumfad> adresine yükleyebilirsiniz. Ayrıca, dergimiz akademik danışma kurulunu ve hakem havuzunu genişletmeyi hedeflemektedir. Bu bağlamda dergimizin danışma kurulunda yer almak isteyen veya hakem olarak dergimize katkıda bulunmak isteyen değerli araştırmacılar özgeçmişlerini skockanat@cumhuriyet.edu.tr adresine e-posta ile gönderebilirler. Hakem sertifika işlemleri Dergipark üzerinden yürütülmektedir. Bu nedenle hakem sertifikası almak isteyen hakemlerimizin Dergipark üzerinden başvuruda bulunmaları gerekmektedir.

Nitelikli ve özgün çalışmalarla bir sonraki sayıda buluşmak üzere...

Doç. Dr. Serdar KOÇKANAT
Editör
Ağustos, 2023



Analysis of Flight Based Airport Passenger Arrival Patterns

Merve Gözde Sayın^{1,a,*}, Mustafa Bolat^{1,b}

¹TAV Technologies, 34485, İstanbul, Türkiye

*Corresponding author

Research Article

History

Received: 03/01/2023

Accepted: 02/05/2023

Copyright



This work is licensed under
Creative Commons Attribution 4.0
International License

ABSTRACT

Maintaining effective and successful work in uncertainty is challenging in a niche sector such as aviation and all industries and situations. The situation is a little more complicated, especially in a sector such as the aviation sector, where the rules are not stretched and where one should always be on the alert. For these reasons, it is precious for businesses that carry out airline operations to analyze arriving passengers and understand whether there is a pattern among passengers. Although there are many factors affecting the arrival patterns of passengers, some of them are particularly noteworthy. For example, factors such as whether the flight is domestic or international, the season in which the flight takes place, and the flight hours take place to provide a broad perspective on the arrival patterns of the passengers at the airport. For example, it can be stated that while passengers on international flights see earlier arrival patterns at the airport, last-minute arrivals are more frequent on domestic flights. Similarly, in domestic flights, different passenger arrival patterns have been determined for the arrival airport, depending on the seasonality of the countries. On the other hand, according to the seasonality of the nations (for example, the opening of schools and national holidays), different passenger arrival patterns have been determined for the destination airport. Analyses were carried out in Python and Excel and included case study outputs.

Keywords: Aviation, Pattern Analysis, Passenger, flights.

^a gozde.sayin@tav.aero

^b <https://orcid.org/0000-0002-6213-2549>

^b mustafa.bolat@tav.aero

^b <https://orcid.org/0000-0001-8169-0629>

How to Cite: Sayın M.G., Bolat M. (2023) Analysis of Flight Based Airport Passenger Arrival Patterns, Journal of Engineering Faculty, 1(1): 1-10

Introduction

Although it is not very long ago that people make sense of data in the business world, the development of the concept of data analysis has accelerated with the digitalization of our world [1]. The key to successful business progress is correctly analyzing the factors affecting the business. Data analysis has gained meaning, especially recently, and it has given importance to the work done by providing various predictions to business owners. If the data analysis is done correctly, it is helpful to see the business's different aspects and negative or positive factors. It even enables accurate and successful predictions by taking it one step further. Considering the value that a business model built on successful forecasts will bring, the importance of data analysis is emphasized.

Since the aviation industry, whose rules are strictly defined, is a niche industry, the results are striking when data analysis is performed. Factors such as flight time, departure and arrival point, flight season, and whether the flight is on weekdays or weekends are essential factors in the classification of flights as well as passengers. A meaningful data analysis can only be made from existing data, new features can be created using existing data, and extended results can be obtained by including them in the analysis.

Researchers in transportation and operations management have extensively studied airport passenger arrival patterns. These studies aim to understand the behavior of passengers arriving at airports and to develop strategies to manage the associated risks and challenges. Airport passenger arrival patterns refer to the distribution of passenger traffic at an airport throughout the day, week, month, and year. This concept is vital in airport planning, design, and management. Understanding passenger arrival patterns help airport operators optimize resource allocation, plan for adequate staffing levels, and ensure the passenger experience is as smooth and efficient as possible. Studies have shown that various factors, including flight schedules, holiday periods, economic conditions, and local weather conditions, influence passenger arrival patterns. For example, a study by Chen and Li [2] found that passenger arrival patterns at Beijing Capital International Airport were strongly influenced by flight schedules, with the majority of passengers arriving in the early morning and late evening. Similarly, a study by Wang and Zhang [3] found that passenger arrival patterns at Shanghai Pudong International Airport were influenced by holiday periods,

with increased passenger traffic during national holidays and peak travel periods. Advanced technologies, such as artificial intelligence and predictive analytics, have also been useful in modeling and understanding airport passenger arrival patterns. For example, a study by Wang et al. [4] used machine learning algorithms to predict passenger arrival patterns at Guangzhou Baiyun International Airport and found that the models could accurately predict passenger traffic levels with a high degree of accuracy.

One of the latest studies on airport passenger arrival patterns was conducted by Yang et al. [5] using data from two major airports in China. The authors analyzed the passenger arrival patterns based on flight schedules and passenger travel characteristics and found that passengers tend to arrive at the airport in clusters before their flight departure time, leading to congestion and delays. Another recent study by Kim et al. [6] used data from an airport in South Korea to examine the impact of passenger arrival patterns on airport resource utilization, such as parking spaces, check-in counters, and security checkpoints. The authors found that passenger arrival patterns have a significant impact on the utilization of airport resources and recommended the use of dynamic resource allocation strategies to improve airport operations and reduce passenger waiting times. In a study by Chen et al. [7] the authors used simulation and optimization models to analyze the impact of passenger arrival patterns on airport security checkpoint operations. The study found that passenger arrival patterns significantly impacted the efficiency and effectiveness of airport security operations and recommended using dynamic queuing strategies to improve the performance of security checkpoints.

Overall, the latest research indicates that passenger arrival patterns play a crucial role in the performance and efficiency of airport operations. Developing strategies to manage passenger arrival patterns is essential for improving airport performance and reducing passenger waiting times. In conclusion, these studies provide valuable insights into the behavior of airport passengers in arriving at airports and the impact of their arrival patterns on airport operations. They highlight the importance of understanding passenger arrival patterns and developing strategies to manage the associated risks and challenges, which can help to improve airport performance and reduce passenger waiting times. Moreover, the literature suggests that various factors, including flight schedules, holiday periods, economic conditions, and local weather conditions, influence airport passenger arrival patterns. The use of advanced technologies [8] such as machine learning algorithms, can also be useful in understanding and predicting passenger arrival patterns. These models can be used to support decision-making in the context of airport planning, design, and management.

Before the data world was so digitalized, descriptive statistical analyses were carried out. Then exploratory data analysis (EDA) [9][10] and later machine learning analyses

developed with the development of technology [11]. Simultaneously, data visualization processes have also improved. Advanced data analyses and visualizations are now performed on Excel and in programming languages such as Python and R libraries. In this way, data analysis and visualization have reached vital importance not only in the academic field but also in the industry. Descriptive Statistical Analysis only describes the data, but exploratory data analysis (EDA) questions whether there are any anomalies or salient points in the data [12]. In this case, descriptive analysis is performed by accepting the hypothesis at first, then exploratory data analysis (EDA) is applied to the dataset, and the data is visualized so that it can be read meaningfully. Data that makes sense with visuals are frequently encountered in business reports. Instantly changing pages in many sectors, such as the aviation industry, are based on these analyses. For example, interactive graphics can be included on the home pages of the applications to track the instantaneous change in passenger numbers according to various factors. Thus, both passengers and airline operators can follow instant changes and take action for their own benefit.

Indeed, recent studies have continued to analyze and understand airport passenger arrival patterns to understand the factors that influence passenger traffic and develop models that can be used to predict passenger arrival patterns. with a focus on utilizing advanced technologies and data analysis techniques. For example, a study by Gursoy et al. [13] used statistical models to analyze passenger arrival patterns at Denver International Airport. The study found that flight schedules influenced passenger arrival patterns, and the authors developed a model that could be used to [14] predict passenger arrival patterns based on flight schedules. Another study by Hu et al. [15] used a queuing theory model to analyze passenger arrival patterns at Hong Kong International Airport. The study found that passenger arrival patterns were influenced by a combination of flight schedules, local weather conditions, and other factors, and the authors developed a model that could be used to predict passenger arrival patterns based on these factors. In addition, several studies have analyzed the impact of airline alliances and codeshare arrangements on passenger arrival patterns. For example, a study by Song et al. [16] found that codeshare arrangements between airlines significantly impacted passenger arrival patterns at Incheon International Airport in South Korea. In addition, the authors found that passenger arrival patterns were more spread out when airlines had codeshare arrangements as compared to when they did not.

One recent Li et al. [17] study used big data analytics to analyze passenger arrival patterns at Beijing Capital International Airport. The authors found that a variety of factors, including flight schedules, holiday periods, and local weather conditions influenced passenger arrival patterns. Additionally, the authors used machine learning algorithms to develop a model that could be used to predict [18] passenger arrival patterns, with the aim of improving airport planning and management. Another recent study by Chen et al. [19] analyzed passenger arrival patterns at San Francisco International Airport using a combination of spatial analysis and machine learning techniques. The authors found that a

range of factors, including flight schedules, airport accessibility, and local demographic characteristics, influenced passenger arrival patterns. As a result, the authors developed a model that could be used to predict passenger arrival patterns based on these factors, and they suggest that this information could be used to improve airport planning and management.

In conclusion, recent studies have continued to analyze and understand airport passenger arrival patterns, utilizing advanced technologies and data analysis techniques. Results from these studies suggest that a range of factors, including flight schedules, holiday periods, local weather conditions, airport accessibility, and local demographic characteristics, influences passenger arrival patterns. A variety of models have been developed to [20] analyze and predict passenger arrival patterns and improving airport planning and management, including statistical models, queuing theory models, big data analytics and machine learning algorithms.

Ease of Use

The study was analyzed on real data from a niche sector such as the airport. It is comparable to analyzes for airports and includes actionable results for a better passenger experience. As different data sets can be created at various airports, passenger behaviors vary according to many factors. Therefore, much more data is needed to generalize the outputs. For example, analysis

results may differ when data containing more airports and flights are included.

Analysis

This paper uses our private airport data, which has 32907 rows and 27 columns, however some of the columns are not relevant and unnecessary for this analysis therefore it was used only 18 of them. Columns are listed in the table-1 with descriptions, non-null counts, types, and examples. Also, new features were generated based on the Scheduled Time Departure (STD) column listed in Table 2 with the same explanations as Table 1. Therefore, there are 18 columns came from raw data and 7 columns from generated data so that total 25 column was used to make an analysis.

The Python libraries used in the analysis are mainly as follows; *pandas*, *numpy*, *matplotlib*, *seaborn* and *datetime*. *Matplotlib* and *seaborn* libraries are used for visualization. Year, month, and week are generated with the Python *datetime* library based on the STD column. Monday, Tuesday, Wednesday, Thursday, and Friday are weekdays, and Saturday and Sunday are weekends. Seasons are generated with the following rule: December, January, and February are defined as winter; March, April, and May are defined as spring; June, July, and August are defined as summer; and September, October, and November are defined as fall seasons.

Table 1. Raw Data set (Some Features)

Column Name	Column Description	Non-Null Count	Data Type	Example
INT/DOM	Whether the flight is international or domestic	320907	Object	I
STD	Scheduled Time Departure	320907	Datetime64[ns]	2021-11-07 11:50:00
tota_pax_count_all_points	Total passenger number for all points at the airport	320907	Int64	185
total_pax_count_checkin	Check in Passenger number	320907	Int64	145
checkin_rate	Rate of check ins	320907	Float64	0.7837
360-330	Time slot before 360-330 minutes of the flight (There are 12 time slot columns at half hour intervals)	320907	Int64	0
delay	Delay of flight in minutes	320907	Float64	27.000

Table 2. Generated Features

Column Name	Column Description	Non-Null Count	Data Type	Example
day_of_week	Day of the week for flight	32854	Int64	0
week	Weekday or weekend information	32854	Object	weekday
day_of_year	Day of the year for flight	32854	Int64	101
month	Month of the flight	32854	Int64	3
seasons	Seasons of the year	32854	Object	Summer
my_timezones	According to hours, name the timezone	32854	Object	Morning
flight_count	Whether the flight is less than 400 or not	32854	Object	Few_flight

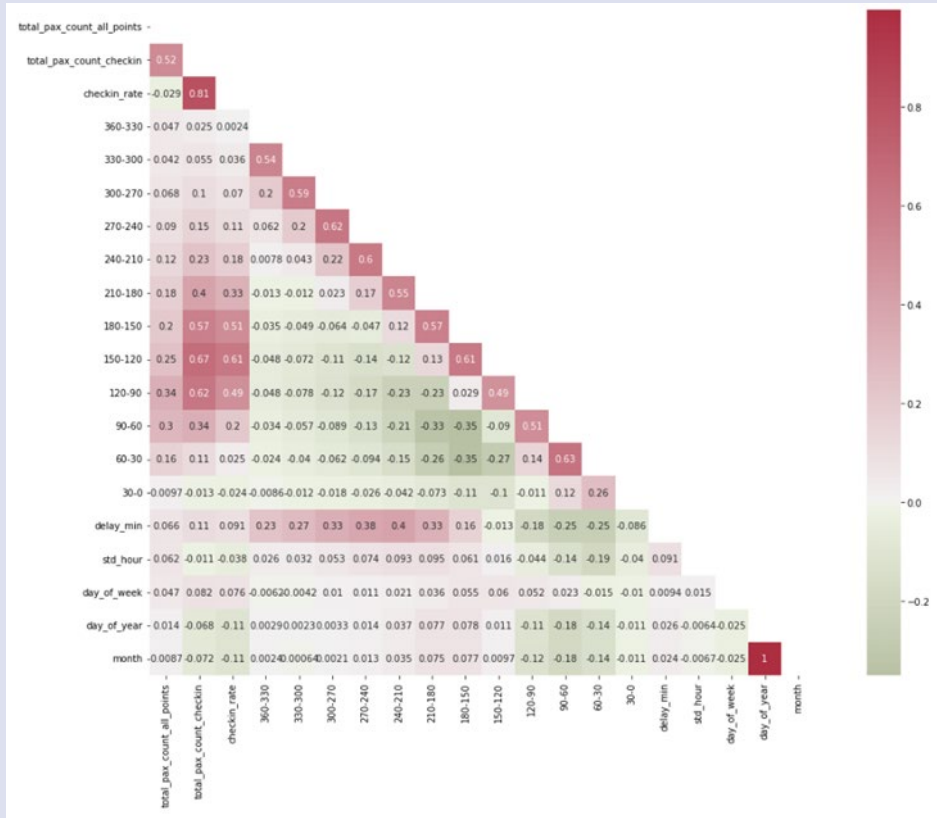


Figure 1. Correlation Heatmap of Data Set

According to the flight industry, between 2 AM and 5 AM are defined as night, between 5 AM and 11 AM as the morning, between 11 AM and 8 PM as noon, and between 8 PM and 2 AM are defined as evening. The dataset needs to be well-distributed for the number of flights, so flights with less than 400 views are labeled as few, and flights with more than 400 views are labeled as many.

After generating new features, there might be irrelevant rows in the data frame; for instance, if there are no passengers in all time slots, this analysis will be unnecessary; therefore, these rows are deleted. In our private data, all departure airports are ADB, so it is nonsense to use the *from_airport* feature so that the column is deleted. Moreover, there are some unknown aircraft types written as 'XXX,' which is also irrelevant to the analysis; therefore, rows with aircraft types are XXX also deleted. Finally, data is not well distributed, so there are various airlines and flights. For the analysis's sake, airlines that occurred less than six times are deleted from the data set.

Correlation values were calculated based on pairwise correlation of columns, excluding NA/null values with python *corr()* function [21] and shown on a heatmap in order to see the features that may be related to each other in the data set. Correlation is calculated between the numeric values in the data frame, and other than the numeric values are ignored in the calculation. Although there are three main calculation methods for correlation, such as Pearson, Kendall, and Spearman, python takes Pearson standard correlation coefficient as default, so in this analysis, Pearson calculation is used. Calculation

results rely on -1 and 1. 1 means a perfect positive relationship, -1 means a perfect negative relationship, also 0 means there is no relationship between variables [22]. Pearson standard correlation coefficient is calculated as given in the equation 1, where \bar{X} is mean of X variable and \bar{Y} is the mean of Y variable. It has 4 assumptions:

- Each observation should have a pair of values.
- Each variable should be continuous.
- It should be the absence of outliers.
- It assumes linearity and homoscedasticity.

$$r = \frac{\sum(X-\bar{X})(Y-\bar{Y})}{\sqrt{\sum(X-\bar{X})^2 \cdot \sum(Y-\bar{Y})^2}} \quad (1)$$

According to the heatmap in Fig. 1, a high positive correlation was observed between the periods in the 180-90 range and the check-in rate. In other words, it can be said that the passengers arriving at the airport during this period are those who have checked in. As seen in the following chapters of the study, most passengers arriving at the airport by checking in between 180-90 times are passengers on international flights. In addition, a relatively high correlation was calculated between the delay time and the 240-210-time interval. Negative correlation computed values do not make sense since they are very close to 0. Therefore, in general, it can be said that there is no negative correlation.

The analysis is based on the flights, passengers, check-in rates, and flight delays.

Flights

In Fig. 2, the x-axis gives the number of flights, and the y-axis shows the information on domestic/international, weekend/weekday, and time zone of flights. Colors are distributed for the seasons.

According to the Fig. 2, flights are grouped with international/domestic, weekday/weekend, time zone, and seasons. It can be said that a maximum number of flights occurs in Domestic, weekday, and morning during the fall season, and the minimum number of flights occurs a domestic, weekend, and night for all seasons. Also, domestic, weekday and noon flights are much more than the rest of the data set. For international flights, it can be said that the maximum number of flights are in the summer season with the information of weekdays, noon. It can be stated that for the international weekday night flights, in the winter season, there are few flights. Overall, it can be noted that the fewest flights took place at night. While the mornings are suitable for domestic flights, noon is preferred for international flights.

Passengers

Passenger analyses are made into three groups. The first group is named all passengers, and the second is check-in passengers. The third group is analyzed under the 12-time slots based on their arrivals at the airport. Moreover, data is grouped with domestic/international flights, weekend/weekday flights, time zones, and the seasons of flights.

In Fig. 3, the x-axis gives the number of passengers, and the y-axis gives the information on domestic/international, weekend/weekday, and time zone of flights. Colors are distributed for the seasons. According to the Fig. 3, like the distribution of the flights, there is a difference between international and domestic flights. For domestic flights, weekday morning and weekday noon are the most preferred time zones in all seasons. On the contrary, weekday and weekend nights are the least preferred time zones for domestic flight passengers.

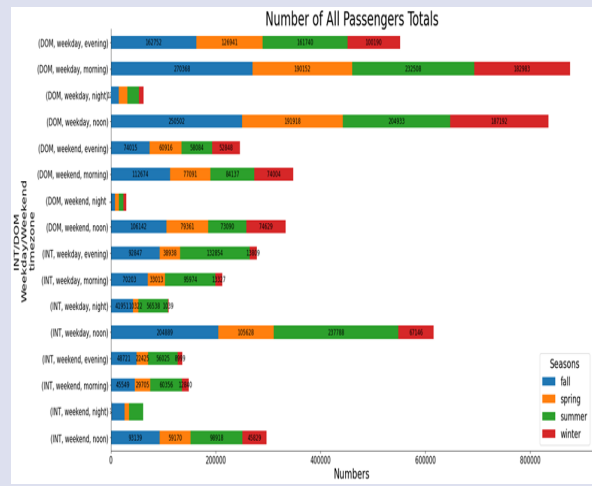
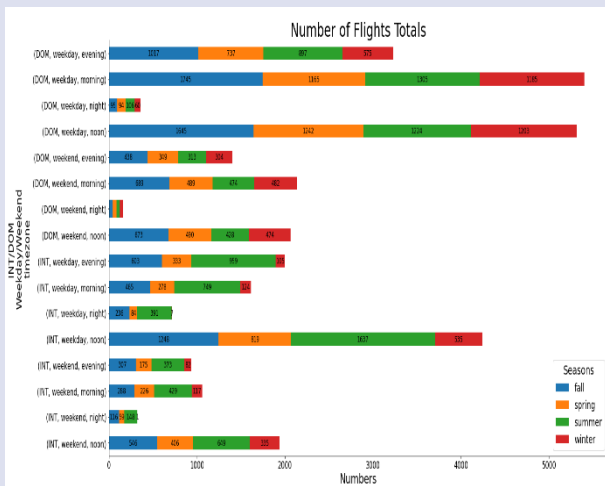


Figure 2. Distribution of Flights

Figure 3. Distribution of All Passengers

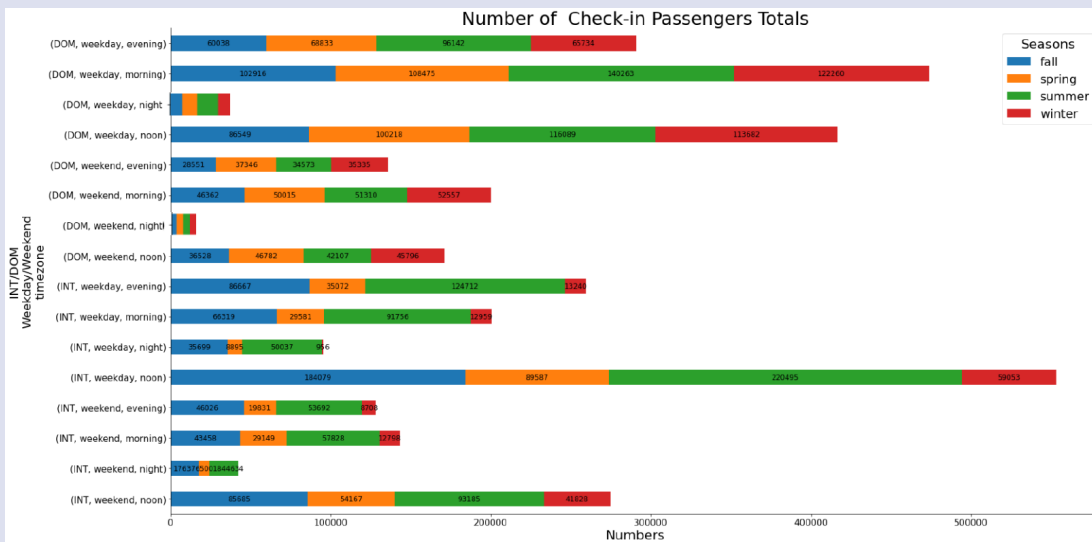


Figure 4. Distribution of Check in Passengers

For international flights, passengers preferred weekday noon flights with respect to other time zones in all seasons. It can be said that international flights are increased in the fall and summer seasons. However, the winter season is the least preferred season for international flights. The preferences are based primarily on the national holidays and the exact seasons, such as school opening closings.

In Fig. 4, the x-axis gives the number of passengers who made check-in procedures at the airport, and the y-axis shows the information on domestic/international, weekend/weekday, and time zone of flights. Colors are distributed for the seasons. Contrary to the all-passenger plots in Fig. 3, international passengers are made check-in procedures more than domestic passengers especially on weekday, noon group. Even though, domestic passengers also made check-in procedures at the airport specifically on weekdays morning and noon, total number of check-in passengers of domestic flights are quite a few than total number of check-in passengers of international flights. Therefore, in Fig. 4, the maximum number of passengers is located on the international, weekday, and noon flights, especially for the summer and fall seasons. It can be said that international passengers tend to make check-ins for the summer flights but not for the winter flights. It can be seen from the Fig. 4; check-in procedures are made less for domestic flights. On the contrary to international flights, domestic flights mostly happen in the summer and winter seasons. Most domestic passengers preferred weekday mornings for their flights.

Passengers over Time Slots

Passengers are grouped by the 30 minutes periods. It starts with a 360-300 slot that is 360 minutes before the flight and continues like that. The difference is noticeable, especially for domestic and international flights. Most of the passengers arrive at the airport between 120-90 minutes; from Fig. 13, it can be easily seen the number of passengers from the x-axis. For domestic flights, the last period arrivals are more usual than for international flights, specifically between 90-0 minutes. However, when international flight passenger arrives at the airport between 180-120 minutes, domestic flight passenger has yet to be seen at the airport.

Since both international and domestic flight passengers usually choose to come to the airport between 120-90 time slots, it can be stated from Fig. 5-16 that arrival patterns are distributed mainly on the type of flight domestic or international.

Check in Rates

When the check-in rates of incoming passengers are examined according to whether the flight is domestic or international, season, time, and weekdays, it can be seen from Fig. 7 that the most significant difference is between domestic and international flights. The check-in rates of domestic flights are much lower than the check-in rates of international flights. Especially in the autumn period, there is a severe proportional difference between them. Therefore, check-in rate differences may be due to the fact that domestic flights are fewer in autumn.

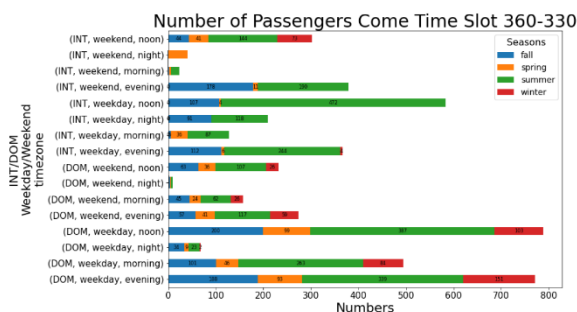


Figure 5. Distribution of Check-in Passengers come in Time Slot 360-330

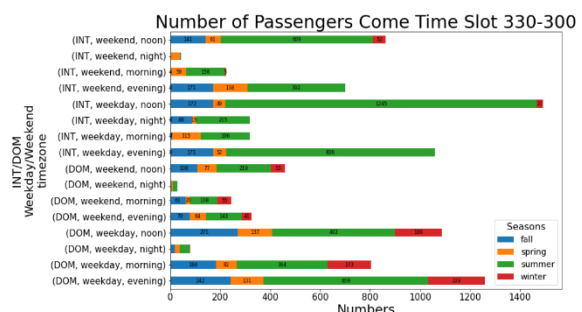


Figure 6. Distribution of Check-in Passengers come in Time Slot 330-300

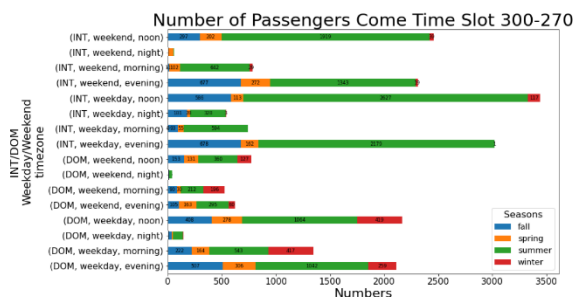


Figure 7. Distribution of Check-in Passengers come in Time Slot 300-270

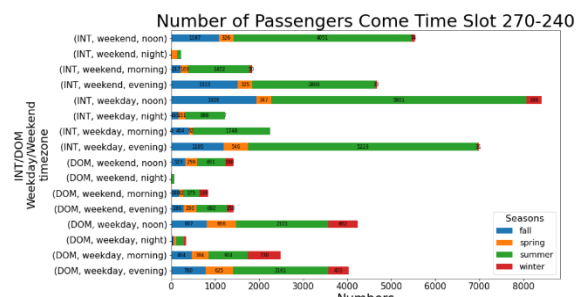


Figure 8. Distribution of Check-in Passengers come in Time Slot 270-240

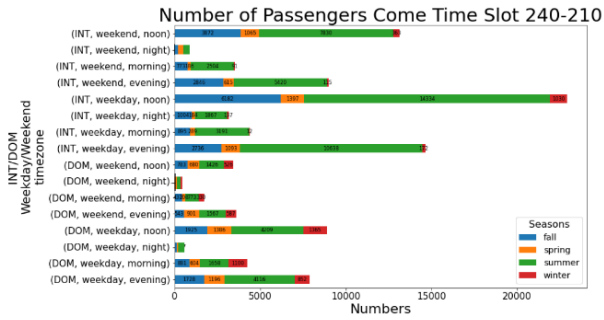


Figure 9. Distribution of Check-in Passengers come in Time Slot 240-210

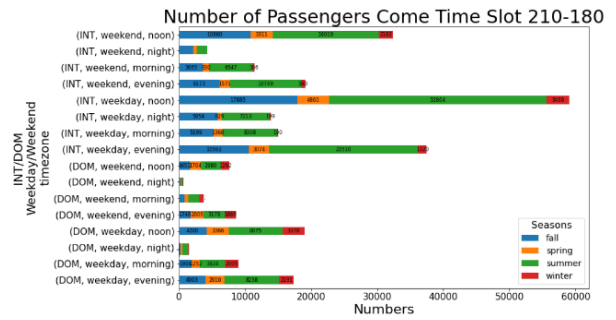


Figure 10. Distribution of Check-in Passengers come in Time Slot 210-180

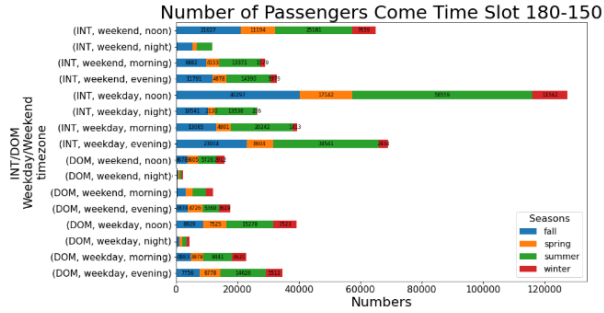


Figure 11. Distribution of Check-in Passengers come in Time Slot 180-150

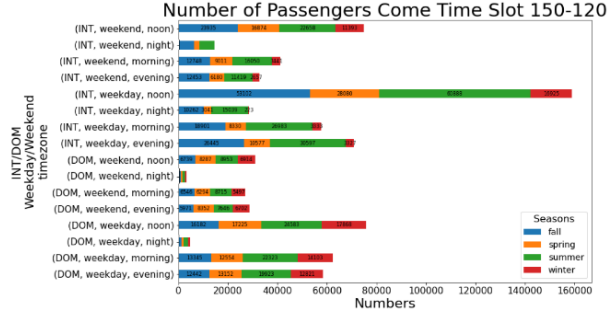


Figure 12. Distribution of Check-in Passengers come in Time Slot 150-120

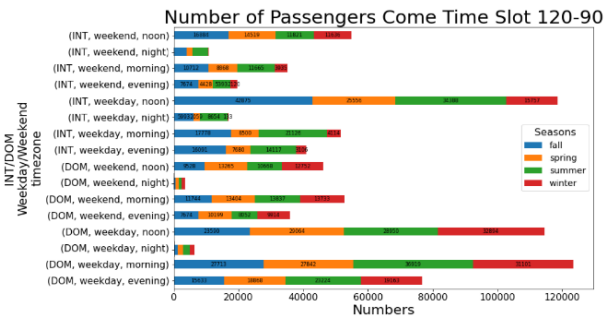


Figure 13. Distribution of Check-in Passengers come in Time Slot 120-90

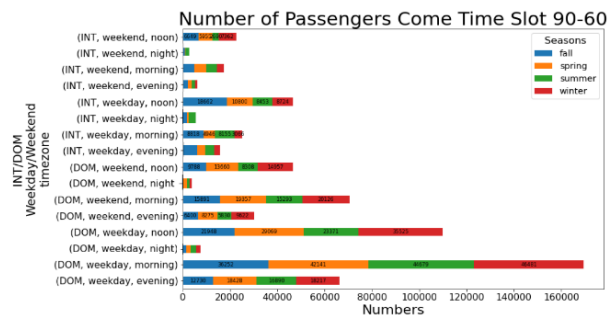


Figure 14. Distribution of check-in Passengers come in Time Slot 90-60

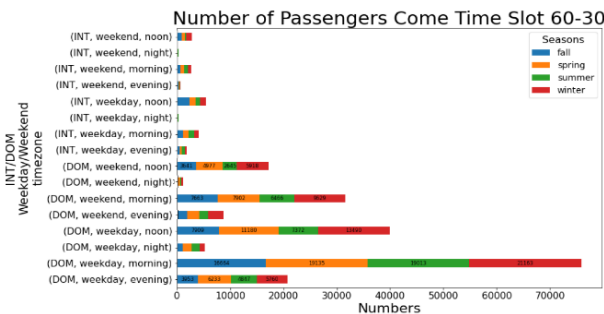


Figure 15. Distribution of Check-in Passengers come in Time Slot 60-30

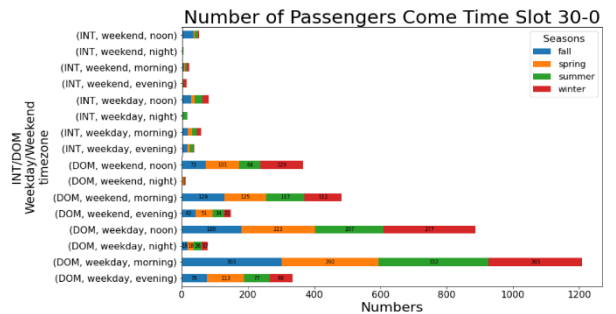


Figure 16. Distribution of Check-in Passengers come in Time Slot 30-0



Figure 17. Distribution of Check in Rates

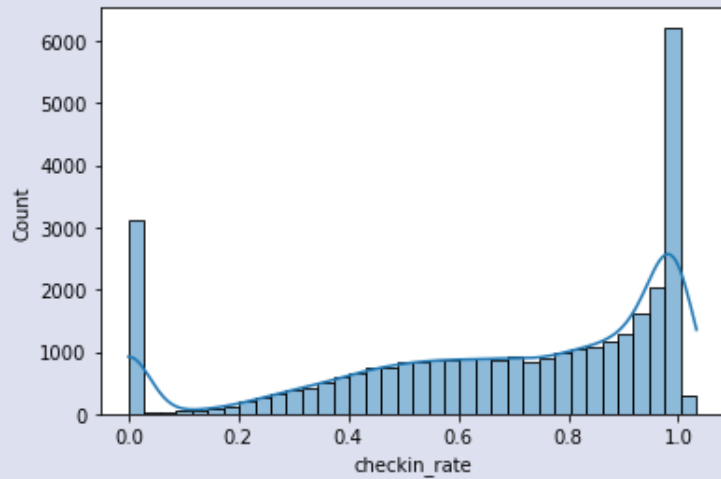


Figure 18. Distribution of Check in Rates-Ungrouped

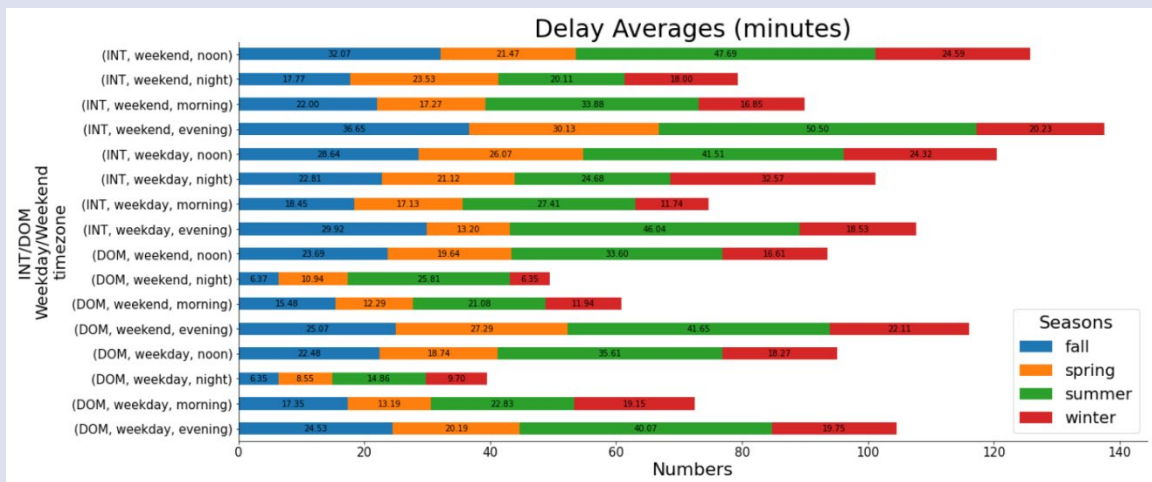


Figure 19. Distribution of Delays in Averages

The check-in rate distribution of all flights without any grouping can be found in Fig. 8. The reason for the check-in rate appearing above 1 is that there are people who appear twice in our dataset, but we decided to keep it as this did not disrupt the course of the analysis. When we look at the check-in rate distribution graph, it is possible to say from Fig. 8 that 0s and 1s are in weight, but the average is 0.5.

Delay Averages

Fig. 9 shows the average delays of the flights. Accordingly, it can be said that most delays occur in the summer months. In this chart, the distribution according to the season distinction and the period of the day of the flight rather than the domestic/international distinction draws attention. The average delays are directly proportional to the excess flights in those periods. The highest average in international, weekend, and evening summer flights was recorded as 50.50 minutes. The lowest average was recorded as 6.35 minutes for domestic flights in the winter and autumn, from the periods with the least flights.

Discussion and Further Works

Analyzing flight-based airport passenger arrival patterns is an essential aspect of airport management. It provides valuable insights into passenger behavior and helps airport authorities optimize their resources to improve the overall efficiency of airport operations. By analyzing passenger arrival patterns, airport authorities can identify the busiest times of the day, week, or year and allocate resources accordingly, such as deploying more staff at peak times, opening additional security checkpoints, or providing more parking spaces. The relevant analysis leads to a more seamless and efficient passenger experience, reducing wait times and congestion and enhancing the airport's overall reputation.

Moreover, analyzing passenger arrival patterns also has implications for airport security. By monitoring passenger arrival times, airport authorities can identify potential security risks, such as suspicious behavior or irregular travel patterns, which enables airport security personnel to respond quickly and appropriately, enhancing the safety and security of the airport and its passengers.

Firstly, data analytics techniques such as statistical analysis, data mining, and machine learning can be used to analyze passenger arrival patterns and identify trends and patterns. Then, data visualization tools such as heat maps, scatter plots, and histograms can be used to display and interpret the data. For example, a study by Chen et al. (2019) [23] used data mining and visualization techniques to analyze Hong Kong International Airport passenger arrival patterns. The study found that most passengers arrived between 6 am and 8 am and 2 pm and 6 pm and recommended that airport authorities allocate more resources during these peak periods.

Secondly, predictive modeling techniques such as regression analysis, time series analysis, and neural networks can be used to predict passenger arrival

patterns and forecast demand. For example, a study by Gao et al. (2019) [24] used a predictive modeling approach to estimate passenger arrival times at Beijing Capital International Airport. The study found that the model achieved an accuracy of over 80% in predicting passenger arrival times and recommended that airport authorities use it to optimize their resources and improve airport efficiency.

In this study, a special data set was created, and some analyzes were carried out by questioning the similarities and differences of the flights in different categories, the analysis of the behavior of the passengers at the airports, and whether there was a specific pattern. The most apparent difference from the outputs is the differences between domestic and international flights. The following output is that the flight frequency increased and decreased according to the time of day the flight took place. In addition, seasonal flight differences also differed in domestic and international flights. Flights and passengers were examined in terms of season, flight type, and temporal, as well as flight delays and check-in rates. In addition, the features that can be positively or negatively related to each other according to the correlation between the components in the data set were examined.

Overall, the analysis of flight-based airport passenger arrival patterns is crucial for optimizing airport operations, improving the passenger experience, and enhancing airport security. As airports continue to grow in size and complexity, the importance of this analysis will only increase, making it a vital area of research for airport management professionals.

Future studies it is aimed to develop the analysis with a more extensive and diverse data set. The scope and results of the analysis will be developed with data from different airports and parameters that can be generated. Thus, the passenger arrival pattern will be drawn, the flights will be classified, and studies will be carried out to provide a more effective airport experience.

Despite the importance of analyzing flight-based airport passenger arrival patterns, several challenges and limitations exist. For instance, data collection and processing can be time-consuming and costly, requiring significant investment in technology and resources. Additionally, the accuracy and reliability of the data can be impacted by several factors, such as incomplete or inconsistent data, errors in data entry or processing, or changes in passenger behavior.

To address these challenges, researchers and practitioners must continue to explore and develop new techniques and tools for analyzing flight-based airport passenger arrival patterns. For instance, machine learning algorithms and predictive modeling techniques can help accurately identify and predict passenger arrival patterns, enabling airport authorities to plan and allocate resources more effectively. Similarly, new data collection methods like mobile applications and sensors can help capture real-time data on passenger arrival patterns, providing a more comprehensive and accurate view of airport operations.

Moreover, as airports continue to face increasing pressure to reduce their environmental impact, analyzing passenger arrival patterns can also promote sustainable airport operations. Airport authorities can optimize ground transportation and reduce congestion and emissions by identifying peak times and routes and upgrading more sustainable and efficient transport systems.

In conclusion, the analysis of flight-based airport passenger arrival patterns is an important area of research for airport management professionals. By leveraging new technologies and data collection methods, researchers and practitioners can develop more accurate and effective strategies for optimizing airport operations, improving the passenger experience, and enhancing airport security and sustainability.

Acknowledgements

We would like to thank Gökhan Koç for helping with this research paper and for providing guidance and feedback throughout this analysis. Also, we would like to thank Dr. Yakup Genç for his guidance and support in this matter. We would also like to thank Talha Koç, his support is very important to us.

References

- [1] Tsai C.W., Lai C.F., Chao H.C., et al., Big data analytics: A survey, *Journal of Big Data*, 2(21) (2015) 1-32, <https://doi.org/10.1186/s40537-015-0030-3>.
- [2] Chen L., Li J., Study on passenger arrival patterns at Beijing Capital International Airport, *Journal of Transportation Systems Engineering and Information Technology*, 10(3) (2010) 190-195.
- [3] Wang X., Zhang Y., Analysis of passenger arrival patterns at Shanghai Pudong International Airport during holiday periods, *Journal of Air Transport Management*, 23 (2012) 41-45.
- [4] Wang X., Wu J., Wang J., Prediction of airport passenger arrival patterns using machine learning algorithms, *Journal of Air Transport Management*, 61 (2017) 87-96.
- [5] Yang Y., Li X., Wang X., Analysis of passenger arrival patterns at airports, *Journal of Air Transport Management*, 93 (2021) 101700.
- [6] Kim J., Kim Y., Lee Y., The impact of passenger arrival patterns on airport resource utilization, *Transportation Research Part A: Policy and Practice*, 144 (2021) 455-466.
- [7] Chen X., Wang X., Li X., Analysis of passenger arrival patterns at airport security checkpoints, *Journal of Air Transport Management*, 98 (2022) 101743.
- [8] Government of Canada investing in research collaborations between colleges and entrepreneurs, (2019), MENA Report.
- [9] Tukey W.J., The future of data analysis, *Annals of Mathematical Statistics*, 33(1) (1962) 1-67.
- [10] Tukey W. J., *Exploratory Data Analysis*, (1977), Addison-Wesley.
- [11] Kürzl H., Exploratory data analysis: Recent advances for the interpretation of geochemical data, *Journal of Geochemical Exploration*, 30(1-3) (1988) 309-322, doi:10.1016/0375-6742(88)90066-0.
- [12] Kolassa S., EDA, Descriptive statistics, *Visual Analytics*, (2017).StackExchange.<https://stats.stackexchange.com/q/309837>
- [13] Gursoy D., Chi X., Lu L., & Lu Y., Passenger arrival patterns and their impact on airline scheduling, *Transportation Research Part A: Policy and Practice*, 38(3) (2004) 193-212.
- [14] Sweeney J., Tran V., Improving Protection Against Cybersecurity Attacks of Emergency Dispatch Centers, In *International Conference on Cyber Warfare and Security*, (2022) 315.
- [15] Hu Y., Wang X., Wang J., Analysis of passenger arrival patterns at Hong Kong International Airport using queuing theory, *Journal of Air Transport Management*, 41 (2015) 38-43.
- [16] Song H., Kim J., Lee H., The impact of airline alliances and codeshare arrangements on airport passenger arrival patterns, *Transportation Research Part A: Policy and Practice*, 102 (2017) 365-376.
- [17] Li Y., Zhang Y., Li J., Big data analytics of passenger arrival patterns at Beijing Capital International Airport, *Journal of Air Transport Management*, 89 (2020) 101935.
- [18] Corum K., Garofalo J., Analyzing 3D-printed artifacts to develop mathematical modeling strategies, *Technology and Engineering Teacher*, 78(2) (2018) 14.
- [19] Chen W., Li Z., Ye Y., Spatial analysis and machine learning for predicting airport passenger arrival patterns: A case study of San Francisco International Airport, *Journal of Transport Geography*, 91 (2021) 102947.
- [20] Zhou Z., Szymanski B., Gao, J., Modeling competitive evolution of multiple languages, *PLoS One*, 15(5) (2020) e0232888.
- [21] McKinney W., *Data Structures for Statistical Computing in Python*, `pandas.DataFrame.corr` - `pandas 1.5.3` documentation. Retrieved February 27, 2023, from <https://pandas.pydata.org/docs/reference/api/pandas.DataFrame.corr.html>
- [22] Sarmiento D. (n.d.), Chapter 22: Correlation Types and When to Use Them, Retrieved February 27, 2023, from <https://ademos.people.uic.edu/Chapter22.html>
- [23] Chen J., Wang Y., Yu Q., Yu M., Analysis of passenger arrival patterns at Hong Kong International Airport using data mining and visualization techniques, *Transportation Research Part C: Emerging Technologies*, 100 (2019) 133-148.
- [24] FlyData. (n.d.). FlyData project. Retrieved from <https://smartcities.berkeley.edu/projects/flydata/>



Categorical and Binary Brain Tumor Classification Using Transfer Learning Techniques

Ayşe Gül Eker ^{1,a,*}, Gamze Korkmaz Erdem ^{2,b}, Nevcihan Duru ^{3,c}

¹Department of Computer Engineering, Kocaeli University, Kocaeli, Türkiye

²Department of Computer Engineering, Kocaeli University, Kocaeli, Türkiye

³Faculty of Engineering and Natural Sciences, Kocaeli University of Health and Technology, Kocaeli, Türkiye

*Corresponding author

Research Article

History

Received: 01/02/2023

Accepted: 16/06/2023

Copyright



This work is licensed under
Creative Commons Attribution 4.0
International License

ABSTRACT

The quality and length of life may be affected by brain tumors, which are created when cells in the head region proliferate out of control. Patients with misdiagnosed or late-diagnosed brain tumors and untreated patients have a lower chance of survival. Images obtained from MR imaging equipment are typically used to diagnose brain cancers. Given the rising number of patients and the high doctor density, computer-assisted techniques are particularly helpful in the diagnosis and categorization of brain tumors. In this study, transfer learning techniques were used to classify brain tumors from MRI data. In the study, a 4-class dataset made up of glioma, meningioma, pituitary, and no-tumor was used in addition to a binary data set of tumor and no-tumor. Repetitive and unneeded regions in the images were eliminated by applying image preprocessing techniques to the datasets. Following that, classification was performed using the EfficientNet, XceptionNet, and CoAtNet models, which modified the last layer and used the weight values of the models trained on very large datasets (imagenet). As a result, show that CoAtNet performed best in multiclassification validation accuracy (98.26) and EfficientNet in binary classification (99.98). When compared to high-success studies with similar datasets, it was observed that the success metrics were quite close to those of these studies

Keywords: transfer learning, coatnet, efficientnet, xceptionnet, brain tumor, classification, medical image

^a aysegul.eker@kocaeli.edu.tr

^b <https://orcid.org/0000-0003-0721-2631>

^c gamze.erdem@kocaeli.edu.tr

<https://orcid.org/0009-0000-3979-0175>

^c nevcihan.duru@kocaelisaglik.edu.tr <https://orcid.org/0000-0003-2154-7067>

How to Cite: Eker A.G., Korkmaz Erdem G., Duru N. (2023) Categorical and Binary Brain Tumor Classification Using Transfer Learning Techniques, Journal of Engineering Faculty, 1(1): 11-16

Introduction

The brain is a massive, intricate structure that governs the whole nervous system in humans and comprises about 100 billion nerve cells [1]. This vital organ is formed in the brainstem, the core of the neurological system. Therefore, any type of irregularity in the brain could be dangerous for people's health. The most severe of these anomalies are brain tumors.

Brain tumors are defined as abnormally growing cells in the skull region. Typically, abnormal and uncontrolled cell division is what causes a brain tumor. Both the brain and the skull can develop these tumors; they can also start in the tissues surrounding the brain.

According to the World Health Organization, brain tumors account for less than 2% of all human cancers, but because of their high morbidity and comorbidities, early diagnosis is a critical idea in contemporary medicine [2].

The World Health Organization (WHO) has categorized brain tumors into four classes [1]. Meningiomas are an example of grade 1 and grade 2 tumors, while grade 3 and grade 4 tumors are more serious ones (e.g., glioma). Meningioma, pituitary, and

glioma tumor incidence rates in clinical practice are roughly 15%, 15%, and 45%, respectively.

Meningiomas, pituitary adenomas, and schwannomas are the most commonly seen benign tumors, while gliomas, which account for 78% of all malignant brain tumors, are included in the category of malignant tumors. Most benign intracranial tumors, or 10 to 15% of all neoplasms, are meningiomas, which are the most frequent type. After meningiomas, gliomas, and schwannomas, pituitary adenomas are the most frequent intracranial tumors, commonly affecting patients in their 30s and 40s. Schwannomas, which form along nerves and are made up of cells that normally provide the nerve cell's electrical insulation, also affect patients frequently in these age groups. Glia, the brain's supporting cells, give birth to gliomas, which include ependymomas, medulloblastomas, astrocytomas, and Glioblastoma multiforme (GBM), the most aggressive kind of glial tumor [3].

Depending on the location, size, and kind of tumor, there are many treatment options for brain tumors. Surgery is currently the most popular method of treating brain tumors because it has no negative consequences on the brain [4].

The inside state of the human body can be observed using a variety of medical imaging technologies, including computed tomography (CT), positron emission tomography (PET), and magnetic resonance imaging (MRI). Since MRI is the only non-invasive, non-ionizing imaging technique that provides useful information in 2D and 3D formats regarding the kind, size, shape, and location of brain tumors, it is regarded as being the most advantageous among all imaging modalities [5].

There are many artificial intelligence applications for brain tumors such as automatic brain tumor classification, brain tumor segmentation, and finding optimal routes to the tumor as we developed before, and it is a very important field [6].

Brain tumor classification is a multidomain problem that requires designing the data collection, pre-processing, denoising, segmenting, feature extraction, feature selection, classification, and post-processing procedures.

In this study, multiple brain tumor classification was performed with two datasets from Kaggle. The Kaggle BR35H dataset [7] was used for binary classification (normal/tumor), and the Kaggle Brain Tumor Classification dataset [8] was used for multi-class classification (normal, glioma tumor, meningioma tumor, and pituitary tumor).

The work is organized as follows. In Section 2, the most recent studies in the literature that perform automatic brain tumor classification images datasets are presented. Methods are explained in Section 3. Information about the dataset used, architectures of transfer learning models, and the deep learning model is given. And explains how the experimental study was carried out. The preprocessing applied to the images and the hyperparameters of the models are presented. In Section 4, the experimental results and the success of the models are presented. In Section 5, the conclusion and discussion are presented and future work is mentioned.

Literature Review

For automatic brain MRI classification using machine learning and deep learning approaches, many different methods have been presented. Numerous studies using cutting-edge deep convolutional neural networks have been written to address binary and multiclass brain tumor diagnosis difficulties.

For quick and accurate tumor classification performance, Kushwaha and Maidamwar [9] suggest a model that combines the Saliency map with VGGNet, AlexNet, Inception Net, and Xception Net models. The model's 95% accuracy, 94.1% precision, and 95.6% recall make it suitable for low-error applications for brain tumor classification. Kang et al. [10] used many pre-trained deep Convolutional neural networks (CNNs) to extract important features from the MRI scans and ML algorithms to classify the MRI scans of three freely available datasets. According to the results, the Support Vector Machines (SVM) with radial basis function kernel outperforms other machine learning classifiers.

Deep tumor networks, as defined by Amran et al. [11], were proposed by Google Net and CNN model hybrids for the detection of CTs. The proposed model was built on top of the GoogleNet model. The final five layers of GoogleNet were

removed, and 14 layers—each one deeper than the previous—of the CNN model were replaced. Although the fundamental CNN architecture was left unmodified, the ReLU AFs were converted to a leaky Re-AF. After the modifications were made, the layers increased from 22 to 33 in total. The hybrid model that is advised acquired the maximum level of classification accuracy, 99.10%.

In another study, Four real-world data sets were successfully used to test and suggest a novel method for the diagnosis of brain cancers based on genetic algorithm-based deep learning. According to experiments on the Gazi Brain Data Set 2020 dataset, this inference was supported by four separate metrics outcomes. The proposed model achieved %85 accuracy. While the conventional CNN model had a success rate of 78%, the proposed CNN+GA model had a success rate of 85% [12].

Papageorgiou [13] proposed a model to follow while creating an automated and cost-effective categorization tool that will help medical professionals everywhere identify brain tumors from MRI scans. The proposed model provides 99.62% testing accuracy utilizing a cross-entropy loss function and was trained and verified using MRI images.

Sert et al. [14] and Özyurt et al. [15] propose ResNet for the first component of the CNN-SVM architecture, whereas resolution improvement and entropy segmentation approaches were used for image preprocessing. On the same dataset, Özyurt et al. [15] compare their model to a CNN-KNN with a 90.62% accuracy. The research in these articles is based on MRI image segments that simply show the tumor tissue. Sajja and Kalluri's [16] use of a CNN on a BRATS dataset of 577 photos yields an accuracy of 96.15% when tested on 182 images, showing another successful attempt to identify images with and without brain tumors.

Using a CNN to combine five separate models into one, Mittal and Kumar [17] identify MRI images in relation to three tumor classifications and a class for the negative diagnoses, achieving a testing accuracy of 98.8%. On two databases comprising three kinds of malignancies (meningiomas, pituitary adenomas, and gliomas), Sultan et al. [18] confirm their CNN model with overall accuracies of 96.13% and 98.7%.

Using pre-trained CNNs [19] is another strategy. On two datasets with three and four tumor types, respectively, accuracy rates of 97.64% and 98% were achieved. In order to segment the image regions containing the tumor and categorize these parts into five groups with an accuracy of 81%, Zhao and Jia [20] use a deep convolutional neural network.

Methods

In this section, firstly, the datasets will be introduced. Then, the preprocessing steps applied on the datasets will be explained. Then, the used transfer learning models will be introduced and the parameters and model structure used will be mentioned.

Datasets

In the study, two different data sets were used for binary and multiple classifications. The BR35H for a binary dataset is also shared as open source on Kaggle. In this dataset, there are a total of 3000 MR images in 2D format, consisting of 1500 tumor images and 1500 healthy images. These images are in JPEG format [21]. For multi-classification, a data set shared as open source on Kaggle was used. This dataset contains 2870 data for 4 classes for training; glioma, meningioma, pituitary, and no-tumor MR images in 2D jpeg format[22].

Image PreProcessing

In both brain MRI datasets, nearly all of the images have unwanted gaps and areas, resulting in below-average classification performance. Therefore, it is very important to cut photos to eliminate unnecessary parts and use only relevant information.

First, the image dimensions are set to 224*224 pixels. It is necessary to calculate the size of the unwanted black areas in the images. Thresholds are applied to images. However, before that, Blurring is performed on the images so that the Threshold process can be applied more successfully. For this, the GaussianBlur method of the OpenCV library is used. The 'otsu' threshold is an OpenCV technique where pixel values are assigned according to the threshold value provided. Each pixel value is compared with the threshold value, if the pixel value is less than the threshold value, it is set to 0. Otherwise, it is set to the maximum value. As a result of this process, the outside of the region we are interested in is masked. Then we contour with the coordinates of the top, bottom, right and left endpoints of the region of interest. The area inside this contour is considered the area we are interested in and the crop is done according to these coordinates. By re-sizing, the images are prepared to be given to the model.

Transfer Learning

It is a machine learning approach in which a deep learning network (usually convolutional networks) previously trained for a task is taken with weights and used as a starting point for a different task [23]. Transfer learning has been successfully used in several fields recently, including the segmentation and classifications of medical images. In this study, preprocessed images for brain tumor classification were classified with EfficientNet, XceptionNet, and CoAtNet.

EfficientNet; It is considered a group of convolutional network models. The ImageNet classification problem consisting of more than 14 million images, reaches 84.4% accuracy with 66 M parameters and is among the state-of-the-art models [24]. EfficientNet; It consists of 8 different models between B0 and B7. The B0 model was used in this study. In EfficientNet, an activation function called Swish is used instead of Rectifier Linear Unit- ReLU. Google Brain Team: They noted that the Swish activation function tended to work better than ReLU when applied in deeper models on a group of datasets. XceptionNet; It is a 71-layer convolutional neural network model trained on the ImageNet classification problem and achieved 79% accuracy in ImageNet. It was basically developed by adding on the InceptionV3 network. In the convolution section, in addition to InceptionNet, smart depth convolution and smart point convolution sections have been added [25]. In this way, it is aimed to prevent over-learning by using fewer parameters.

For large-scale image identification and classification, CoAtNet offers a special mix of depthwise convolutions (1) and self-attention (2) that enables quick and precise progress. The suggested design is based on the finding that self-attention models typically demonstrate higher capacity whereas CNN's typically show better generalization. If the model hyperparameters are mentioned; Weight values for all models are from 'imagenet'. Validation split is =0.2. Training is 30 epochs. optimizer is Adam (lr= 1e-4). Other parameters are given in Table 1.

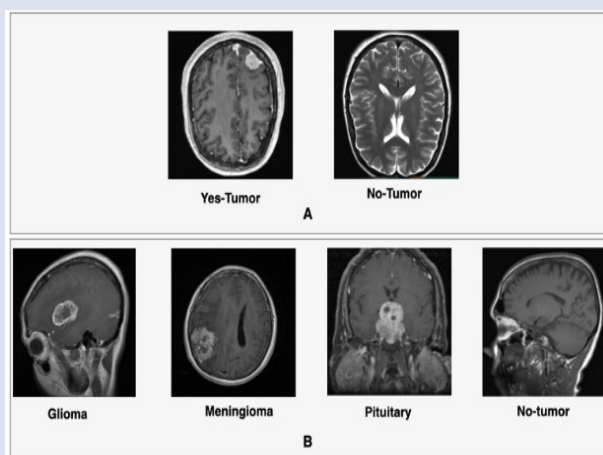


Figure 1. A- Example image from dataset for binary classification, B- Example image from dataset for multiclassification

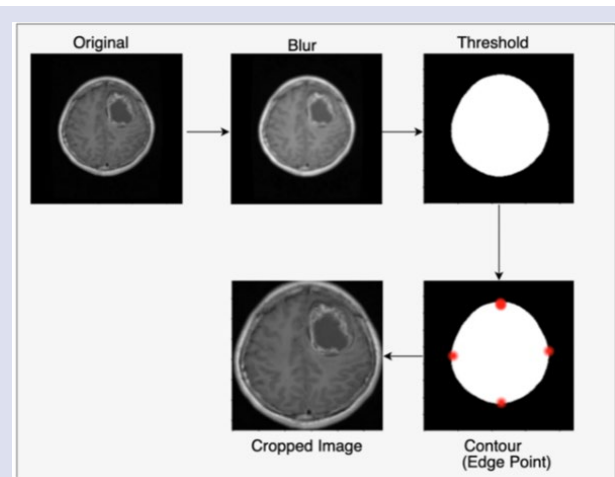


Figure 2. Image preprocessing steps

Table 1. Hyperparameters

Model	Hyperparameters	
	Binary	Multi-class
EfficientNet	Last_activation=sigmoid,loss=binary__crossentropy	Last_activation=softmax,loss=categorical_crossentropy Version=EfficientNetB0,
XceptionNet	Last_activation=sigmoid,loss=binary__crossentropy	Last_activation=softmax,loss=categorical_crossentropy Version='XceptionNet',
CoatNet	Last_activation=sigmoid,loss=binary__crossentropy	Last_activation=softmax,loss=categorical_crossentropy Version='CoatNetv0',

Table 2. Success Values For Multiple Classification

Model	Accuracy	AUC	Precision	Recall
EfficientNetB0	98.12	98.99	98.12	98.12
XceptionNet	95.63	99.40	95.63	95.63
CoAtNetv0	98.26	99.39	98.26	98.26

Table 3. Success Values For Binary Classification

Model	Accuracy	AUC	Precision	Recall
EfficientNetB0	99.98	1	99.90	1
XceptionNet	97.50	99.30	1	94.67
CoAtNetv0	99.38	99.18	99.6	99.2

Table 4. Success Values for Similar Datasets

References	Model	Dataset	Classification	Accuracy
Kushwaha and Maidamwar [9]	VGGNet, AlexNet, InceptionNet, XceptionNet	Kaggle BR35H Brain Tumor Dataset, IEEE Data Port Dataset	Multi	95
Kang et al. [10]	CNN	BT-small-2c, BT-large-2c, BT-large-4c	Binary and Multi	98.17
Amran et al. [11]	GoogleNet, CNN	Kaggle BR35H Brain Tumor Dataset	Binary	99.10
Özdem et al. [12]	CNN+GA (Genetic Algorithm)	Gazi Brain Data Set 2020	Binary	85
Papageorgiou [13]	CNN	Kaggle BR35H Brain Tumor Dataset, Kaggle Brain MRI Images for Brain Tumor Detection	Binary	99.62
Sert et al. [14]	ResNet	TCGA-GBM	Binary	95
Özyurt et al. [15]	NS-CNN	TCGA-GBM	Binary	95.62
Sajja and Kalluri [16]	CNN	BRATS	Binary	96.15
Mittal and Kumar [17]	AiCNN	Two private datasets	Multi	98.8
Sultan et al. [18]	CNN	Dataset from Tianjing Medical University, REMBRANDT	Multi	98.7
Ari et al. [19]	CNN	RIDER, Figshare, REMBRANDT	Multi	99
Zhao and Jia [20]	DCNN	BRATS	Multi	81
Our Study	CoAtNetv0	Kaggle Brain Tumor Classification (MRI)	Multi	98.26
Our Study	EfficientNetB0	Kaggle BR35H Brain Tumor Dataset	Binary	99.98

Experimental Results

The results obtained in this section will be presented in tables. First, the validation success values for transfer learning in multiple classification are given in Table 2.

Accordingly, the highest accuracy values for multiple classifications were obtained with the CoatNetv0 model.

In Table 3, validation success values for transfer learning in binary classification are presented.

Accordingly, the highest accuracy values for binary classification were obtained with the EfficientNetB0 model.

In Table 4, the comparisons of studies with similar datasets and the achievements obtained with the transfer learning model are presented. It is observed in the table that many methods are used for brain tumor binary and multiple classifications and the most successful models are CNN-based.

Conclusions

Brain tumors, which are formed by the uncontrolled proliferation of cells in the head region, can cause a decrease in the quality and duration of life. Patients with misdiagnosed or late-diagnosed brain tumors and untreated patients have a lower chance of survival. Diagnosis of brain tumors is usually provided by images taken from MR imaging systems. It is very useful to use computer-aided systems in the detection and classification of brain tumors due to the increasing number of cases and the high density of doctors. The development of artificial intelligence and deep learning models and automatic classification of brain tumors are very common areas of study in recent years.

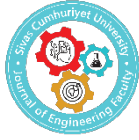
In this study, brain tumor classification from MRI images was performed by transfer learning methods. In the study, a binary dataset of tumor and no-tumor, as well as a 4-class dataset consisting of glioma, meningioma, pituitary, and no-tumor, was used. By applying image preprocessing steps to the datasets, redundant and unnecessary areas in the images were removed. Then, classification was carried out with EfficientNet, XceptionNet, and CoAtNet models, which used the weight values of the models trained with very large datasets (imagenet) and changed the last layer.

According to the results of the study, while EfficientNet gave the highest success values in binary classification (validation accuracy is 99.98), CoAtNet gave more successful results in multi-classification (validation accuracy is 98.26), which is a more challenging task. EfficientNet is a model that uses a compound scaling method to increase the depth, width, and resolution of the network in a coordinated way. This allows EfficientNet to be a more efficient and scalable network with improved performance. The CoAtNet model, based on both CNN and Vision Transformer (ViT) architectures, is one of the most successful models developed in recent years. CoAtNet takes advantage of both of these strengths by using a hybrid architecture that combines CNNs and transformers. When compared to high-success studies with similar datasets, it was observed that the success metrics were quite close to those of these studies. In future studies, it is aimed to achieve the highest success values by performing different transfer learning studies with more datasets for brain tumor classification.

References

- [1] Louis D.N., Perry A., Reifenberger G., Deimling A.V., Figarella-Branger D., Cavenee W.K., Ohgaki H., Wiestler O.D., Kleihues P., and Ellison D.W., The 2016 World Health Organization classification of tumors of the central nervous system: A summary, *Acta Neuropathol.*, 131 (2016) 803–820.
- [2] De Angelis L.M., Brain tumors, *New England J. Med.*, 344(2): (2001) 114-123. <https://doi.org/10.1056/NEJM200101113440207>.
- [3] Gladson C.L., Prayson R.A., Liu W., The pathobiology of glioma tumors, *Annual Review of Pathology: Mechanisms of Disease*, 5 (2010) 33-50. <https://doi.org/10.1146/annurev-pathol-121808-102109>.
- [4] Mehrotra R., Ansari M.A., Agrawal R., Anand R.S., A Transfer Learning approach for AI-based classification of brain tumors, *Mach. Learn. Appl.*, 2 (2020) 10–19.
- [5] Pereira S., Pinto A., Alves V., and Silva C.A., Brain tumor segmentation using convolutional neural networks in MRI images, *IEEE Trans. Med. Imaging*, 35 (2018) 1240–1251.
- [6] Dundar T.T., Yurtsever I., Pehlivanoglu M.K., Yildiz U., Eker A., Demir M.A., Mutluer A.S., Tektaş R., Kazan M.S., Kitis S., Gokoglu A., Dogan I., Duru N., Machine Learning-Based Surgical Planning for Neurosurgery: Artificial Intelligent Approaches to the Cranium, *Front Surg.*, 9 (2022) 863633. doi: 10.3389/fsurg.2022.863633. PMID: 35574559; PMCID: PMC9099011.
- [7] Hamada A., Br35H Brain Tumor Detection 2020 Dataset, Available online: <https://www.kaggle.com/ahmedhamada0/brain-tumor-detection>.
- [8] Sartaj, "Brain Tumor Classification (MRI) Dataset", Available online: <https://www.kaggle.com/datasets/sartajbhuvaji/brain-tumor-classification-mri>.
- [9] Kushwaha V., Maidamwar P., BTFCNN: Design of a brain tumor classification model using fused convolutional neural networks, 2022 10th International Conference on Emerging Trends in Engineering and Technology-Signal and Information Processing (ICETET-SIP-22), (2022) 1-6, doi: 10.1109/ICETET-SIP-2254415.2022.9791734.
- [10] Kang J., Ullah Z., and Gwak J., MRI-Based Brain Tumor Classification Using Ensemble of Deep Features and Machine Learning Classifiers, *Sensors (Basel)*, 21(6) (2021) 2222. doi: 10.3390/s21062222.
- [11] Amran G.A., Alsharam M.S., Blajam A.O.A., Hasan A.A., Alfaifi M.Y., Amran M.H., Gumaei A., Eldin S.M., Brain Tumor Classification and Detection Using Hybrid Deep Tumor Network, *Electronics*, 11(21) (2022) 3457. <https://doi.org/10.3390/electronics11213457>.
- [12] Özdem K., Özkaya Ç., Atay Y., Çeltikçi E., Börcek A., Demirezen U., and Sağiroğlu Ş., A GA-Based CNN Model for Brain Tumor Classification, 2022 7th International Conference on Computer Science and Engineering (UBMK), (2022) 418-423, doi: 10.1109/UBMK55850.2022.9919461
- [13] Papageorgiou V., Brain Tumor Detection Based on Features Extracted and Classified Using a Low-Complexity Neural Network", *Traitement du Signal.*, 38 (2021) 547-554. doi:10.18280/ts.380302.
- [14] Sert E., Özyurt F., and Doğantekin A., A new approach for brain tumor diagnosis system: Single image super resolution based maximum fuzzy entropy segmentation and convolutional neural network, *Medical Hypotheses*, 133 (2019) 109413.
- [15] Özyurt F., Sert E., Avci E., and Doğantekin E., Brain tumor detection on Convolutional Neural Networks with neutrosophic expert maximum fuzzy sure entropy, *Measurement*, 147 (2019) 106830. <https://doi.org/10.1016/j.measurement.2019.07.058>.
- [16] Sajja V.R., and Kalluri H.K., Classification of brain tumors using convolutional neural networks over various SVM methods, *Ingénierie des Systèmes d'Information*, 25(4): (2020) 489-495. <https://doi.org/10.18280/isi.250412>
- [17] Mittal A., Kumar D., AiCNNs (artificially-integrated convolutional neural networks) for brain tumor prediction, *EAI Endorse Transactions on Pervasive Health and Technology*, 5 (2019) 1-18. <http://doi.org/10.4108/eai.12-2-2019.161976>.

- [18] Sultan H.H., Salem N.M., Al-Atabany W., Multi-classification on brain tumor images using deep neural network, IEEE Access, 7 (2019) 69215-69225.
- [19] Ari A., Alcin O.F., Hanbay D., Brain MR image classification based on deep features by using extreme learning machines, Biomedical Journal of Scientific and Technical Research, 25: (2020) 19137-19144.
- [20] Zhao L., Jia K., Multiscale CNNs for brain tumor segmentation and diagnosis, Computational and Mathematical Methods in Medicine, (2016) 1-17. <https://doi.org/10.1155/2016/8356294A>.
- [21] Hamada A., Br35H: Brain Tumor Detection, (2020), <https://www.kaggle.com/datasets/ahmedhamada0/brain-tumor-detection>.
- [22] Sartaj, Classify MRI images into four classes, (2020), <https://www.kaggle.com/datasets/sartajbhuvaji/brain-tumor-classification-mri>.
- [23] Szegedy C., Liu W., Jia Y., Sermanet P., Reed S., Anguelov D., Rabinovich A., Going deeper with convolutions, In Proceedings of the IEEE conference on computer vision and pattern recognition, (2015) 1-9.
- [24] Lumini A., Nanni L., Deep learning and transfer learning features for plankton classification, Ecological informatics, 51 (2019) 33-43.
- [25] Dandıl E., Serin Z. Derin, Sınır Ağları Kullanarak Histopatolojik Görüntülerde Meme Kanseri Tespiti. Avrupa Bilim ve Teknoloji Dergisi, (2020) 451-463.



Fast And High Preciously Estimator Design With Differential Evolution Algorithm For Shaking Table

Serdar Koçkanat^{1,a}

¹Department of Electrical and Electronics Engineering, Cumhuriyet University, 58140, Sivas, Türkiye

^aCorresponding author

Research Article

History

Received: 14/07/2023

Accepted: 24/07/2023

Copyright



This work is licensed under
Creative Commons Attribution 4.0
International License

ABSTRACT

The shaking table is an experimental system in which the behavior of buildings and vehicles against ground shocks can be examined. A shaking table consists of electrical, mechanical and hydraulic parts to provide the desired technical specifications. In particular, harmonics are inevitable in the nonlinear shaking table system designed by these aforementioned parts. Harmonic is an undesirable disturbing signal that reduces the control performance of a system and distorts the output signal obtained from the system. Therefore, the identification and elimination of harmonics is an important design problem. In this paper, an acceleration harmonic estimator based differential evolution algorithm has been designed to determine the harmonics that occur especially in sinusoidal vibration tests. The proposed estimation approach was analyzed with both simulation and real-time harmonic signals including six harmonics. In addition, the amplitude and phase estimation results were compared with the results obtained by the simulated annealing algorithm. In short, fast and high preciously estimator design was realized by using differential evolution algorithm and its advantages were demonstrated with the obtained estimation results in literature.

Keywords: estimation; acceleration harmonics; shaking table; differential evolution; optimization.

skockanat@cumhuriyet.edu.tr

<https://orcid.org/0000-0001-6415-0241>

How to Cite: Koçkanat S. (2023) Fast And High Preciously Estimator Design With Differential Evolution Algorithm For Shaking Table, Journal of Engineering Faculty 1(1): 17-29

Introduction

In earthquake and civil engineering, the experimental system, in which the performance analyzes of structures and vehicles in low, medium and high intensity shocks can be examined and simulated, is called a shaking table [1]. In addition, the shaking table can be used successfully to simulate earthquakes that have occurred or are expected to occur.

The shaking tables can be designed up to 3 axes to simulate the desired or previously occurred earthquake motions. Also, shaking table designs including electrical, mechanical and hydraulic components have been developed. Thus, shaking tables can be produced to efficiently work at the desired load, precision and speed and they can also be used for different aims such as small scale structural mechanics, earthquake, ground and geological engineering experiments [2].

The electrical, mechanical and hydraulic components used in the design of the shaking table form a nonlinear control system and due to the aforementioned nonlinear factor, unwanted harmonics were especially shown in sinusoidal vibration tests. Harmonics are disturbing signals that negatively affect both the control performance of the system and the acceleration output signals generated by the system. Therefore, the identification and elimination of these disruptive harmonics arising from the internal components of the shaking table is an important engineering design problem [3, 4]. The key solution of this design problem is crucial for improving the control performance of the system and trustworthiness of the analysis results obtained from the aforementioned experiments [5]. Therefore, the greatest focal point of the design problem is to estimate the

amplitude and phase values of each harmonic with high accuracy and to quickly perform the estimation process. As a result, the fast execution time and high accuracy in harmonic estimation will positively affect the control performance of the system and the reliability of the experimental analysis results.

In recent years, optimization algorithms have rapidly gained importance in solving many linear and nonlinear, one-dimensional or multi-dimensional, discrete or continuous engineering problems. Especially, suggested approaches based optimization algorithms provide fast computation and high accuracy for the estimation of amplitude and phase values of harmonics occurring in complex and nonlinear systems such as electrical power systems and shaking table. So, they have come to the fore with the aforementioned advantages. The well-known basic optimization algorithms such as least mean square (LMS), normalized LMS and recursive least square (RLS) algorithms have been used for acceleration harmonic estimation problems of the shaking table system [6-8]. However, when the harmonic order increases and the problem becomes nonlinear and more difficult, a deterioration in the estimation performance is observed. Also, the relative error in the phase estimation increases and the estimation speed slows down. In order to overcome the disadvantages of the aforementioned classical approaches and to obtain better estimation results, new estimation approaches have been proposed using metaheuristic algorithms that have better convergence rate in solution space and are more robustness in the solutions of nonlinear problems.

Particle swarm optimization (PSO) algorithm has been successfully applied for the harmonic estimation in power systems and PWM inverter systems [9, 10]. Therefore, an acceleration harmonic estimation approach based PSO algorithm has been proposed and better results have been obtained compared to the method reported in literature [11]. In addition, both the estimation and convergence performances of the PSO algorithm were compared with those of the LMS algorithm. A new approach for acceleration harmonic estimation was proposed using water cycle algorithm (WCA), and the performance criteria of the real-time calculation, convergence rate and estimation accuracy were analyzed [12]. Also, in order to improve the estimation results of the previously reported PSO algorithm, two suggested approaches based bat algorithm (BA) and artificial bee colony (ABC) algorithm have been applied for acceleration harmonic estimation problem and the results have been compared. Thus, the estimation results obtained in the literature have been improved [13, 14]. An approach based ABC algorithm has been proposed to solve the high-order acceleration harmonic estimation problem and the effect of increasing nonlinearity on estimation performance has been investigated [15]. The RLS method and the simulated annealing (SA) algorithm were used for the acceleration harmonic estimation approach and compared in practice [8]. The harmonic estimation accuracy and real-time convergence rate of the SA

algorithm against the RLS algorithm were evaluated. Metaheuristic algorithm versus classical algorithm has been analyzed using performance criteria in multidimensional and nonlinear estimation problem.

From the discussions mentioned above, it is seen that the problem of acceleration harmonic estimation is an important design problem in electrical, mechanical or hydraulic systems and the estimation and elimination of harmonics have positive effects on the shaking table systems. Therefore, it is important to develop fast and accurate harmonic estimation approaches. In this study, to the best of our knowledge, differential evolution (DE) algorithm, that has fast convergence rate and powerful search ability, was used and analyzed for the first time ever in the acceleration harmonic estimation approach. It is also an important advantage that the proposed approach does not require any prior knowledge as with Kalman filters. For estimating the amplitude and phase values of the acceleration harmonics occurring in the shaking table system, the suggested approach based DE algorithm was examined for a literature test signal and an experimental signal with 6 harmonics. In both simulation and experimental study, the estimated amplitude and phase values were compared with the estimation approach based on the latest reported SA algorithm. Calculation time, convergence rate and estimation accuracy were selected as two important criteria in the simulation and experimental analyzes and the approaches were evaluated using these criteria for a fair comparison. As a result, the proposed approach based DE algorithm has shown a very accurate and rapid amplitude and phase estimation performance for both simulation and experimental acceleration harmonic signals.

Servo Electro-Mechanical Shaking Table

In Figure. 1, the servo electro-mechanical shaking table is shown. It is a single-axis shaking table and its size is 50x50 cm. This portable shaking table is often preferred in many university research laboratories or company research offices, because it has the ability to simulate recorded earthquakes and to apply defined waves such as sine, cosine and triangle signals and any acceleration or position profile defined by the user. The aforementioned system has a servo motor, closed loop PID controller, analog to digital converter, accelerometer sensors and a mechanical platform where vibration occurs. In addition, this system is a servo electro-mechanical shaking table with a weight of 45 kg, 1000 N power, 500 mm/s speed and operating frequency up to 20 Hz.

In this study, the performance of the proposed approach based DE algorithm is analyzed for acceleration harmonic estimation problem in servo electro-mechanical shaking table. The analyzes were carried out in two stages. At the first stage, the preferred simulation signal with 5 Hz fundamental frequency in the literature was used. And, at the second stage, the experimental signal with 3 Hz fundamental frequency was produced using the servo electro-mechanical vibration table in Figure. 1.



Figure. 1. Servo Electro-Mechanical Shaking Table

Differential Evolution

Differential evolution (DE) algorithm is a metaheuristic algorithm which is accepted in the class of population-based and evolutionary algorithms. Its mechanisms are mutation, crossover and selection and they are very similar to genetic algorithm (GA). The DE algorithm is a powerful population-based algorithm developed by Storn and Price between 1996 and 1997 [16].

In the DE algorithm, crossover, mutation and selection operators are used as in GA algorithm. In addition, the DE algorithm uses a mutation operator based on the difference of randomly selected solutions, while applying each operator to the whole population respectively in order to obtain better solutions. Through mutation and crossover processes, new individuals are formed by selecting three randomly selected chromosomes individually. By comparing the suitability values of the new chromosome obtained with the existing chromosome, the individual with the better fit is transferred to the next population as the new individual. Thus, the selection operator is also used. The quality of each solution is measured by the fitness value obtained by replacing it in the objective function. The basic steps of the DE algorithm are given as follows.

Step 1: Producing the initial population according to the objective problem.

Step 2: Evaluation of randomly generated population and determination of fitness values.

Step 3: repeat

Step 4: Mutation

Step 5: Crossover (Recombination)

Step 6: Evaluation the population

Step 7: Selection

Step 8: until (cycle = maximum number of cycles)

The basic control parameters of the DE algorithm can be expressed as population size (NP), scaling factor (F), crossover ratio (CR) and maximum number of cycles. The basic flowchart of differential evolution algorithm is shown in Figure. 2.

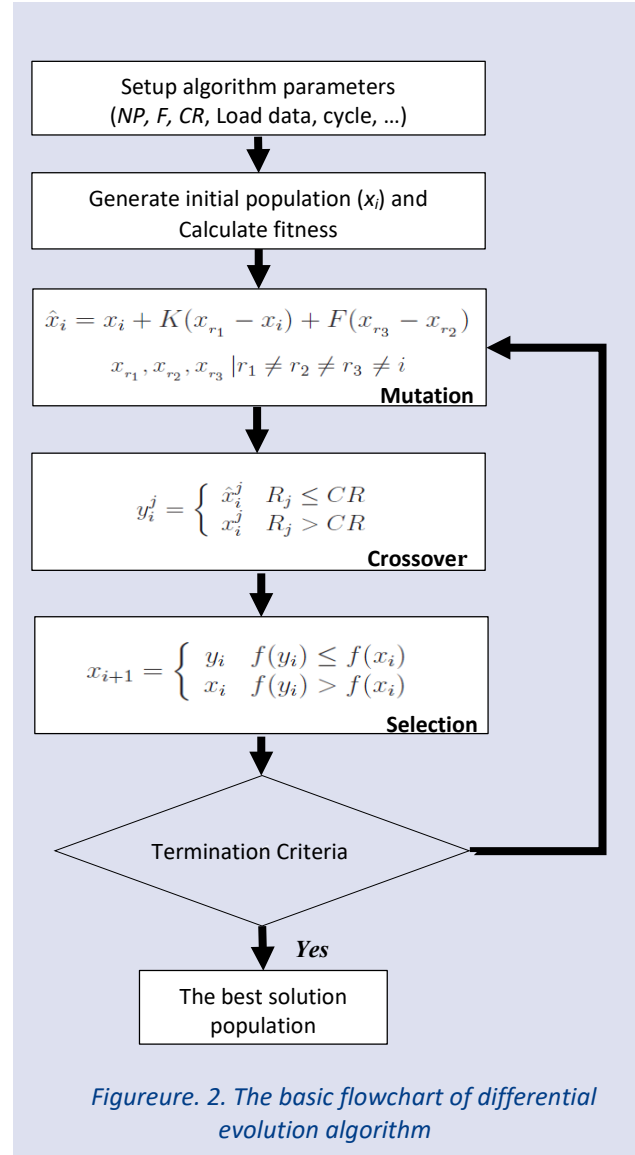


Figure. 2. The basic flowchart of differential evolution algorithm

Acceleration Harmonic Estimation Problem

In shaking table design problem, an acceleration harmonic signal can be modeled as the sum of the higher degree harmonics of the unknown amplitude and phase values and it is shown as

$$a(t) = \sum_{n=1}^N A_n \sin(2n\pi f_0 t + \varphi_n) \quad (1)$$

where f_0 is the fundamental frequency, A_n and φ_n are the unknown magnitude and phase values of the n th harmonic. N represents harmonic order and $\omega_n = n2\pi f_0$ is the angular frequency of the n th component. Then, acceleration harmonic signal is sampled with the desired sampling period T_s . $a(t)$ continuous signal is transformed to the $a(k)$ discrete harmonic signal and it can be expressed as

$$a(k) = \sum_{n=1}^N A_n \sin(\omega_n k T_s + \varphi_n) \quad (2)$$

Here, discrete harmonic signal $a(k)$ can be modeled using sine and cosine functions and it can be rewritten as

$$a(k) = \sum_{n=1}^N [A_n \sin(\omega_n k T_s) \cos \phi_n + A_n \cos(\omega_n k T_s) \sin \phi_n] \quad (3)$$

Later, $a(k)$ discrete signal in Equation 3 is converted to the parametric form as

$$a(k) = H(k)\theta(k) \quad (4)$$

where $H(k)$ is given as

$$H(k) = [\sin(\omega_1 k T_s) \cos(\omega_1 k T_s) \dots \sin(\omega_N k T_s) \cos(\omega_N k T_s)]^T \quad (5)$$

Also, the vectors of unknown parameters is presented as

$$\theta(k) = [A_1 \cos \phi_1 \ A_1 \sin \phi_1 \dots A_N \cos \phi_N \ A_N \sin \phi_N]^T \quad (6)$$

Using estimation vector in Equation 6, A_n and ϕ_n of the nth harmonic can be calculated.

An objective function in optimization is an important part of minimization or maximization operation and it is employed for optimizing the weight vector of the problem. In the acceleration harmonic estimation problem, the objective function is modeled as the mean square error between a_k and $\hat{a}_{k_{estimated}}$ signals and expressed as

$$J = \min \left(\sum_{k=1}^K e^2(k) \right) = MSE(a_k - \hat{a}_{k_{estimated}}) \quad (7)$$

where, a_k is the simulation or experimental harmonic signal and $\hat{a}_{k_{estimated}}$ represents the estimated harmonic signal by the proposed approach based DE algorithm. Also, k is the sample number. In Figure. 3, the flowchart of suggested approach based DE algorithm for acceleration harmonic estimation is represented.

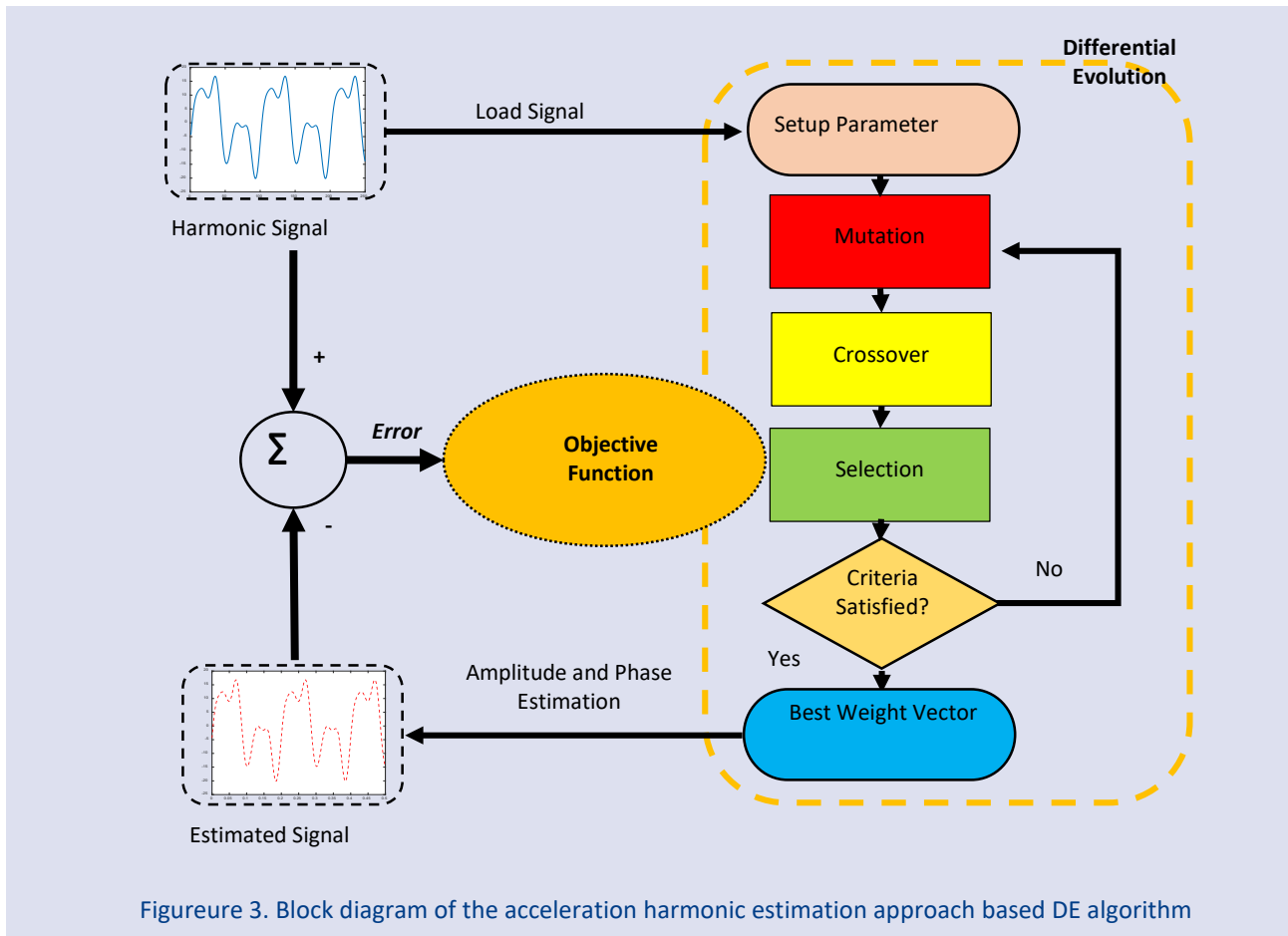


Figure 3. Block diagram of the acceleration harmonic estimation approach based DE algorithm

The block diagram of the acceleration harmonic estimation approach based DE algorithm can be illustrated with Figure. 3. Harmonic signal represents the sinusoidal acceleration output in shaking table system and estimated signal is generated by the estimated amplitude and phase values. The difference between harmonic signal and estimated signal is error signal and it is used to drive objective function for error minimization. In the flowchart, firstly, the initial setup parameters are

determined and harmonic signal is loaded. Then, initial population is passed through mutation, crossover and selection mechanism. Each candidate solution is evaluated and calculated fitness value using objective function driven by error signal. At the end, the best weight vector is achieved and memorized. Amplitude and phase estimation is realized and estimated signal is produced. So, the estimation steps are successfully completed.

Simulation and Results

Firstly, at the simulation step, a simulation harmonic signal including six harmonics are generated according to the estimation approaches in literature [8]. The simulation harmonic signal is given as

$$a(t) = 10\sin(10\pi t) + 8\sin(20\pi t - 1.2) + 6\sin(30\pi t + 0.55) + 4\sin(40\pi t - 0.8) + 2\sin(50\pi t + 1.4) + 1\sin(60\pi t + 1) \quad (8)$$

The simulation signal contains 6 harmonics and the fundamental signal is at 5 Hz. The frequencies of other harmonics are at 10, 15, 20, 25 and 30 Hz, respectively.

For the DE algorithm, population size (*NP*), scaling factor (*F*), crossover ratio (*CR*) and cycle number were experimentally determined as 24, 0.5, 0.8 and 250, respectively. Also, for achieving the best solution, the strategy is selected as DE/rand/1/bin from all strategies. For a fair and accurate assessment, DE algorithm was run 30 times with different initial seeds and the mean values of these multiple runs were evaluated and compared.

After determining the setup parameters, the simulation signal is applied to the suggested approach based DE algorithm for the amplitude and phase estimation. At the end of the calculation process, estimated amplitude and phase values using DE algorithm are listed in Table 1 for 6 harmonics. The harmonic estimation results obtained by DE algorithm are very close to the actual values and the relative errors are very small compared with those of the SA algorithm. When the reported harmonic estimation results taken into account, it is concluded that proposed approach based DE algorithm is a high preciously estimator design for acceleration harmonic estimation in shaking table system. Also, it has superior performance than that of the SA algorithm.

In Figure. 4, harmonic estimation period is observed and the overlap between the actual simulation signal suggested in literature and estimated signal by DE algorithm is analyzed. In the initial estimation, the fluctuation decreases within 0.05 seconds and the actual and estimation signals overlap in complete agreement. After 0.1 seconds, a perfect agreement between two signals is occurred.

Table 1. Harmonic estimation results of SA and DE algorithms

Algorithms	Parameters	Harmonics Degree					
		Fund.	Second	Third	Fourth	Fifth	Sixth
Actual	Frequency (Hz)	5	10	15	20	25	30
	Amplitude (m/s ²)	10	8	6	4	2	1
	Phase (radian)	0	-1.2	0.55	-0.8	1.4	1
SA Algorithm [8]	Amplitude (m/s ²)	9.9998	8.0004	5.9999	4.0007	1.9993	0.9998
	Error (%)	0.0018	0.0052	0.0025	0.0172	0.0358	0.0224
	Phase (radian)	-0.0000	-1.2000	0.5500	-0.7998	1.4000	0.9997
	Error (%)	0.0000	0.0008	0.0064	0.0238	0.0002	0.0272
DE Algorithm	Amplitude (m/s ²)	10.0000	8.0000	6.0000	4.0000	2.0000	1.0000
	Error (%)	0.0004	0.0001	0.0002	0.0000	0.0001	0.0012
	Phase (radian)	0.0000	-1.2000	0.5500	-0.8000	1.4000	1.0000
	Error (%)	0.0000	0.0000	0.0004	0.0000	0.0001	0.0008

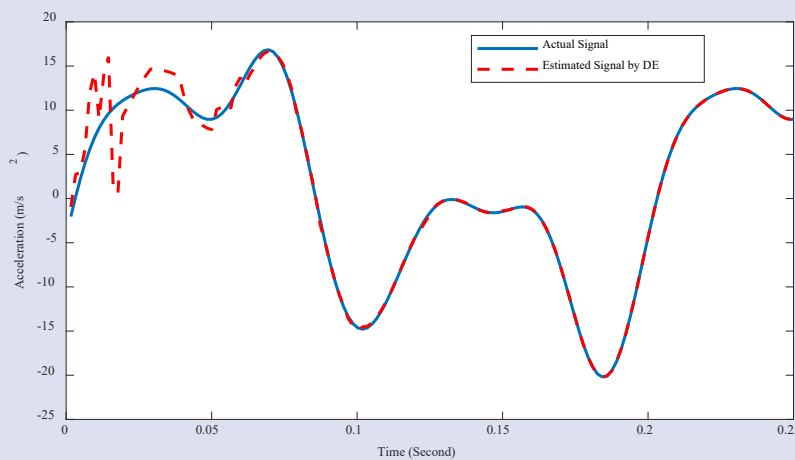


Figure 4. Actual signal and estimated signal by DE algorithm

In Figure. 5 and 6, the estimated amplitudes and phases by applying DE algorithm are shown in detail. For each harmonic, amplitude-time and phase-time curves are drawn. In the initial estimation interval for both amplitude and phase, random fluctuations can be observed. As mentioned above, the randomly generated weight vector causes this change. But, after about 0.1 seconds, the estimated amplitude and phase values of each harmonic converge to the predefined actual values. The convergence time is very small compared with that of the SA algorithm, because SA algorithm completes the optimization within about 0.4 seconds.

In Figure. 7, for each harmonic, generated waveform by generating estimated amplitude and phase values is shown. From this Figureure, it is shown that acceleration harmonic estimation problem in shaking table system is solved and computed with 0.1 seconds using proposed approach based DE algorithm.

When the reported harmonic estimation results in simulation taken into account, it is obvious that fast and high preciously estimator design with differential evolution algorithm is realized and efficiently applied at the simulation stage.

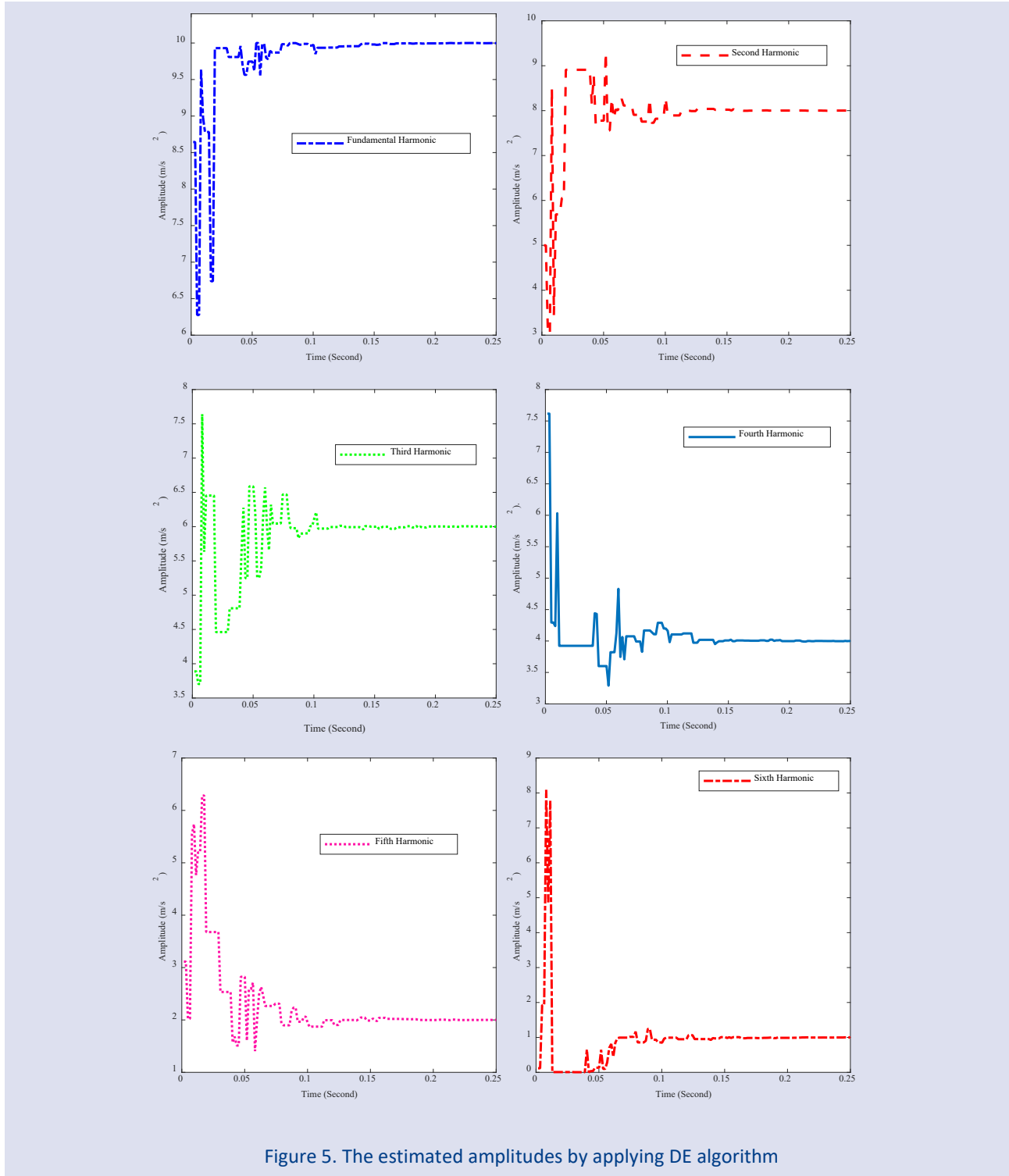


Figure 5. The estimated amplitudes by applying DE algorithm

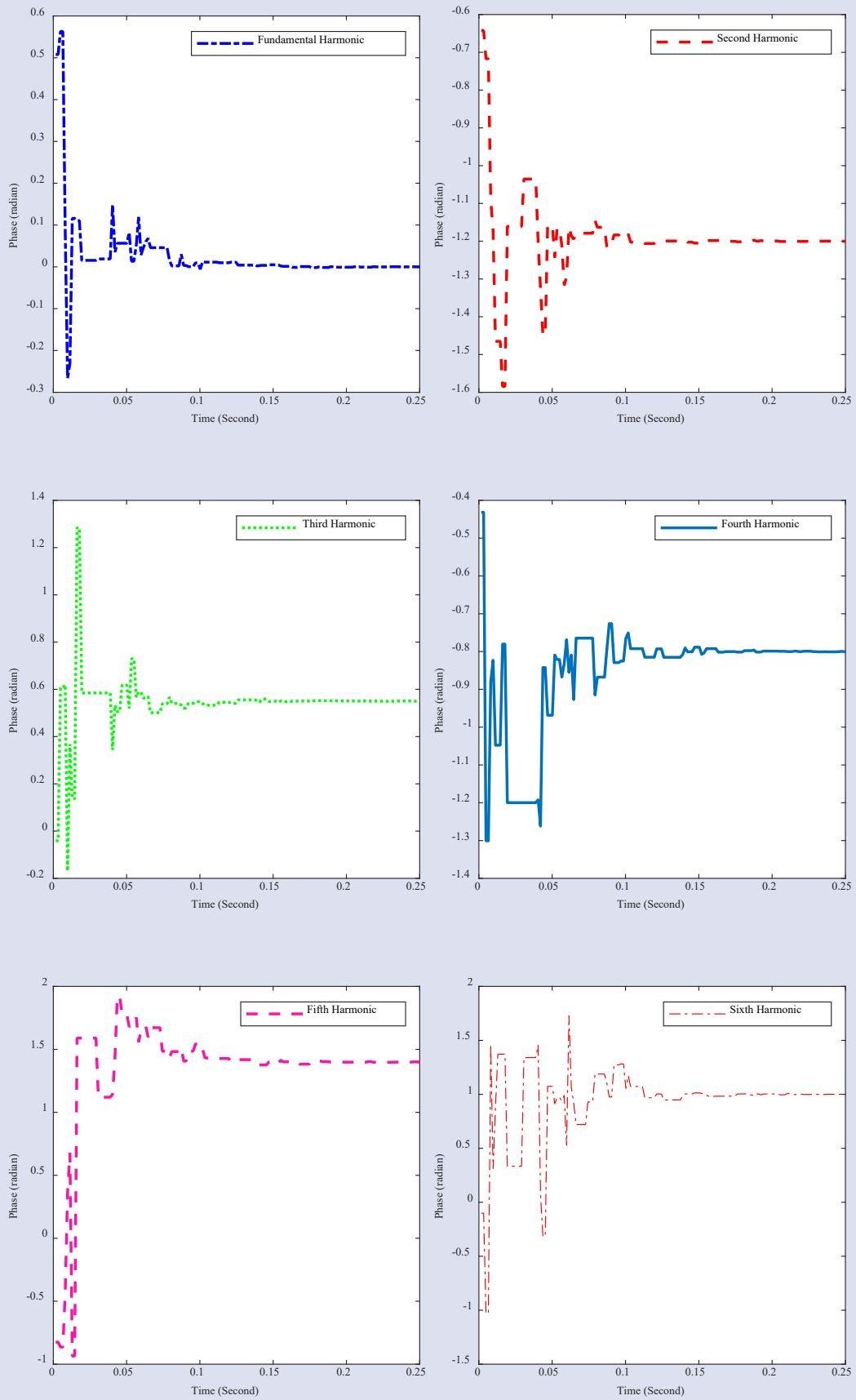


Figure 6. The estimated phases by applying DE algorithm

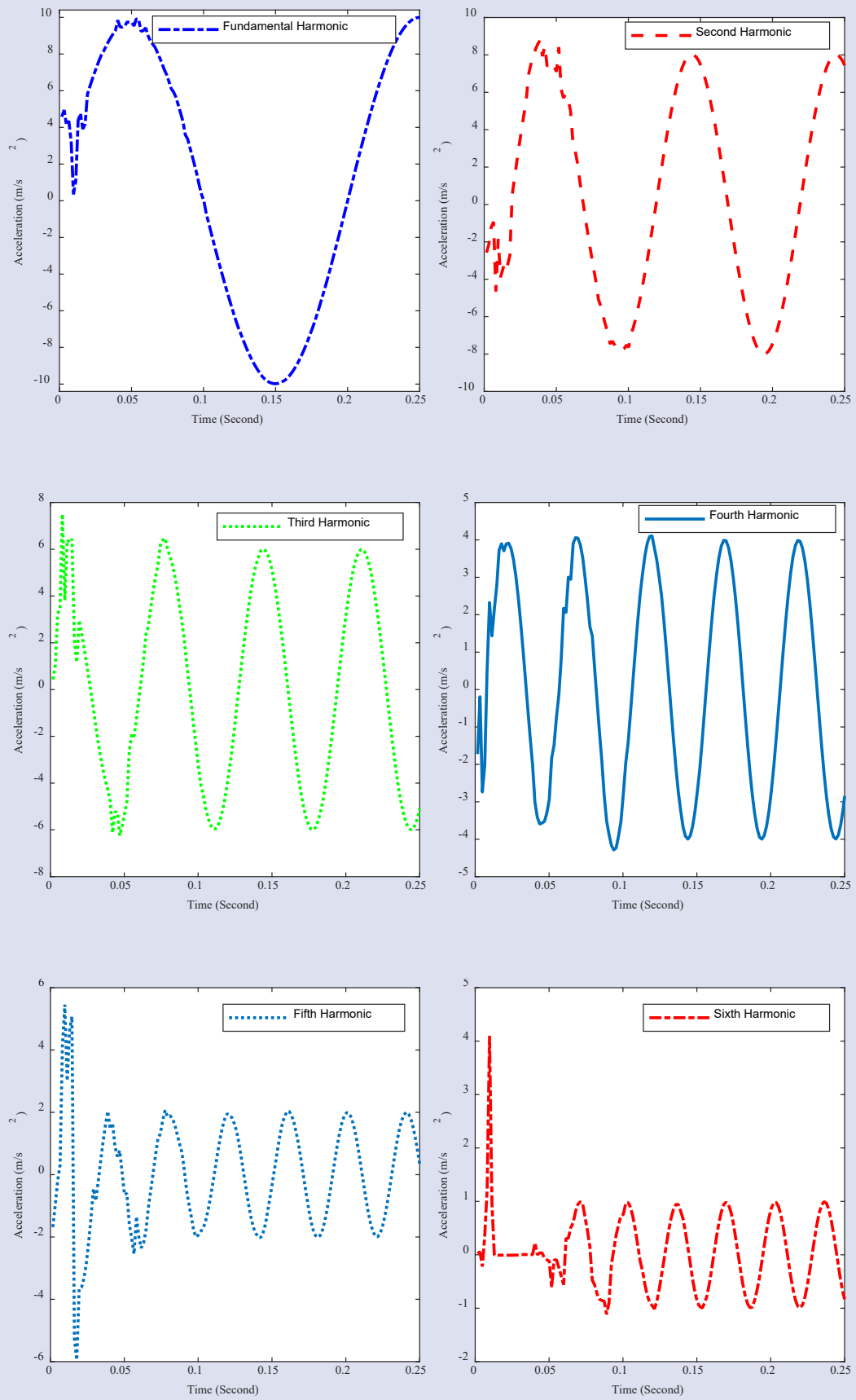


Figure 7. Harmonic waveforms by generating estimated amplitude and phase values

Experiment and Results (3 Hz)

Secondly, at the experimental stage, an experimental harmonic signal is obtained from the servo electro-mechanical shaking table in real-time. The experimental signal contains 6 harmonics and the fundamental signal is at 3 Hz. The frequencies of other harmonics are at 6, 9, 12, 15 and 18 Hz, respectively. The setup parameters are selected as previous section.

In real-time application, proposed approach based DE algorithm is operated after the third seconds, because real-time data acquisition and experiment begin at this start time. Also, above aforementioned optimization steps have been realized.

In Figure. 8, the actual experimental signal and estimated signal by DE algorithm are shown. The tracking ability of the proposed approach depends on the fast and accurate estimated amplitude and phase values and it is quite satisfactory. Because, after 3.1 seconds, the agreement between two harmonic signal is growing at perfect level. The best fit is achieved within 3.2 seconds. Also, at the end of real-time estimation, the obtained results using proposed approach based DE algorithm is tabulated in Table 2. When the Figure. 8 and Table 2 taken into account, it is concluded that the high precisely estimator design computes successively the amplitude

and phase values of harmonics in simulation and experimental applications.

The estimated amplitudes and phases by applying DE algorithm are given in Figure. 9 and 10 for real-time application. As can be seen from the Figureures, fluctuations continue in amplitude and phase estimation, though the estimated amplitude and phase values of each harmonic converge to their stable values. After about 3.2 seconds, amplitude estimation process is exactly completed for each harmonic. But, phase estimation process of the 2nd, 4th and 6th harmonics is finished after about 3.4 seconds.

In Figure. 11, waveforms of all harmonics by generating estimated amplitude and phase values is presented. For real-time acceleration harmonic estimation, proposed approach based DE algorithm solves the desired results within 0.2 seconds.

To sum up, when the estimated amplitude and phase values, generated waveforms of all harmonics, and convergence times in simulation and experimental conditions taken into account, it is evident that the proposed estimator design not only has the fast and preciously solution ability, but also it is suitable for real-time application. Also, the proposed design show better estimation performance than those of the SA and RLS algorithm.

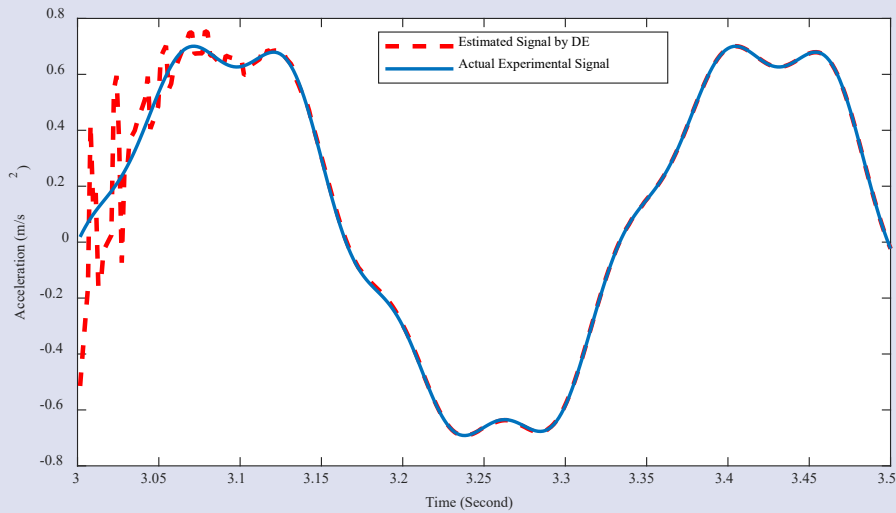


Figure 8. Actual experimental signal and estimated signal by DE algorithm

Table 2. Harmonic estimation results of DE algorithm

Harmonic Degree	Amplitude (m/s ²)	Phase (radian)
Fundamental	-0.7185	3.0242
Second	-0.0033	1.0666
Third	-0.0381	-2.5075
Fourth	0.0076	-2.4615
Fifth	0.0745	1.8149
Sixth	-0.0044	1.5760

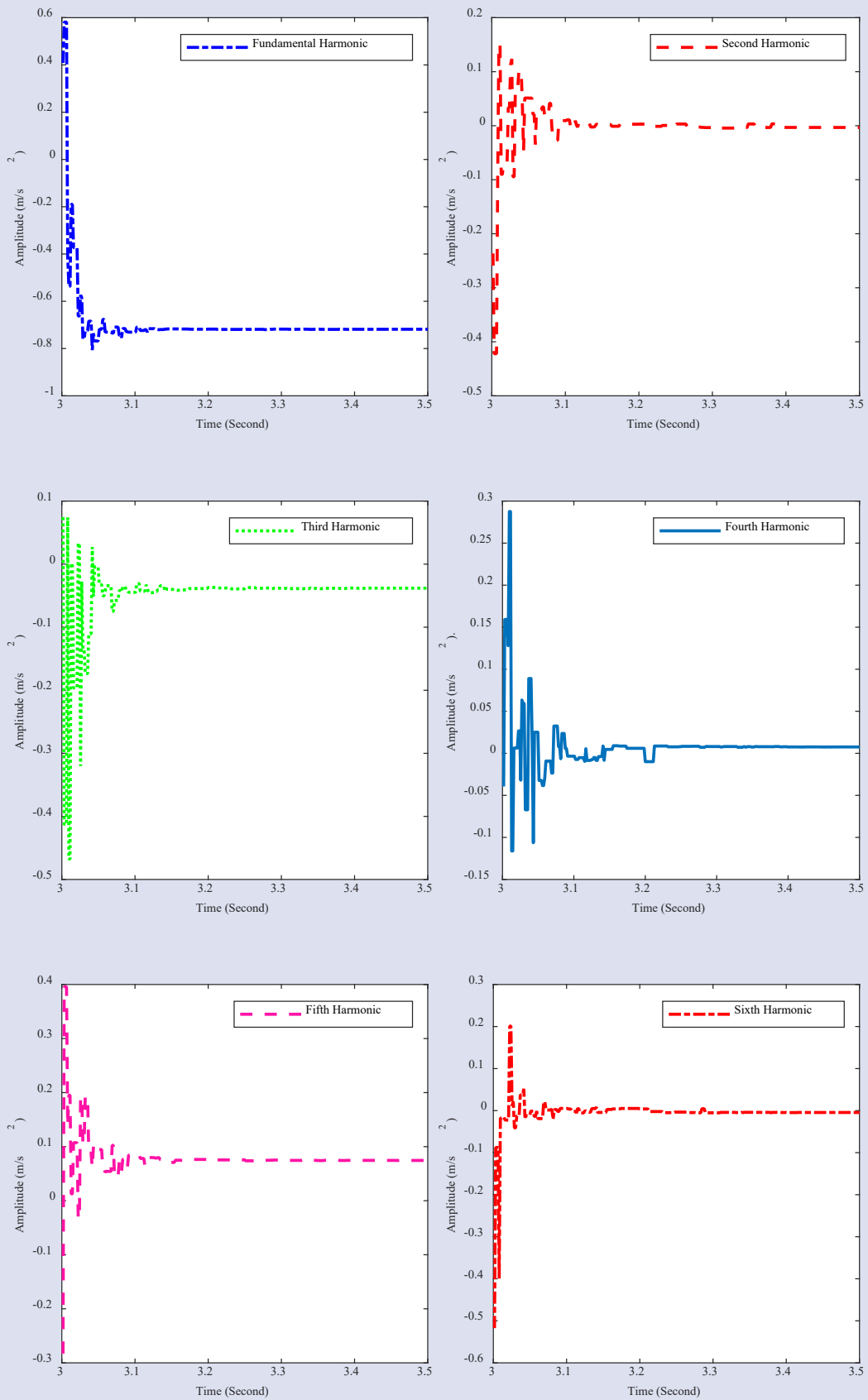


Figure 9. The estimated amplitudes by applying DE algorithm

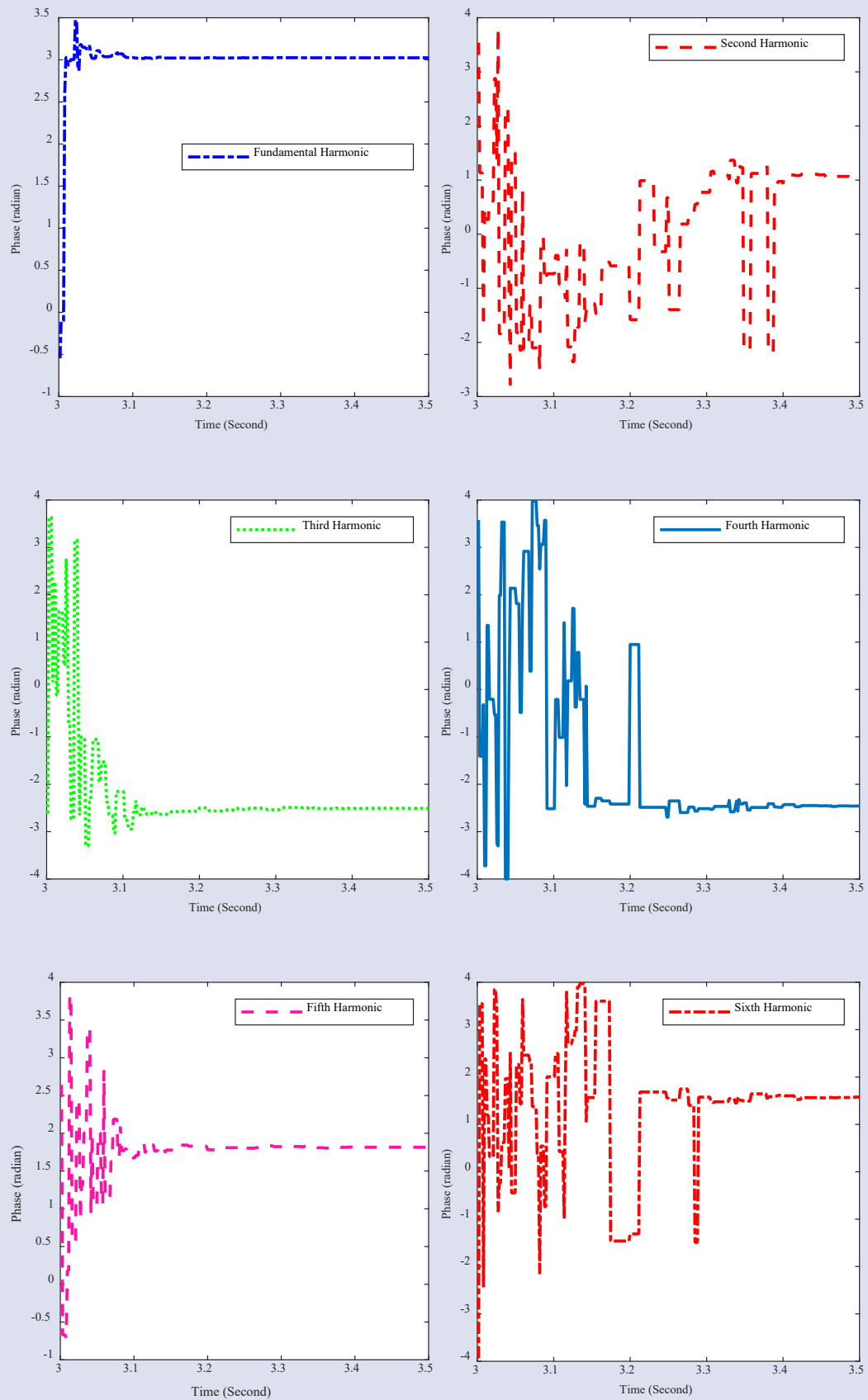


Figure 10. The estimated phases by applying DE algorithm

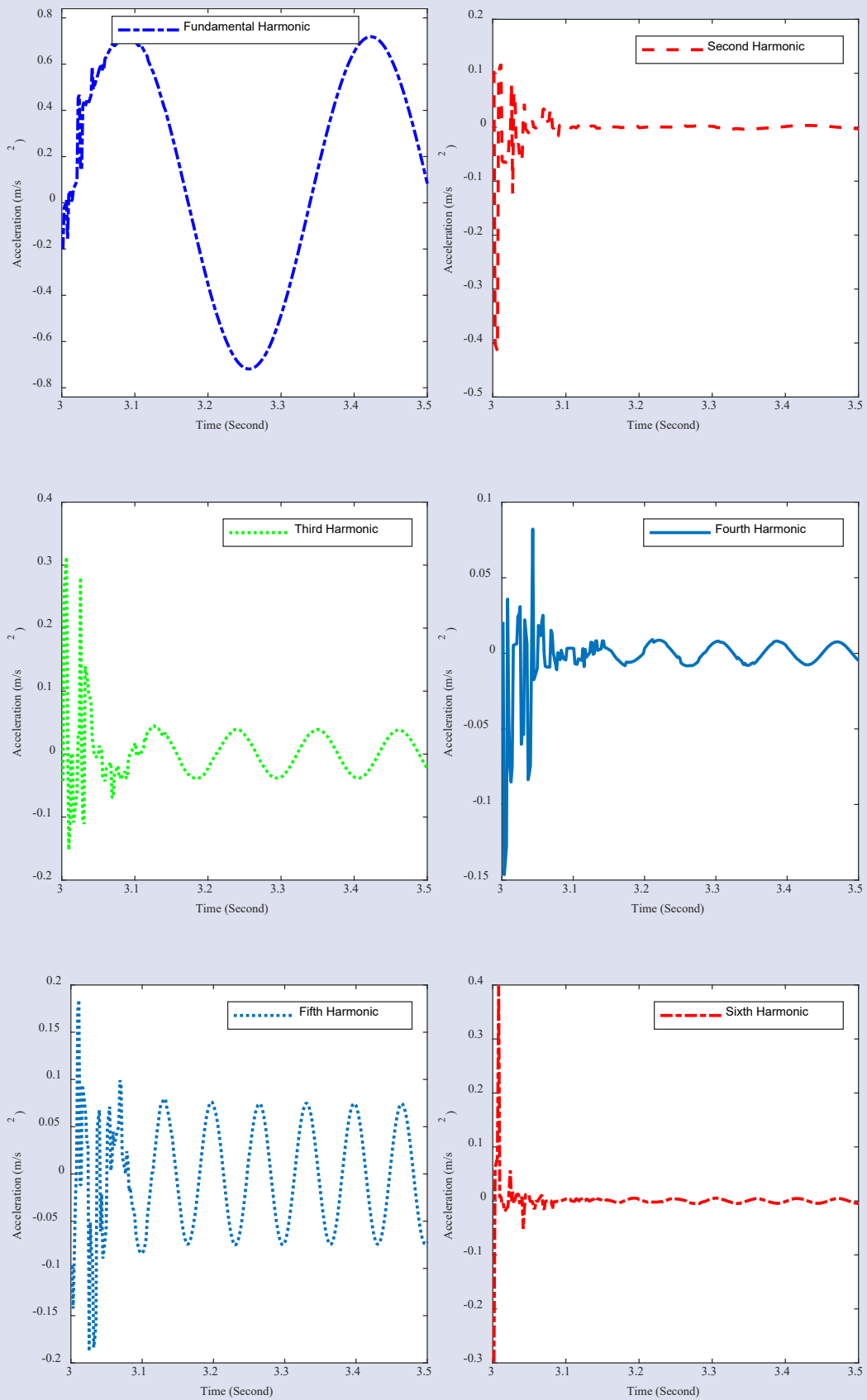


Figure 11. Harmonic waveforms by generating estimated amplitude and phase values

Conclusions

In this study, fast and high precisely harmonic estimator design with differential evolution algorithm is developed and coded. In particular, a key solution has been proposed for the determination of harmonics in the shaking table system. Unlike many solutions using optimization algorithms, the harmonic estimator design has been analyzed for both simulation and experimental cases. At the simulation stage, a simulation signal with 6 harmonics was used. The fundamental frequency is 5 Hertz. With the proposed harmonic estimator, amplitude and phase values of each harmonic in the simulation signal are estimated. All estimation results obtained by DE algorithm are shown in Table 1. The best relative error in amplitude estimation was 0.0000, while the worst relative error was 0.0012. In the phase estimation, the best relative error value was 0.0000, while the worst relative error value was 0.0008. In addition, the estimation process was completed within 0.1 seconds. When the estimation results, graphics and convergence time are taken into account, a more successful harmonic estimation was performed compared with the SA algorithm. At the experimental stage, a real-time harmonic signal with a fundamental frequency of 3 Hertz was used. Up to 6 harmonics were estimated for the experimental signal and it was obtained from servo electro-mechanical shaking table system. The estimated amplitude and phase values are given in Table 2. Relative error values could not be calculated because the actual amplitude and phase values were not known. However, the amplitude and phase estimation figures of each harmonic show that the designed harmonics estimator works successfully. In addition, the estimation process was completed in 0.2 seconds. To sum up, when the reported harmonic estimation results, figures and convergence rate in simulation and experimental conditions taken into account, it is concluded that fast and high precisely estimator design with differential evolution algorithm is efficiently realized and its performance is better than that of the SA algorithm.

References

- [1] Ji X., Kajiwara K., Nagae T., Enokida R., Nakashima M., A substructure shaking table test for reproduction of earthquake responses of high-rise buildings, *Earthquake Engineering and Structural Dynamics*, 38 (12) (2009) 1381-1399.
- [2] Shen W., Wang J.Z., Wang S.K., The control of the electro-hydraulic shaking table based on dynamic surface adaptive robust control, *Transactions of the Institute of Measurement and Control*, 39(8) (2017) 1271-1280.
- [3] Yao J., Yan H., Xiao R., Di D., Jiang G., Gao S., Yu H., Sinusoidal acceleration harmonic estimation using the extended Kalman filter for an electro-hydraulic servo shaking table, *Journal of Vibration and Control*, 21(8) (2015) 1566-1579.
- [4] Yao J.J., Hu S.H., Fu W., Han J.W., Impact of excitation signal upon the acceleration harmonic distortion of an electro-hydraulic shaking table, *Journal of Vibration and Control*, 17(7) (2011) 1106-1111.
- [5] Yao J., Acceleration Harmonic Cancellation of Electro-hydraulic Servo Shaking Table, *Chinese Journal of Mechanical Engineering*, 46(3) (2010).
- [6] Yao J., Jiang G., Di D., Liu S., Acceleration harmonic identification for an electro-hydraulic servo shaking table based on the normalized least-mean-square adaptive algorithm, *Journal of Vibration and Control*, 19(1) (2013) 47-55.
- [7] Yao J., Hu. S, Fu. W, et al., Harmonic cancellation for electro-hydraulic servo shaking table based on LMS adaptive algorithm, *Journal of Vibration and Control*, 17(12) (2011) 1862-1868.
- [8] Yao J., Wan Z., Fu Y., Acceleration Harmonic Estimation for Hydraulic Servo Shaking Table by Using Simulated Annealing Algorithm, *Applied Sciences*, 8(4) (2018) 524.
- [9] Lu Z., Ji T.Y., Tang W.H., et al., Optimal Harmonic Estimation Using A Particle Swarm Optimizer, *IEEE Transactions on Power Delivery*, 23 (2) (2008) 1166-1174.
- [10] Ray R.N., Chatterjee D., Goswami S.K., An application of PSO technique for harmonic elimination in a PWM inverter, *Applied Soft Computing*, 9(4) (2009) 1315-1320.
- [11] Yao J., Yu H., Dietz M., Xiao R., Chen S., Wang T., Niu Q. Acceleration harmonic estimation for a hydraulic shaking table by using particle swarm optimization, *Transactions of the Institute of Measurement and Control*, 39(5) (2017) 738-747.
- [12] Yao J., Wan Z., Fu Y., Acceleration Harmonic Estimation in a Hydraulic Shaking Table Using Water Cycle Algorithm, *J Shock and Vibration*, (2018) 12.
- [13] Koçkanat S., Acceleration Harmonic Estimation for Hydraulic Shaking Table Using Bat Algorithm, *European Journal of Science and Technology*, 15 (2019) 387-393.
- [14] Koçkanat S., Acceleration Harmonic Estimation using an Approach based Artificial Bee Colony Algorithm: A Hydraulic Shaking Table Application, 2019 27th Signal Processing and Communications Applications Conference (SIU), (2019) 1-4.
- [15] Yao J., Wan Z., Fu Y., et al., An Artificial Bee Colony Algorithm for Solving Hydraulic Shaking Table Acceleration Harmonic Estimation Problem, *ASME 2018 Noise Control and Acoustics Division Conference*, (2018) 1-5.
- [16] Storn R., Price K., Differential Evolution – A Simple and Efficient Heuristic for global Optimization over Continuous Spaces, *Journal of Global Optimization*, 11 (4) (1997) 341-359.



Investigation of liquefaction behavior of Geyve county of Sakarya province soils with GIS

Ayşe Eda Özdin^{1,a,*}, İsa Vural^{2,b}

¹ Sakarya University of Applied Sciences, Graduate Education Institute, Department of Civil Engineering, Sakarya, Türkiye

² Sakarya University of Applied Sciences, Faculty of Technology, Department of Civil Engineering, Sakarya, Türkiye

*Corresponding author

Research Article

History

Received: 13/07/2023

Accepted: 27/07/2023

Copyright



This work is licensed under
Creative Commons Attribution 4.0
International License

ABSTRACT

The objective of this study is to create a liquefaction map with sample zoning for Sakarya, Geyve. For this purpose, Geyve county was chosen as an example, because it is the largest county of Sakarya in terms of area and also the 3rd largest county in terms of population, and it is possible to have an alluvial soil that carries the risk of liquefaction due to its location near the Sakarya River. Analyses were carried out with the data of 290 drilling points in the ground survey reports obtained from the Geyve Municipality, Directorate of Reconstruction and Urbanization. Liquefaction analyses were made according to the Türkiye Building Earthquake Code 2018 (TBEC). The gathered information is transferred from geographic information system (GIS) mapping to the MapInfo application. Classification of soil in Geyve county, corrected SPTN (SPTN*), water content (W_N), fine grain content (FGC), liquid limit (W_L), plastic limit (W_P), groundwater table (GWT) and soil liquefaction mapping was designed with the transferred data. This study shows that there is no risk of liquefaction in the Geyve county generally but only low risk in some zones.

Keywords: Geyve, GIS, MapInfo, Soil liquefaction map

^a y190007003@subu.edu.tr

^b <https://orcid.org/0009-0003-5591-757X>

^a ivural@subu.edu.tr

^b <https://orcid.org/0000-0003-2370-7597>

How to Cite: Özdin, A.E., Vural, İ. (2023) Investigation of liquefaction behavior of Geyve county of Sakarya province soils with GIS, Journal of Engineering Faculty, 1(1): 30-37

Introduction

The North Anatolian Fault Zone (NAFZ) passing through the Marmara Region is divided into three lines in this area. The 1999 Marmara Earthquake, which occurred in this fault zone, significantly damaged the engineering structures as a result of liquefaction.

In the last 1600 years, there have been earthquakes with a magnitude of 6.8 and more in our country. Also in the last century, there have been 10 earthquakes with a magnitude of 6.0 and more [1].

Liquefaction which damages, especially human life and then the economy, can be interpreted that it occurs on the water-logged, dune, low clay content ground under repetitive tensions like earthquakes in parallel with the effective tension decreases on the ground and acts as if it is liquid [2].

One of the significant arguments from the Adapazarı Ground Charette, organized at Sakarya University is that the main problem is the Sakarya River's uncontrolled streaming and this causes liquefaction in some areas of Sakarya [3].

When all these data are taken into account, in this study Geyve county was chosen as the sample area because it is the biggest county of Sakarya in terms of area, it is located in the south part of the North Anatolian Fault and generates a risk of liquefaction.

Within this study, data in every 1.5 m / 3 m / 4.5 m / 6 m / 7.5 m / 9 m / 12 m depth received from Geyve Municipality, Construction and Urbanization Directorate ground reports of 290 drilling points were transferred to the MapInfo program from the GIS programs. Thematic area grade in every 1.5 m / 3 m / 4.5 m / 6 m / 7.5 m / 9 m / 12 m depth related to drills, corrected SPTN, W_N , FGC, W_L , W_P , GWT and soil liquefaction maps were generated. Examining the liquefaction maps, is aimed at identifying the areas at risk of liquefaction. This liquefaction map, which was created by taking into account the seismicity of Sakarya, will be a guide for the construction areas of the Geyve region and will provide prevention for risky areas.

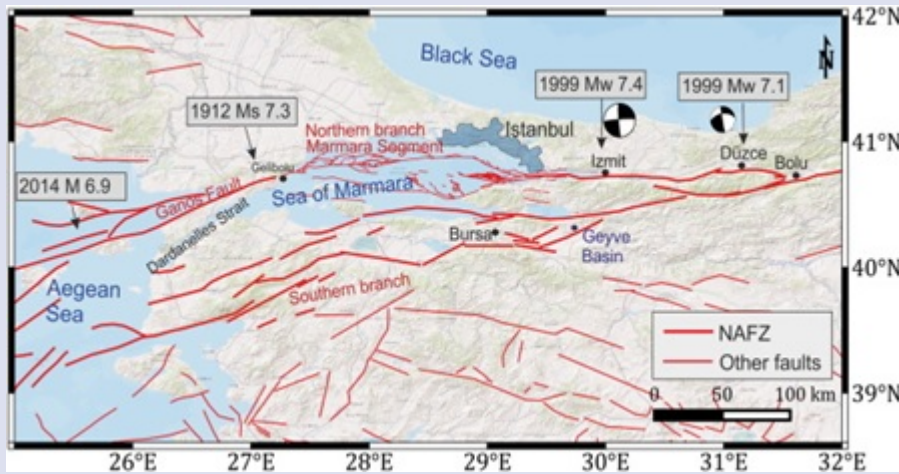


Figure 1. North Anatolian Fault sections [4]

Literature

Erken and his colleagues investigated how sand, silt and clay soils behave under the effect of earthquake-like dynamic loads. As a result of the research, they observed that the bearing capacity of water-saturated sand and low plasticity silt soils was destroyed as a result of liquefaction due to earthquakes, while the bearing capacity of soft plastic silt and clay soils decreased significantly [5].

Karavul and his colleagues, in their study on the compactness of Adapazarı soil, made mappings with the GIS mapping method and observed that the soil of the region where the settlement in the center of Adapazarı is high is mostly composed of materials showing loose compactness. In addition, they stated in their study that the groundwater level in this region varies between 0.5 m-4 m [2].

Bayraktar and his colleague prepared an earthquake scenario by using the Gölcük earthquake intensities map in Sakarya province in their study. In their study, they used the geographic information system (ArcGIS) to map the damages to be caused by the earthquake scenario. They stated that the damage that will occur in the event of a possible earthquake in Sakarya province will be serious, especially in Adapazarı county, and stated that a tent city should be established in all counties of Sakarya province to help the disaster victims after the earthquake in public green areas [6].

Material and Method

As liquefaction, a result of repetitive tensions causes much loss of life and property, there may be large settlements on the ground and this can bring about major property damage. In the geological past, it is common to accumulate alluvion in the river bed and the near abroad. Thus Geyve county located near Sakarya river which obtains the liquefaction potential of alluvial soil was chosen as the field.

Method used the analysis

There are several analysis methods using field studies and laboratory experiments for the liquefaction analysis on grounds with the potential of liquefaction. This study applied liquefaction analysis applying the standard penetration test (SPT) results method explained in TBEC 2018 chapter 16B. This approach, known as Simplified Method, was first discovered by Seed and Idriss (1971) and was later gathered by Youd (2001), taking the final form. It is the approach that is most frequently applied in the literature [7,8].

Equation 1 was used to fix the raw SPT data from the soil study report.

$$N_{1,60} = N * C_N * C_R * C_B * C_S * C_E \quad (1)$$

$N_{1,60}$ = The amount of energy corrected SPT stroke

N = SPT impact value measured on the ground

C_N = Cover load correction parameter

C_E = Energy ration correction parameter

C_B = Drilled well correction parameter

C_R = Rod length correction parameter

C_S = Sampler method correction parameter

The cover load correction parameter (C_N) in Equation 1 is calculated by Equation 2.

$$C_N = 9,78 * \sqrt{\frac{1}{\sigma'_{v0}}} \leq 1.70 \quad (2)$$

The vertical effective stress (σ'_{v0}) in this equation is calculated according to the land conditions when the SPT is taken [9].

Corrected SPT numbers according to the fine grain content ($N_{1,60f}$) are calculated with Equation 3.

$$N_{1,60f} = \alpha + \beta * N_{1,60} \quad (3)$$

Fine grain content correction parameters (α , β) are calculated from the equations below.

$$\alpha = 0 ; \beta = 1 \text{ (FGC} < \%5) \quad (4.1)$$

$$\alpha = \exp [1.76-(190/FGC^2)] ; \beta = 0.99+FGC^{1.5}/1000 \text{ (\%5 < FGC } \leq \text{ \%35)} \quad (4.2)$$

$$\alpha = 5 ; \beta = 1.2 \text{ (FGC } \geq \text{ 35)} \quad (4.3)$$

Liquefaction resistance (τ_R) is calculated with Equation 5.

$$\tau_R = CRR_{M7.5} * C_M * \sigma' \quad (5)$$

Cyclic strength ratio ($CRR_{M7.5}$) corresponding to an earthquake with a moment magnitude of 7.5 in Equation 5 is calculated with Equation 6.

$$CRR_{M7.5} = \frac{1}{3.4-N_{1,60f}} + \frac{N_{1,60f}}{135} + \frac{50}{(10*N_{1,60f}+45)^2} - \frac{1}{200} \quad (6)$$

The earthquake magnitude correction parameter (C_M) in Equation 6, for design earthquake moment magnitude (M_w) 7.5, is calculated according to the Equation 7.

$$C_M = 10^{2.24/M_w - 2.56} \quad (7)$$

Repetitive shear stress in the ground ($\tau_{\text{earthquake}}$) is analyzed with total vertical stress (σ_{v0}) in the liquefaction analyzed soil, stress relief parameter (r_d) and short period spectral acceleration (S_{Ds}) as shown in Equation 8.

$$\tau_{\text{earthquake}} = 0.65 * \sigma_{v0} * 0.4 * S_{Ds} * r_d \quad (8)$$

The stress relief parameter (r_d) is analyzed according to the liquefaction depth (z) as shown in Equation 9.

$$r_d = 1 - 0.00765z \quad z \leq 9.15 \text{ m} \quad (9.1)$$

$$r_d = 1.174 - 0.0267z \quad 9.15 < z \leq 23 \text{ m} \quad (9.2)$$

$$r_d = 0.744 - 0.008z \quad 23\text{m} < z \leq 30 \text{ m} \quad (9.3)$$

$$r_d = 0.50 \quad z > 30 \text{ m} \quad (9.4)$$

The factor of safety against the liquefaction (FS), is calculated by dividing the liquefaction resistance (τ_R) by repetitive shear stress ($\tau_{\text{earthquake}}$) (Equation 10).

$$\tau_R / \tau_{\text{earthquake}} \geq 1.10 \quad (10)$$

Mapping Methods

Interpolation is a method that is used the estimated value at a different point whose value is unknown between to points, starting from the existing value points. Today, interpolation methods are used in the creation of many thematic maps [9].

In this study, using the MapInfo program, one of the GIS programs, the thematic soil class in 1.5 m / 3 m / 4.5 m / 6 m / 7.5 m / 9 m / 12 m depths related to the 290 drills, SPTN*, W_N , FGC, W_L , W_p , GWT and soil liquefaction maps were created. While creating these maps, natural neighbor interpolation (NNI) for soil maps, for SPTN* and liquefaction maps triangular irregular network method

(TIN), and inverse distance weighting interpolation method (IDW) for the other maps were used.

Inverse Distance Weighting (IDW) Interpolation

The IDW method, which is frequently used in Geographic Information Systems (GIS), works on the principle of obtaining the values at the unknown point by entering the known points values. Since the value of the point to be estimated is proportional to the distance between to the known point and the points, the value of the point to be estimated varies depending on this distance. When at least two known point values are entered and the radius of the region to be estimated is specified, the unknown point value is estimated using only the points in the circle area covering this region [10].

As in the example in Figure 2, when the red dot value and the radius value to be estimated (the area to be interpolated) are entered to estimate the purple dot, the estimation is only made for the red area and value of the purple dot is estimated. The point to be considered here is that only the points in the area within the specified radius will be used when making the estimation [10,11].

The formula used in the IDW method is as shown in the Equation 11 [12].

The formula used in the IDW method is as shown in the Equation 11 [12].

$$z_p = \frac{\sum_{i=1}^n (z_i/d_i^p)}{\sum_{i=1}^n (1/d_i^p)} \quad (11)$$

In this Equation, n is the number of known (baseline) points, z is the property value of known (baseline) points (altitude, temperature, etc.), d is the distance between the point to be interpolated (estimated) and the known (baseline) point, and p is the power parameter, generally accepted as 2 in literature [10].

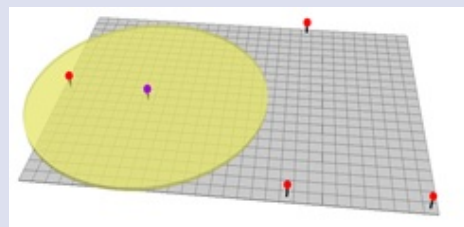


Figure 2. An example of finding an unknown point with the IDW method [12]

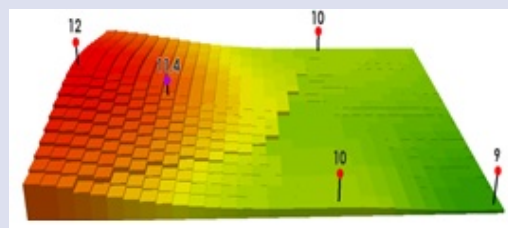


Figure 3. Example created by using Equation 11[12]

Triangular Irregular Network (TIN) Interpolation

The TIN forms circles around each of the nearest neighboring points, and the intersections of these circles form the triangles so that their intersections do not overlap. It estimates the values inside these triangles and thus creating a triangular surface and map [11].

As seen in Figure 4 triangular regions are created by creating circles around the red points so that the intersections of these circles do not overlap. The inner parts of these triangular regions are interpolated, the calculation is made and the surface is created [11].

Looking at the methods described so far, while no interpolate is made outside the triangle boundaries created in the TIN method (Figure 4), it is understood that in the IDW method, interpolate is made from the point found in a circular way as the radius of the region where interpolate is required (Figure 3).

Natural Neighbor Interpolation (NNI)

The NNI is a method based on quickly and reliably determining a weighted average surface from available data points [13].

In the NNI, Voronoi polygons are formed with the available data. A subset is determined by interpolating in line the weighted average of the distance between two points forming these polygrams, and a Voronoi polygram (white space) is created as in Figure 5 for this subset. The new polygrams formed in this way separate the transition boundaries better and allow the detailing of the transition boundaries [13,14].

The reason why we used the natural neighbor interpolation method (NNI) for the soil class in this study is that it is the best method to show heterogeneous transitions in soil types [13]. This method developed by Robin Sibson and based on the bond polygon system, calculates the weighted average for the Voronoi polygrams for every point given x,y coordinates of subset. Sibson represented every contribution to the calculation of the formed Voronoi polygram with λ (lambda). The Equation created by Sibson is seen in the Equation 12 [15].

$$\lambda_i(x) = (A(x_i))/(A(x)) \quad (12)$$

λ_i : Polygon values from 1 to N

$A(x_i)$: The intersection between the new polygon to be created and the the known polygon

$A(x)$: Total area of new polygon to be created

The new Voronoi polygon created by taking the interpolation weights of polygons is seen in Figure 5. Here, the areas of the polygons indicated by each number are their interpolation areas. The white colored polygon in the middle is the new Voronoi polygon created by taking the weight average (Equation 12) of these interpolated areas.

Results

In this study, the soil class at 1.5 m / 3 m / 4.5 m / 6 m / 7.5 m / 9 m / 12 m depths of each soil survey report, received from the Geyve county Directorate of Reconstruction and Urbanization corrected SPTN, W_N , FGC, W_L , W_P , GWT etc. were obtained and liquefaction calculations were made according to the TBEC 2018 with the same soil types that are under the risk of liquefaction.

In accordance with these calculations, with the MapInfo program, soil classifications for each depth in Sakarya province Geyve county at 1.5 m / 3 m / 4.5 m / 6 m / 7.5 m / 9 m / 12 m, corrected SPTN, W_N , FGC, W_L , W_P , GWT, and soil liquefaction mapping were created.

Example Liquefaction Analysis

In this section, the liquefaction analysis will be explained step by step which is carried out in Alifuatpaşa Town 157 Block 1 Parcel obtained from Geyve Directorate of Reconstruction and Urbanization. Table 1 shows some information of borehole number 2 in the soil survey report. In addition to this information, the unit volume weight of the water was considered as (γ_w) 9,81 kN/m³.

When liquefaction analysis is made with SPT values, first of all the soil parameters are determined and then SPT value correction is made, afterwards the liquefaction resistance (τ_R) is analyzed and finally the shear stress in the ground ($\tau_{\text{earthquake}}$) is analyzed, it is checked whether there is a risk of liquefaction on the ground according to the safety numbers.

Soil Parameters and SPTN Values

In accordance with the collective test report, the total vertical stress value calculated from Equation 10 is 114 kN/m², the total vertical effective stress value calculated from Equation 11 is 84.57 kN/m² and pore pressure value calculated from Equation 12 is 29.43 kN/m².

Analysis of The $N_{1,60f}$

The value of the cover load correction coefficient using Equation 2 is calculated as $C_N = 1.06$. Here when $C_N > 1.7$, $C_N = 1.7$ should be accepted [9].

In line with the information in the ground survey report, when the SPTN correction coefficients taken from Table 1 $C_R = 0.85$, $C_S = 1$, $C_B = 1$, $C_E = 1$ values are placed in Equation 1, $N_{1,60}$ is calculated as 7.21.

According to the Equation 4.2, α is analyzed as 2.91 and β is analyzed as 1.06. When α and β values are placed in the Equation 3, $N_{1,60f}$ is analyzed as 10.55.

Analysis of The T_r

When the $N_{1,60f}$ value found as 10.55 is placed in Equation 6, $CRR_{M7.5}$ is analyzed as 0.14. When M_w is selected as 7.5, C_M is obtained as 0.99 according to the Equation 7. In liquefaction analyses, the M_w is always chosen as 7.5 [15]. These obtained data from Equation 5 are placed, τ_R is analyzed as 11.72.

Analysis of The $T_{\text{earthquake}}$

σ_{v0} at the liquefaction analyzed depth is placed according to the Equation 9.1, if the r_d and S_{DS} are substituted in Equation 8, $\tau_{\text{earthquake}}$ is analyzed as 31.81.

Analysis of The FS

According to the TBEC 2018, safety number must be at least 1.1 so that there is no risk of liquefaction (Equation 10). According to the Equation 10, there is a risk liquefaction since the safety number is analyzed as 0.37 when the τ_R value for the relevant depth is divided by the $\tau_{\text{earthquake}}$ value.

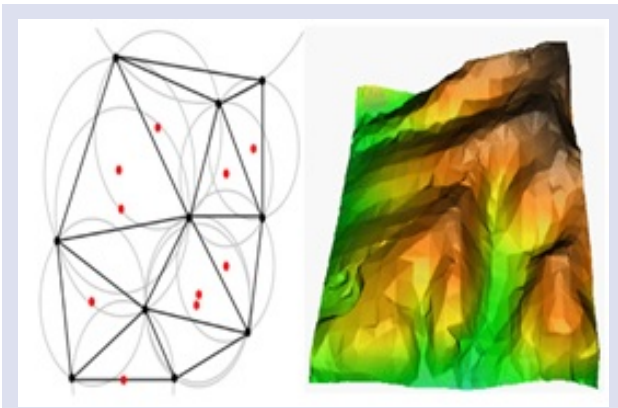


Figure 4. Example of creating a surface with the TIN method [12]

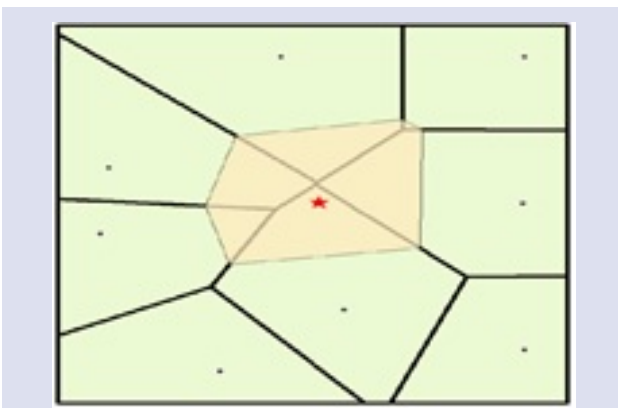


Figure 5. New polyram created by the weighted average of neighboring polygons [14]

Table 1. Drilling log information

Information	Value
Soil Class	SM
Depth (m)	6
FGC (%)	16.58
GWT (m)	3
γ_{natural} (kN/m ³)	18
$\gamma_{\text{saturated}}$ (kN/m ³)	20
S_{DS}	1.125

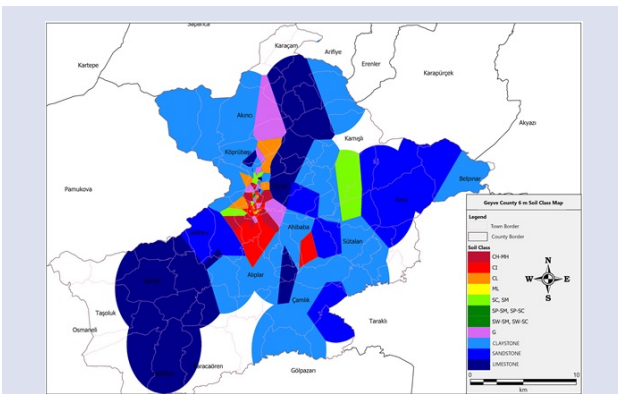


Figure 6. 6 m soil class map

Assumption Made in the Analysis

While the liquefaction analysis is made, in soil investigation report where γ_n ve $\gamma_{\text{saturated}}$ values are not given, these values are accepted according to the TS 498 standard [16].

In Türkiye Building Earthquake Regulation, soils with the potential of liquefaction are described as gravelly sand non-plastic silt and silt-sand mixture below ground water [9].

According to Karl von Terzaghi (1925), who is regarded as the father of soil mechanics, “liquefaction can occur when the weight of the solid particles forming the soil is transferred to the surrounding water during the subsidence of the saturated soil. As a result of this, the hydrostatic pressure of the soil with increasing hydrostatic water pressure at the relevant depth becomes close to the unit weight of the soil submerged in water [17].

In another definition, liquefaction is the rapid loss of strength that occurs in cohesionless (permeable) soils subject to cyclic shear stresses caused by earthquakes. Sometimes the shear strength drops below normal, and sometimes it disappears completely. In both cases, it can cause different damages” [18].

Considering all these definitions, since there will be no liquefaction in claystone, sandstone, limestone soil units, the safety number values for liquefaction in mapping for these research pit reports are taken as 2. Since the soils are above the groundwater level, liquefaction calculation was not made in the drillings where the groundwater level is not encountered [9].

In most of the ground survey reports received from the Geyve Directorate of Reconstruction and Urbanization, it was observed that this area was crossed with a research pit, since drilling could not be done due to the hardness of the ground. Considering the hardness of the ground in the reports passed with the research pit, the SPTN values were taken as 100.

Liquid limit values for non-plastic soil types were taken as 10 in reports of hard soils such as sandstone, claystone and limestone, which were observed to be passed by the survey pit during mapping [19].

Mapping Studies

In most of the ground survey reports received from the Geyve Directorate of Reconstruction and Urbanization, it was observed that these areas were crossed with a research pit, since drilling could not be done due to the hardness of the ground. Therefore, the sample for SPTN*, W_N , FGC, W_L , W_P and GWT maps was limited in a very small area. These mappings were made to cover the limited area that includes Gazi Süleymanpaşa, Alifuatpaşa, Orhaniye, Epceler, Camikebir, Tepecikler, Eşme and Sarıgazi towns, where construction is more intense.

Looking at the ground map in Figure 6, coarse-grained gravel units are observed in the county center at a depth of 6 m, while silty clayey sand units are observed in the east of the center.

When looking at the county center, a very variable soil profile, such as coarse-grained gravel and fine grained clay units, is seen in Figure 7.

Looking at the map in Figure 8, it is seen that the SPTN* number is generally 30 hits or more throughout the study area at a depth of 6 m 30.

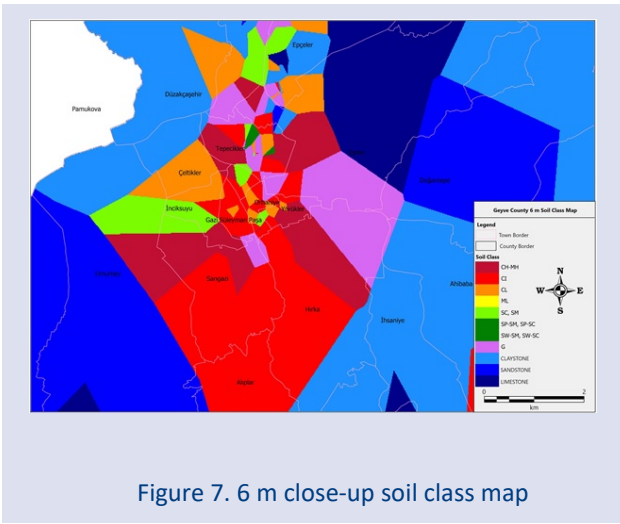


Figure 7. 6 m close-up soil class map

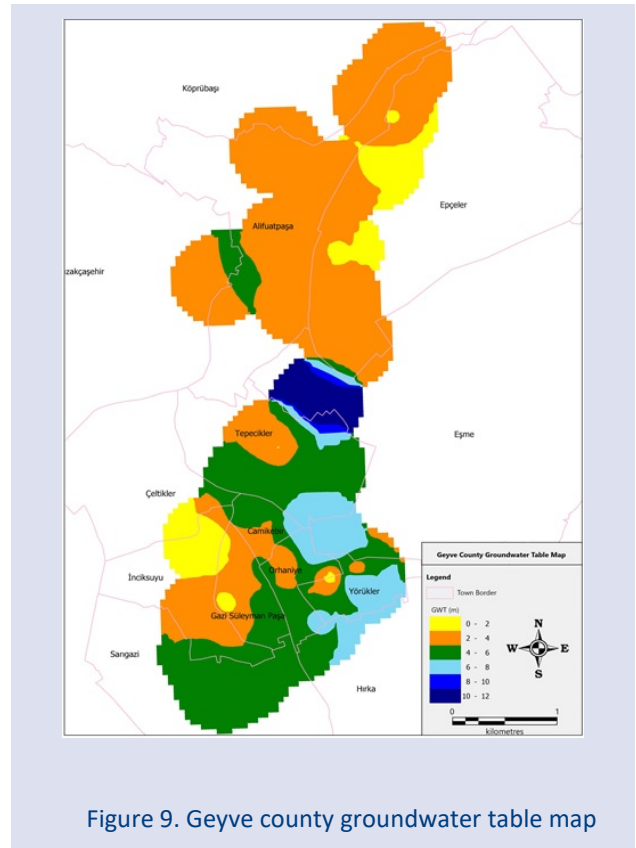


Figure 9. Geyve county groundwater table map

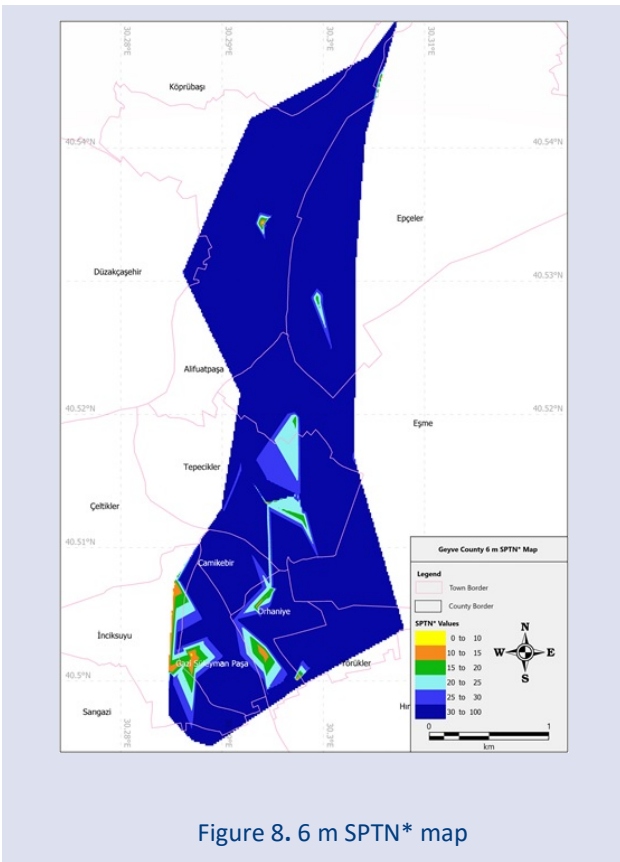


Figure 8. 6 m SPTN* map

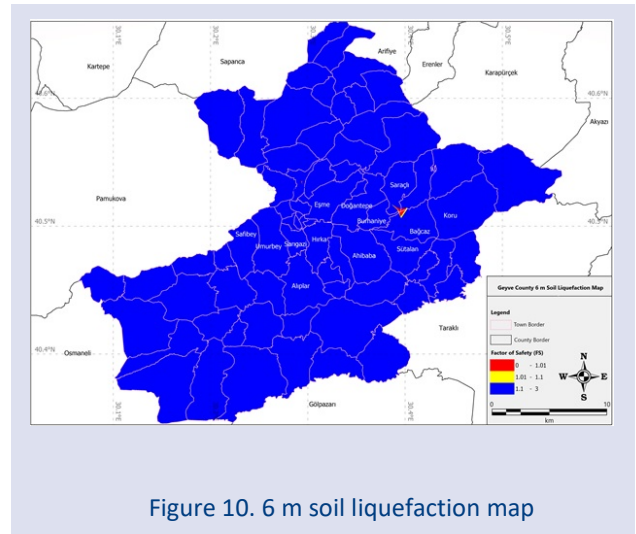


Figure 10. 6 m soil liquefaction map

In Figure 9, looking at the GWT map created with the available data, it is seen that the groundwater table is generally between 2-4 m in the south of the towns covering the sample area, and it is generally between 4-6 m in the north of the towns covering the sample area. The increase in groundwater table in the north-east of the region is thought to be related to the presence of mountainous areas

Figure 10 shows the soil liquefaction map for 6 m depth. On the map, the parts with a safety factor of less than one and a high risk of liquefaction are shown in red, and the parts with a safety coefficient between 1-1,1 and a low risk of liquefaction are shown in yellow. According to the map, it can be said that there is generally no risk of liquefaction at 6 m depth

Discussion and Conclusion

Within the scope of the study, the Geyve county of Sakarya province was selected. In order to make a thematic mapping in the selected region, the drilling data in the reports obtained from the previous ground survey studies in the region were used.

Looking at the soil maps prepared for the Geyve county of Sakarya province, it has been observed that hard soil units in the form of sandstone, claystone and limestone are dominant throughout the county. When we look at the central towns (Alifuatpaşa, Gazı Süleymanpaşa, Orhaniye, Camikebir, Eşme, Sarıgazi) where the settlement is the largest in the county, a complex soil profile is observed, mostly dominated by fine-grained clay, as well as coarse-

grained sand and gravel units up to 6 m deep. After 6 m of depth, it was observed that there was an increase in coarse grained (gravel) soil units in the counties.

Based on the soil maps prepared for Geyve, it can be said that the fine-grained soil unit (silt) which has high liquefaction potential is very few in the region. Therefore, the liquefaction analysis made with TBEC 2018 was considered sufficient.

When the corrected SPTN maps prepared for Geyve county covering the most populated central counties are examined, it is seen that the majority of the study area at 1.5 m depth is below 20 impact numbers. It was observed that the number of impacts increased at 3 m of depth. After 3 m depth, it was found that almost all of the study area had 30 or more impacts. When the corrected SPTN maps are compared with the ground maps, it can be said that the fine-grained soils up to 6 m depth are hard and compact soils. In addition since it is known that there is an increase in coarse-grained soil (gravel) units in the ground maps after the 6 m depth, it has been observed that the ground maps and the corrected SPTN maps are compatible with each other.

When the W_N maps prepared for Geyve county are examined, it is seen that the water content value, which changes 25% and above until 6 m depth, gradually decreases after 6 m depth and remains below 20%. In addition, since the number of available data decreased, it was observed that the white colored parts in the sample area increased as the depth increased.

When the prepared FGC maps were examined, it was seen that the fine grain ratio was 76% and above up to 4.5 m depth. It is seen that after 4.5 m depth in the sample area, this value drops below 76% and decreases as the depth increases. When the prepared FGC maps were examined, it was seen that the fine grain ratio was 76% and above up to 4.5 m depth. It is seen that after 4.5 m depth in the sample area, this value drops below 76% and decreases as the depth increases. The first is that the soil profile of the town is composed of coarse-grained soils such as gravel and sand and hard claystone units. The second is that the Sakarya river passes over this town and coarse-grained soils dominate at the base levels along the river line.

When the consistency limit maps prepared for Geyve county are examined, it is observed that there is an increase in coarse grained soils due to the increase in depth, although not regularly, there is a decrease in W_L values with depth. The same is true for W_P maps.

When we look at the prepared GWT map, it is seen that the GWT is shallower than 6 m (usually 2-4 m) in most of the county. In regions with mountainous areas, the groundwater table is encountered after 6-10 m.

When the liquefaction maps prepared for Sakarya province Geyve county are examined, it is observed that there is no liquefaction risk in the county except for some small areas. Looking at the close-up maps, areas with a high risk of liquefaction up to 7.5 m depth have been identified in Alifuatpaşa, Gazisüleymanpaşa and Orhaniye towns, where the settlement is dense. Since there are dense zoning areas in these regions that make up the

county center, it is thought that necessary ground and structure improvements should be made despite the risk of liquefaction.

Since the area between Burhaniye-Bağcaz to the east of these maps and where there is a risk of liquefaction is mountainous and there is no settlement, it is thought that even if liquefaction occurs in this region, it will not pose a danger to human life. However, in case of zoning, it is foreseen that detailed ground examinations and ground improvement processes will be carried out in this region. In addition, since there are mountainous lands outside the county center, it is predicted that there will be no risk of liquefaction in these areas based on the data available.

Although this study, which was prepared on the basis of the available data, is in accordance with the general literature, since the existing data are thought to be insufficient, a more detailed liquefaction analysis should be done on the basis of parcels in order to obtain more consistent data and not be considered as an inclusive study in the whole of Geyve county.

Acknowledgements

Authors would like to thank Geyve Municipality and engineer Murat KOZCAZ for his help while supplying ground survey reports for this study.

References

- [1] Yalçın H., Gülen L., Utkucu M., Türkiye ve Yakın Çevresinin Aktif Fayları Veri Bankası ve Deprem Tehlikesinin Araştırılması, *Yerbilimleri Bulletin for Earth*, 34 (3) (2013) 1-168.
- [2] Karavul C., Kurnaz T.F., Beyhan G., Kıyak A.; Coğrafi Bilgi Sistemleri Kullanılarak Adapazarı Zemin Sıklık Durumunun Haritalanması, *Deprem Sempozyumu*, (2005).
- [3] Adapazarı Zemin Çalıştay 22 Mart 2020. Available at: <http://www.aym.sakarya.edu.tr/2020/03/22/adapazarı-zemin-calistayi/>. Retrieved March 2, 2022.
- [4] Bohnhoff M., Martínez-Garzón P., Bulut F., Stierle E., Ben-Zion Y., Maximum Earthquake Magnitudes Along Different Sections of the North Anatolian Fault Zone, *Tectonophysics*, 674 (2016) 147-165.
- [5] Erken A., Özay R., Kaya Z., Ülker M.B.C., Elibol B., Depremler Sırasında Zeminlerin Sıvılaşması ve Taşıma Gücü Kayıpları. *Türkiye Mühendislik Haberleri Dergisi*, No.431 (2004) 20-26.
- [6] Bayraktar H., Hossin A., Sakarya İlinin Depreme Duyarlı Bölgelerinde CBS Tabanlı Hasar Tahmini, *Resilience*, 5(2) (2021) 173-185.
- [7] Seed H.B., Idriss I.M., Simplified Procedure for Evaluating Soil Liquefaction Potential, *Journal of the Soil Mechanics and Foundations Division*, 97(9) (1971) 1249-1273.
- [8] Youd T.L., Idriss I.M., Liquefaction Resistance of Soils: Summary Report From the 1996 NCEER and 1998 NCEER/NSF Workshops on Evaluation of Liquefaction Resistance of Soils, *Journal of Geotechnical and Geoenvironmental Engineering*, 127(4) (2001) 297-313.
- [9] Türkiye Bina Deprem Yönetmeliği Deprem Etkisi Altında Binaların Tasarımı İçin Esaslar, Çevre ve Şehircilik Bakanlığı, 2018.
- [10] Göğsu S., Hastaoğlu K.Ö., Ters Mesafe Ağırlıklı Enterpolasyon Yönteminde Güç Fonksiyonu Etkisinin

- İncelenmesi, 17. Türkiye Harita Bilimsel ve Teknik Kurultayı, Ankara, 2019.
- [11] QGIS training manual. Available at: https://docs.qgis.org/3.28/en/docs/gentle_gis_introduction/spatial_analysis_interpolation.html. Retrieved December 20, 2022.
- [12] GISGeography, Inverse distance weighting (idw) interpolation. Available at: <https://gisgeography.com/inverse-distance-weighting-idw-interpolation/>. Retrieved November 8, 2022.
- [13] Mitas L., Mitasova H., Spatial Interpolation. Journal of Geographical Information Systems: Principles, Techniques, Management and Applications, 1(2) (1999) 481-492.
- [14] ArcGIS 9.2 Desktop Help. Available at: <https://webhelp.esri.com/arcgisdesktop/9.2/index.cfm?TopicName=Natural%20Neighbor%20Interpolation>. Retrieved December 27, 2022.
- [15] Sibson R., A Brief Description of Natural Neighbour Interpolation. Interpreting Multivariate Data, (1981) 21-36.
- [16] TS 498 Yapı Elemanlarının Boyutlandırılmasında Alınacak Yüklerin Hesap ve Tasarım Değerleri, Çizelge 1, (1987).
- [17] Castro G., Liquefaction of sands, Ph. D. Thesis, series, Harvard University, Mass, (1969).
- [18] Mollamahmutoğlu M., Babuçcu F., Zeminlerde sıvılaşma analiz ve iyileştirme yöntemleri. Gazi Kitabevi (2006).
- [19] Çelik S.B., Denizli il merkezi zeminlerinin jeolojik, jeoteknik açıdan incelenmesi ve sıvılaşma duyarlılığının belirlenmesi. Yüksek lisans tezi, Pamukkale Üniversitesi, Fen Bilimleri Enstitüsü, 2003.



Recognition and Performance Evaluation of Handwritten Numbers Using a New Segmentation Method

Sultan Murat Yılmaz^{1,a,*}, Serap Çakar^{2,b}

¹Giresun University, Giresun, 28200, Türkiye

²Sakarya University, Sakarya, 54187, Türkiye

*Corresponding author

Research Article

History

Received: 17/10/2022

Accepted: 13/06/2023

ABSTRACT

Machine learning and computer vision applications have been very trendy recently and have been used in many applications and fields, such as biometric recognition, disease diagnosis and character analysis. Within the scope of this study, an application was developed to make it easier to read and integrate the written or test exam grades in schools and the performances of the classifiers used in the application were evaluated. Grades written by hand on exam papers were defined by using image processing methods. At the stage of recognition of grades, pre-processing, classification and slicing processes were performed on the image and classification processes were carried out on the data set used. Especially in slicing process, a new method was developed by using neighborhood relations of pixels and its performance was evaluated. MNIST dataset, which is frequently preferred in academic studies, was used to train and test the system. In this dataset, there are 60,000 handwritten samples of numbers 0-9 taken from 250 different people. In the image processing stage, a new technique for slicing the characters was used, and appropriate character separation was applied for all situations. After proper slicing, Artificial Neural Networks (ANN), Convolutional Neural Networks (CNN) and K-Nearest Neighbor (K-NN) algorithms were used to classify the data and the performance values were obtained as 98%, 99.4% and 86%, respectively.

Keywords: handwriting recognition, machine learning, classification

Yeni Bir Dilimleme Yöntemi Kullanarak El Yazısı Rakamlarının Tanınması ve Performans Değerlendirmesi

Süreç

Geliş: 17/10/2022

Kabul: 13/06/2023

ÖZ

Makine öğrenmesi ve bilgisayar görmesi uygulamaları son zamanlar oldukça trend olmaya ve biyometrik tanıma, hastalık teşhisi ve karakter analizi gibi uygulamalar başta olmak üzere birçok uygulama ve alanda kullanılmaya başlanmıştır. Bu çalışma kapsamında okullarda yapılan yazılı veya test sınav notlarının daha kolay okunup sistem üzerine entegre edilmesi için bir uygulama geliştirilmiş ve uygulamada kullanılan sınıflandırıcıların performansları değerlendirilmiştir. Sınav kağıtları üzerine elle yazılan başarı notlarının görüntü işleme yöntemleri kullanılarak tanımlanması yapılmıştır. Başarı notlarının tanınması aşamasında görüntü üzerinde ön işleme, dilimleme ve sınıflandırma işlemleri yapılarak kullanılan veri seti üzerinde sınıflandırma işlemleri gerçekleştirilmiştir. Özellikle dilimleme işleminde piksellerin komşuluk ilişkilerinden yararlanarak yeni bir yöntem geliştirildi ve performansı değerlendirildi. Sistemi eğitmek ve test etmek için akademik çalışmalarda sıklıkla tercih edilen MNIST veri seti kullanılmıştır. Bu veri setinde 0-9 arasındaki rakamların 250 farklı kişiden alınan 60.000 el yazısı örneği bulunmaktadır. Görüntü işleme aşamasında karakterlerin dilimleme işlemleri için yeni bir teknik kullanılarak tüm durumlar için uygun karakter ayrımı gerçekleştirilmiştir. Uygun dilimleme işlemi gerçekleştirildikten sonra verileri sınıflandırmak için Yapay Sinir Ağları (YSA- Artificial Neural Networks (ANN)), Evrimsel Sinir Ağları (Convolutional Neural Networks- CNN) ve K-En Yakın Komşu (K-Nearest Neighbor- K-NN) algoritmaları kullanılmış ve performans değerleri sırasıyla %98, %99,4, %86 olarak elde edilmiştir.

Anahtar Kelimeler: el yazısı tanımlama, makine öğrenmesi, sınıflandırma

Copyright



This work is licensed under
Creative Commons Attribution 4.0
International License

^a s.muratyilmaz@giresun.edu.tr

^{id} <https://orcid.org/0000-0001-5386-2219>

^b scakar@sakarya.edu.tr

^{id} <https://orcid.org/0000-0002-3682-0831>

How to Cite: Yılmaz SM, Çakar S (2023) Recognition and Performance Evaluation of Handwritten Numbers Using a New Segmentation Method, Journal of Engineering Faculty, 1(1): 38-47

Giriş

Makine öğrenmesi ve bilgisayar görmesi uygulamalarında özellikle el yazısı tanıma işlemleri bilgi işlemede önemli bir rol oynamaktadır. Son yıllarda geliştirilen teknoloji ve yöntemler sayesinde el yazısı tanıma uygulamalarının kullanımı ve doğruluk oranları artmıştır.

Yazı yazma stilleri kişiden kişiye farklılık gösterir. Bu durum insan el yazısı rakam tanımayı araştırma ve uygulama için ana alan haline getirmiştir. Rakamların farklı stiller ile yazılması ve çok sayıda yazıtların kısa sürede okunabilmesi zor olabileceğinden, bir bireyin rakamları gözden geçirmesi oldukça zor bir görev haline gelir. Bu noktada insanların yerini bilgisayarların alması, süreci kısaltacak ve kolaylaştıracaktır.

Günümüzde el yazısı tanıma aktif bir araştırma alanıdır. Son yıllarda, yüksek tanıma doğruluğu ve güvenilirliği talep eden pratik uygulamalar için birçok el yazısı rakam tanıma sistemi önerilmiştir. El yazısı tanıma günümüzde yaygın olarak kullanılan Makine Öğrenmesi ve Derin Öğrenme yöntemleri mevcuttur. Bu yöntemler el yazılarını tanıma (sınıflandırmada) iyi yöntemler olsalar da el yazısı tanıma hâlâ bir açık araştırma alanıdır. Tanıma doğruluğu, çalışma süreleri, hesaplama karmaşıklığı yönünden çalışma performansını arttıracak yeni yöntemler geliştirilmesi talep edilmektedir. Bu açıdan günümüzde trend bir araştırma alanı olup bu konu ile ilgili literatürde çeşitli çalışmalar mevcuttur.

Tanya Makkar ve arkadaşları [1] yaptıkları çalışmada MNIST data setini kullanarak el yazısı rakamlarının K-NN ve CNN ile tanınması ile ilgili çalışma gerçekleştirdiler. Yapılan bu çalışmada görüntü işlemede en iyi sonuçların alınmasında iki ana etken olduğuna değinilmiştir. Birincisi görüntü özniteliklerinin uygun ve doğru bir şekilde çıkarılması, ikincisi ise iyi bir sınıflandırma yönteminin belirlenmesidir. Görüntü özellikleri çıkarmada Gauss dağılım metodunu kullanarak K-NN ve CNN performanslarını ve zaman karmaşıklığını karşılaştırdılar. Yapılan çalışmada CNN'in K-NN'e göre daha iyi performans verdiğine ancak CNN'in eğitim süresinin göz ardı edilecek seviyede olduğuna değinilmiştir.

Preman Ghadekar ve arkadaşları [2] çalışmalarında MNIST ve EMNIST veri setleri üzerinde K-NN ve Destek Vektör Makinesi (SVM) yöntemlerini kullanarak el yazısı rakamlarının tespitini gerçekleştirdiler. Yapılan bu çalışmada görüntü işleme safhasında görüntülerin özellik çıkarımları için iki ayrı yöntem kullanılmıştır. Hibrit Ayrık Dalgacık Dönüşümü ve Ayrık Kosinüs Dönüşümü kullanılarak görüntü özelliklerini çıkardılar ve bu özellikler K-NN ve SVM yöntemleri kullanılarak rakamların tespiti gerçekleştirildi. SVM yönteminin rakam tespitinde daha avantajlı olduğu sonucuna varılmıştır.

E. Lejeune [3] yaptığı çalışmada farklı bir yöntem kullanarak görüntü işlemede daha az maliyet ve karmaşıklığa sahip meta model yöntemi kullanmıştır. Bu yöntemde Neo-Hookean materyal modeli kullanmıştır. Materyal modeli ile farklı bir özellik çıkarma yöntemi kullanılarak ileri beslemeli YSA modeline göre CNN modelinde daha yüksek performans elde edilmiştir.

O. Kaziha ve T. Bonny [4] geliştirdikleri çalışmada MNIST veri setinden gelen verilerin ve görüntü işlemede kullanılacak görüntülerin boyutlarını kullandıkları yöntem ile küçültürken CNN ve Uzun Kısa Süreli Bellek (LSTM) sinir ağlarında performansını gözlemlidiler. Her iki sınıflandırma yöntemi için 784 olan giriş verilerini 128'e düşürmüşlerdir. Bu sayede sınıflandırma eğitiminde zamandan kazanç sağlanmış, performanslarında CNN için %99,45, LSTM için %99,22 doğruluk oranı elde edilmiştir.

Palvanov A. ve Cho Yi. [5] el yazısı rakamlarının tespitinde en uyumlu derin öğrenme yönteminin seçilmesi için dört farklı derin öğrenme algoritmasını denemişlerdir. MNIST veri setini kullanarak dört farklı derin öğrenme yöntemini gerçek zaman uygulamalarında eğitim ve test sürelerini, bellek kullanımının miktarlarını ve temel indeks değerlerini karşılaştırdılar.

Ricardo F. Alvear-Sandoval ve arkadaşları [6] MNIST veri seti üzerinde CNN performansının iyileştirilmesi için bir çalışma gerçekleştirdiler. CNN performansının iyileşmesi için iki yönlü takip işlemi uyguladılar. Birincisi yığılmış gürültü giderme otomatik kodlayıcı sınıflandırıcılarının CNN birimlerine uygulanması, ikincisi ise CNN mimarilerinin sınırlamalarından yararlanmaya çalışarak önceki tasarımların en iyilerinin çıktısına bir Yığılmış Gürültü Giderici Otomatik Kodlayıcı sınıflandırıcısı uygulamaktan ibarettir. Bu sayede normal CNN modelinden daha üstün performans elde edilmiştir.

E. S. Gati ve arkadaşları [7] Kannada alfabesi için Kannada-MNIST ve Dig-MNIST olarak adlandırılan yeni el yazısı rakamları veri kümesi üzerinde yeni bir boru hattı oluşturarak veriler üzerinde eğitimin başarı oranını artırdılar. Geliştirilen modelde doğruluk oranlarını Kannada-MNIST'de %96,8'den %97,53'e ve Dig-MNIST veri setinde %76,1'den %85,02'ye çıkarmışlardır.

D. Beohar ve A. Rasool [8] çalışmalarında MNIST veri setini ve YSA ve CNN sınıflama yöntemlerini kullanarak el yazısı rakamlarının tanınmasını gerçekleştirdiler. Bu çalışmada el yazısı rakamlarının tanınmasında beş aşamalı bir yöntem önerildi. Aynı zamanda çoklu sinir ağlarında lokal Gradyan yöntemi kullanılarak Gradyan patlaması durumunun engellenmesi sağlanmıştır.

K. Zhang ve arkadaşları [9] MNIST veri setini kullanarak YSA uygulamalarında oluşan hiper parametreleri ve L-2 norm düzenlemelerinin etkilerini gözlemlidiler. YSA uygulamalarında optimizasyon yapmak için manuel, ızgara, rastgele arama ve Gauss Süreçlerini kullanan Bayes optimizasyonu gibi bir dizi yöntem önerilmiştir. Çok küçük öğrenme oranlarının aşırı uyum problemi oluşturacağından L2-norm düzenlemesi ile aşırı uyumun ortadan kaldırılmasının kritik öneme sahip olduğu belirtilmiştir.

A. Garin ve G. Tauzin [10] makina öğrenmesi yöntemi için topolojik veri analizini kullanarak yeni bir öğrenme metodunu sundular. Gri seviyeli resimler üzerinden belirli filtreleme yöntemlerini kullanarak MNIST veri seti üzerinden eğim yapılmasıyla el yazısı rakamlarının tanınması ile ilgili çalışma gerçekleştirdiler.

Dong-yuan Ge ve arkadaşları [11] MNIST veri setini kullanarak CNN tabanlı el yazısı rakam tanıması için yüksek

doğrulukla detektör tasarımı gerçekleştirdiler. TensorFlow üzerinde gerçekleştirilen bu uygulamada konvolüsyon katmanlarındaki özellik haritaları yüksek boyutta ve derinlikte çıkartılmıştır. Bu sayede CNN'in son katmanında fazla sayıda nöron kullanılarak sınıflandırmanın hassasiyeti ve performansı artırılmıştır.

Birjit G. ve arkadaşları [12] MNIST veri setini kullanarak el yazısı rakamların tanınmasında kullanılan beş farklı makine öğrenmesi yönteminin performanslarını karşılaştırdılar. Bu yöntemler için hangi durumlarda hangi yöntemin performansının daha iyi olabileceği belirlenmeye çalışıldı.

AG Hochuli ve arkadaşlarının [16] yaptıkları çalışmada el yazısı rakamlarının dilimleme işlemlerini gerçekleştirerek CNN modelinde eğitimini sağladılar. Yapılan çalışmada el yazısı rakamlarının boylarının (rakamların üst ve alt tepe noktaları farkı) yarısı alınarak C medyan değeri hesaplanıyor. Bu değer üzerinden bit taraması yapılarak rakamların dilimlenmesi sağlanıyor. Bu yöntemde birleşik rakamların ve iç içe geçmiş rakamların dilimlenme işlemleri doğru bir şekilde gerçekleşmiyor. Yapılan ölçümlerde dilimleme işlemi %85 oranında doğru bir şekilde yapılmıştır. Sınıflandırma işleminde CNN modeli kullanılmıştır. NIST veri seti kullanılarak CNN modelinin eğitimi yapıldı. Dilimleme işleminden gelen veriler CNN modeline uygulanmasında %97,12 oranında başarı elde edildi.

Abdülcelil Gattal ,Youcef Chibani ve Bilal Hacı [17] yaptıkları çalışmada el yazısı rakamlarının uygun şekilde dilimlenmesini ve sınıflandırmasını gerçekleştirdiler. Dilimlenme işlemi için görüntü ön işleme kısmında dikey iz düşüm histogram analizi, kontur analizi ve kayan pencere Radon dönüşümüne dayalı olarak üç farklı segmentasyon yöntemi kullanarak dilimleme işlemi gerçekleştirildi. Bu yöntem kesintili rakamların tanınması ve birleşik rakamların tanınmasını sağlamaktadır. Ancak iç içe geçmiş rakamlar için dilimleme aşamasında uygun çözümler sunamamaktadır. Sınıflandırma aşamasında karar destek vektör makinası kullanılmıştır. Veri seti olarak NIST veri seti kullanıldı. Gerçekleştirilen modelin performansı %96,91 olarak ölçüldü.

Mohsine Elkhayati ve arkadaşlarının [18] yapmış olduğu çalışmada Arapça yazıların dilimlenmesi gerçekleştirdiler. Arapça yazılar birleşik yazıldığından bu çalışmada matematik morfolojik işlemler kullanıldı. Ancak bu yöntemin kullanılmasında el yazılarında veri kaybına neden oldu. Bu durumu engellemek için Küresel Genişleme ve Küresel Aşınma yöntemleri kullanıldı. Sınıflandırma için CNN yöntemi kullanıldı. Tüm işlemler sonucunda performans olarak %97,35 oranında doğruluk oranına sahiptir.

Guillaume Renton ve arkadaşlarının [19] yapmış oldukları çalışmada el yazısı metin satırı segmentasyonu için öğrenmeye dayalı bir yöntem sunuyorlar. Tam konvolüsyon ağlarını kullanarak giriş verilerinin giriş verilerinin çözünürlüğünü düşürmeden piksel bazda tarama yapılarak her satırın x ekseninde tespiti yapıldı. Kullanılan bu yöntem %91,3 lük bir performans sağlıyor ancak bu yöntemin kullanılması bellek yönetimi açısından maliyetli olabileceği unutulmamalıdır.

Manoj Kumar Sharma ve Vijay Pal Singh Dhaka [20] yaptıkları çalışmada destek vektör makinası sınıflandırma

yöntemini kullanarak el yazısı kelimelerinin dilimleme işlemini gerçekleştirdiler. Bu çalışmada kayıt, eğitim ve segmentasyon olmak üzere üç aşamaya ayrılmıştır. Eğitim ve test işlemlerinde ICDAR veri seti kullanılmıştır. Segmentasyon aşaması sekiz alt bölümden oluşur ve dilimleme işlemlerinde SURF (Hızlandırılmış Dayanıklı Özellikler) algoritması kullanıldı. Filtrelenmiş destek vektör makinaları kullanılarak dilimleme işlemleri sonucunda %96,48 oranında bir başarı elde edilmiştir.

Payal Jindal ve Balkrishan Jindal [21] yapmış oldukları çalışmada orta nokta algılama tekniği kullanılarak Gurmukhi yazısıyla yazılmış el yazısı metin belgelerinin satır ve kelime bölünmesi işlemi gerçekleştirildi. Bu çalışmada yazarların geliştirdiği satır bölümlenmesi algoritması ve kelime bölümlenme algoritması kullanılarak hem satır hem de kelime bölünmesi işlemi gerçekleştirildi. Burada önerilen orta nokta tespitine dayalı yaklaşımla, basitçe iki satırı veya iki kelimeyi ayıran boşlukların tanınmasına dayanmaktadır. Yapılan testler sonucunda önerilen yöntemin hem satır hem de kelime segmentasyonu için %95 oranında bir performansla çalıştığı bulunmuştur.

Son yıllarda yapılan çalışmalar ve gelişmeler sonucunda yapay zekâ ve derin öğrenme teknikleri karakter tanımda oldukça yüksek performans çıkarmıştır. Bu çalışma kapsamında özellikle kalabalık sınıflarda yapılan yazılı veya test sınav kağıtlarındaki el yazısı notlarının dijital ortamda anlaşılır ve hatasız olarak tespit edilmesi için bir uygulama geliştirilmiştir. Kağıtların üzerindeki notların görüntüsü tarama işleminden geçirilerek dijital ortama taşınmıştır. Dijital ortama aktarılan resimler gerekli ön işleme, dilimleme ve sınıflandırma işlemlerine tabi tutularak el yazısı rakamlarının tanınması işlemleri gerçekleştirilmiştir. Sınıflandırma işlemleri yapılırken Yapay Sinir Ağları (YSA - Artificial Neural Networks), K En yakın Komşu Algoritması (K-NN - K-Nearest Neighbor) ve Evrimsel Sinir Ağları (CNN - Convolutional Neural Networks) yöntemleri kullanılmış ve bu yöntemler arasında performans farklılıkları gözlemlenmiştir.

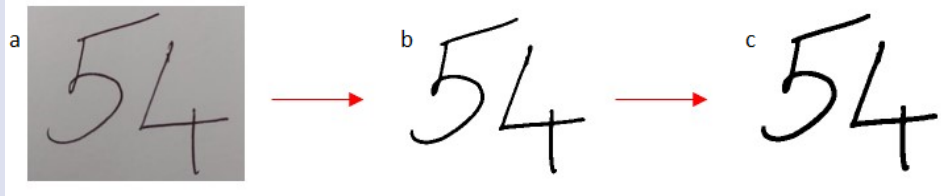
El Yazısı ile Rakam Tanıma Uygulaması

Görüntü işleme uygulamalarında el yazısı tanıma işlemleri çevrim içi (online) ve çevrim dışı (offline) olmak üzere iki kısımda incelenir. Çevrim içi yöntemler anlık el yazısı tanıma uygulamalarıdır. Çevrim içi yöntemlerde özel ekranlar (tablet, dokunmatik ekran vs.) üzerinden el yazısı hareketlerinden yararlanarak el yazıları tanımlanır. Çevrim dışı yöntemler ise el yazıları görüntülerinin analiz için tasarlanan sisteme görüntü olarak aktarılıp, sistem üzerinden tanınmasını sağlayan yöntemdir [13].

Bu çalışma kapsamında çevrim dışı yöntem kullanılmıştır. Sınav kağıtlarında notların yazıldığı alanların görüntüleri alınarak tasarlanan sistem üzerinden görüntünün giriş, ön işleme, dilimleme, sınıflandırma ve sonuç olmak üzere beş aşamalı bir sistemden geçerek el yazısı rakamlarının tanıma işlemi gerçekleştirilmiştir (Şekil 1).



Şekil 1. Uygulama işlem basamakları.
Figure 1. Application process steps.



Şekil 2. (a) Orijinal resim.; (b) Blur, Laplace filtresi ve Siyah-Beyaz dönüşüm uygulaması.; (c) Morfolojik işlem.
Figure 2. (a) Original image.; (b) Blurring, Laplace filtering and black-white conversion applications.; (c) Morphological process.

El yazısı görüntüleri tarayıcı yardımıyla sisteme girişi sağlanır. Sisteme alınan ham görüntüler ön işleme aşamasında belirli manipüle işlemlerinden geçerek özellik çıkarımları yapılır. Dilimleme aşamasında geliştirilen yeni yöntem kullanılarak piksellerin komşuluk ilişkisinden yararlanılarak rakamların dilimlenmesi yapılır. Sınıflandırma aşamasında K-NN yöntemi, evrişimli sinir ağları (CNN) ve yapay sinir ağları (ANN) kullanılarak sınıflandırma işlemleri gerçekleştirilir. Evrişimli sinir ağları ve yapay sinir ağlarının eğitimi için MNIST veri seti kullanılmıştır.

MNIST Veri Seti

Bu çalışmada sistemin eğitimi ve testler için kullanılan veri seti olarak "Modified National Institute of Standards and Technology" (MNIST) veri seti [14] kullanılmıştır. El yazısı rakamlardan oluşan MNIST veri seti uluslararası alanda sıklıkla kullanılmaktadır. MNIST veri seti sıfır ile dokuz arasındaki rakamların görüntülerinden oluşan bir veri setidir. MNIST veri setindeki verilerin 60,000 adedi eğitim verisi, 10.000 adedi test verisi olarak bulunmaktadır. Rakamların her biri 28x28 piksel ölçüsüne sahip görüntülerden oluşmaktadır.

Ön İşleme

Ön işleme bölümünde sisteme alınan ham görüntülerin istenmeyen gürültü, parazit ve gereksiz alanlarını ayırarak görüntülerin istenilen (benzersiz) alanlarını ön plana çıkarmak için kullanılan bir takım manipüle işlemleri gerçekleştirilir. Bu bölümde görüntülerin benzersiz özelliklerini ön plana çıkarmak için belirli manipülasyon işlemleri ve filtreleme yöntemleri kullanılmıştır. Çalışmada sınav notlarının tanınması işlemi gerçekleştirileceğinden her basamak için onluk sayma sistemi rakamlarını (0-9 arası rakamları) tanıma yapılmıştır. Dijital rakamlara baktığımızda tüm rakamlar bütünlük içindedir. Yani dijital rakamlarda yazım stillerinden kaynaklanan kesikler, rakamın tam ve doğru yazılmaması gibi maddi hatalar yoktur. Aslında el yazısı

rakamlarında bu şekilde yazılması beklenilmektedir. İdeal durumda el yazısı rakamların ortak özelliği yazım esnasında bir bütünlüğü olmasıdır. El yazısı ile yazılan her rakam kalemi kaldırmadan yazılabilir durumda olmalıdır. Bu durum da her rakam için bir bütünlük durumu oluşması beklenmektedir. Ön işleme aşamasında temel motivasyonumuz rakamların bir bütünlük içinde olmasıdır. Ancak kişilerin yazım stillerinden kaynaklanan farklılıklar sebebiyle her zaman bu ideal yazım şekli gerçekleşmeyebilir. Bu durumlar için görüntü üzerinde gerekli manipüle işlemi gerçekleştirerek her basamak değeri için hem rakamların bütünlüğünü hem de rakamların birbirlerinden ayrıklığı sağlanmalıdır.

Ön işleme aşamasında sisteme giriş sağlanan el yazısı not görüntülerinde bireysel yazım stillerinden dolayı el yazısı rakamları bütünlük içinde olmayabilir. Bu durum bizim için istenmeyen bir durumdur. Çünkü dilimleme aşamasında bütünlük özelliğinden yararlanarak el yazısı rakamlarının ayrıştırılması sağlanacaktır. Bu durumu engellemek için ön işleme aşamasında gerekli manipüle işlemleri gerçekleştirilir. Aynı zamanda yazım stilleri nedeniyle görüntülerin birbirine bitişik olması da söz konusu olabilir. Bu durum için de bitişik görüntülerin uygun şekilde ayrılması ve saptanması gerekmektedir.

Ön işleme aşamasında öncelikle görüntüdeki bütünlüğü arttırmak ve istenmeyen özellikleri yumuşatmak için 5x5 matris özellikli blur filtrelemesi uygulanır. Ardından istenilen kenar ve özelliklerin çıkarılması için düşük seviyede Laplace filtrelemesi kullanılır. Daha sonra görüntü siyah beyaz görüntüye çevrilir. Görüntüyü siyah beyaz forma dönüştürürken uç özelliklerinden yararlanıldı. Yani görüntü matrisinde siyaha yakın olan piksel değerleri "0", beyaza yakın olan piksellerin matris değerleri ise "255" olarak belirlendi. Bu işlemlerden sonra rakamlarda bütünlük oluşmayabilmektedir. Bu durumun önüne geçmek için ve görüntüdeki rakamların bütünlüğünü sağlamak amacıyla morfolojik işlemlerden yararlanıldı. Görüntümüzdeki son işlem olarak 2x2 matrisli Morfolojik Genişletme işlemi

uygulandı. Tüm işlemlerden sonra görüntüler şekil 2 (a), (b) ve (c)'deki gibi olacaktır.

Dilimleme

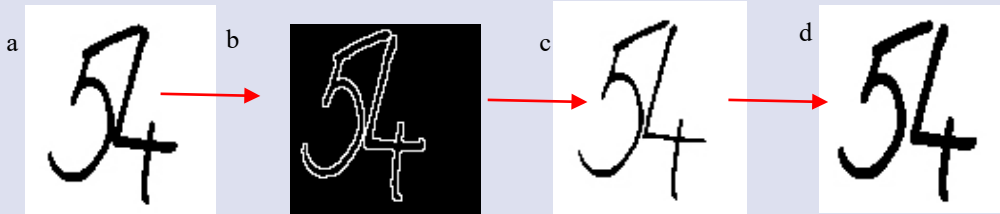
Ön işleme aşaması tamamlandıktan sonra oluşan görüntü birden fazla basamak değerine sahipse görüntüyü basamak değerlerine ayırmak gerekmektedir. Ön işlemeden sonra gelen görüntü (Şekil 2 (c)) iki boyutlu matris halindedir. Görüntüde not değerlerinin olduğu matris değerleri (siyah alanlar) "0", diğer tüm alanların değerleri (beyaz alanlar) "255" değerindedir. Bu değerlerin uç noktalarda tutulması dilimleme ve sınıflandırma aşamasında bize kolaylık sağlayacaktır.

Ön işlemeden gelen görüntüdeki her bir rakam bir bütünlük içerisinde. Rakamlarda kişilerin yazı stillerinden oluşan kopmalar morfolojik işlemler kullanılarak tamamlanmış ve bütünlük sağlanmıştır. Rakamların tamamının bütünlük içinde olması dilimleme işlemleri için kolaylık sağlayacaktır. Ancak burada rakamların bitişik yazılma durumlarının da kontrol edilmesi gerekmektedir. Bunun için ön işleme aşamasından gelen görüntü (Şekil 3 (a)) üzerinde bazı manipüle işlemleri gerçekleştirilmesi gerekmektedir. Bunun için öncelikle görüntüye 2x2 matrisli Morfolojik Gradyan işlemi uygulanır (Şekil 3 (b)). Bu işlemle birleşik görüntünün sınırları belirlenir. Sınır belirleme işleminden sonra belirlenen sınır dışı alanlar 2x2 matrisli Morfolojik Erozyon (Şekil 3 (c)) işlemi ile temizlenir. Temizlenme işlemi sonunda görüntüde bütünlük kaybı olamaması için son işlem olarak 2x2 matrisli Morfolojik Genişletme (Şekil

3 (d)) işlemi yapılır. Bu sayede uç uca birleşik olan rakamlar ayrılmış olur. Bu işlem sonrasında görüntüdeki rakamı ifade eden pikseller "0" değerini taşır. Diğer bütün pikseller "255" değerini taşır. Yani rakamları ifade eden pikseller siyah diğer bütün pikseller beyaz rengini taşır.

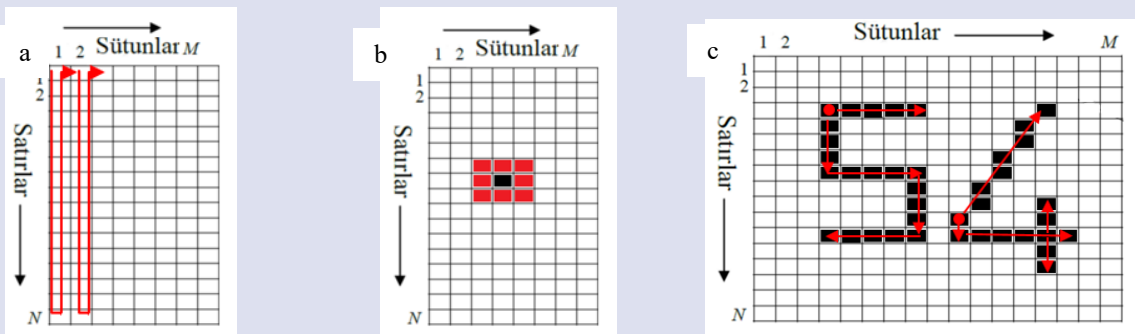
Dilimleme işleminde geliştirilen yeni yöntem CNN ağlarının konvolüsyon işlemlerinden ilham alınarak geliştirilmiştir. Ön işlemeden gelen görüntüdeki rakamlar bir bütünlük içinde olacağından her rakama ait görüntüdeki piksellerin değerleri "0" (Sıfır) olacaktır ve rakamların görüntüleri birbirlerini kesmeyecektir. Rakamların arası ve diğer tüm alanlardaki pikseller "255" değerine sahip beyaz görüntü pikselleri olacaktır. İlk olarak ön işlemeden gelen işlenmiş görüntü başlangıç sütunundan başlanarak sütun bazlı taramaya başlanılır (Şekil 4 (a)).

Taramada bulunan ilk "0" değerine ait matris adresi bizim referans noktamız olarak kabul edilir. Referans noktası bulunduktan sonra ön işlemeden gelen görüntü boyutunda tüm elemanları "255" olan yeni bir matris oluşturulur. Ön işlemeden gelen görüntünün referans noktasından başlanarak komşu pikseli "0" değerine sahip tüm matris adreslerinin değeri tespit edilir ve oluşturulan yeni matriste bu adreslere "0" değeri atanır. Bir piksele ait tüm komşu piksel değerleri şekil 4(b)'de belirtilmiştir. Şekil 4 (b)'de belirtilen siyah alana sahip pikselin tüm komşuları şekil 4 (b)'de belirtilen kırmızı alanlardır. Referans noktasından başlanılarak tespit edilen tüm sıfır değerine sahip pikseller bize görüntüdeki rakamın ilk basamak değerine sahip rakamı verecektir (Şekil 4 (c)).



Şekil 3. (a) Ön işlemeden gelen resim.; (b) Morfolojik Gradyan (2x2); (c) Morfolojik Erozyon (2x2); (d) Morfolojik Genişletme (2x2).

Figure 3. (a) Image from pre-processing.; (b) Morphological Gradient (2x2); (c) Morphological Erosion (2x2); (d) Morphological Expansion (2x2).



Şekil 4. (a) Sütun bazlı tarama işlemi.; (b)Piksel komşuluk gösterimi.; (c) Komşuluk ilişkisinden yararlanarak rakam belirleme işlemi.

Figure 4. (a) Column-based scanning process.; (b) Pixel neighborhood display.; (c) The process of determining numbers using the neighborhood relationship.

Tespit edilen rakam oluşturulan yeni matriste saklanır. Tespit edilen "0" değerine sahip pikseller içinde en büyük sütun değerine sahip piksel yeni referans değerimiz olur. Başlangıç satır değeri (ilk satır) ve yeni referans değerine sahip olan pikselin sütun numarası (0 x yeni referans değeri sütun numarası) değerine sahip pikselden başlanılarak sütun bazlı taramaya devam edilir. Tarama işleminde bulunan ilk "0" değeri yeni referans noktası değeri olur. Bu noktaya sahip pikselden başlanılarak komşusu "0" değerine sahip olan pikseller için tüm değerleri "255" olan işlenmiş görüntü boyutlarında yeni bir matris oluşturulur. Oluşturulan yeni matrise komşuluk ilişkisinden yararlanarak "0" değerine sahip piksellerin atama işlemi gerçekleştirilir (Şekil 4 (c)). Komşuluk ilişkisinden yararlanarak değeri "0" olan pikseller bittiğinde işlem tamamlanır ve en büyük ikinci basamak değerine sahip rakamın görüntüsü oluşturulmuş olunur. Komşusu "0" olan değerler içinde sütun değeri en büyük olan değer hafızada tutulur ve yeni referans değeri olur. Bu işlemler (Şekil 5) görüntüdeki tüm rakamlar tespit edilene kadar (Şekil 6) devam eder. Böylece görüntülerin piksel değerlerinin komşuluk ilişkilerinden yararlanarak tüm basamak değerlerine sahip rakamların değerleri tespit edilir. Dilimleme işlemine ait kaba kod şekil 5'de belirtilmiştir. Dilimleme işleminde tespit edilen tüm rakamlara ait görüntüler sınıflandırma işlemlerinde MNIST veri seti kullanıldığı için son aşamada siyah piksellerin olduğu alanlardan kırılarak 28x28 boyutuna dönüştürülür.

Dilimleme İşleminin Değerlendirilmesi

El yazısı rakamlarının dilimlenme yönteminde çevrim içi el yazılarının tespitine benzer bir yöntem geliştirilmiştir. Bu

yöntemde CNN ağlarının konvolüsyon aşamasına benzer piksel taramalı bir yöntem uygulanmıştır. Literatürde genel olarak el yazısı rakamlarının dilimlenmesinde histogram analizi, kontur analizi, yazı konum bilgilerinden yararlanma, yazı şekilleri vb. yöntemler kullanılmaktadır. Bu çalışma kapsamında sınav kağıtlarında el yazısıyla yazılan başarı notları rakamlarının dilimlenmesi için piksellerin komşuluk ilişkilerinden yararlanılarak yeni bir dilimleme yöntemi geliştirildi. Geliştirilen bu yöntemle rakam görüntüleri ön işleme aşamasında belirtilen manipülasyon işlemlerinden geçirilir. Ön işleme aşamasından başarılı olarak gelen görüntünün siyah piksellerinin komşuluk ilişkisinden yararlanarak dilimleme işlemleri gerçekleştirilmiştir. El yazısı görüntülerinde yazım stillerinden dolayı kaynaklanan küçük kesikli rakamlar morfolojik işlemler kullanılarak bütünleme işlemleri gerçekleştirilir. Ancak yazım stillerinden kaynaklanan büyük kesikli rakamlarda birleştirme işlemleri uygun bir şekilde tamamlanamıyor.

El yazısı görüntülerinde bütün ve ayrı rakamlar ile bitişik bir şekilde yazılan rakamlar ön işleme aşamasından tespit edilip dilimleme işlemi başarılı bir şekilde gerçekleştiriliyor. Ancak iç içe geçmiş el yazısı rakamlarında bu yöntem başarılı kabul edilemez.

Dilimleme işlemlerinin testi için 20 kişiden 50 farklı en az 2 basamaklı rakamlardan oluşan yazım örnekleri alınmıştır. Her kişiden el yazısı rakamlarının 30 tanesi bütün ve ayrı rakamlar (Şekil 2 gibi), 10 tanesi birleşik şekilde yazılan rakamlar (Şekil 3 gibi), 10 tanesi ise iç içe geçmiş rakamlardan oluşmaktadır. Dilimleme işleminin performansı tabloda 1'de belirtilmiştir.

```

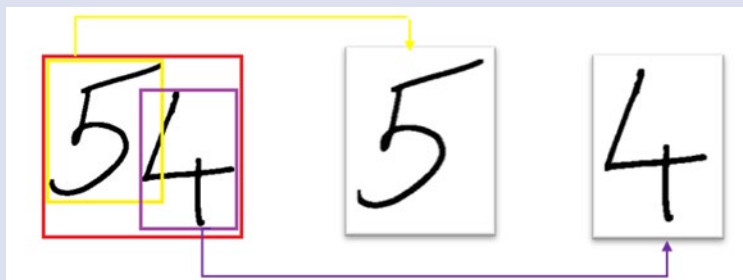
1  Goruntu_on_isleme[m][n]
2  a=0;b=0;
3  i:
4  while(a<m+1){
5  while(b<n+1){
6  if(Goruntu_on_isleme[a][b]==0){
7  tum_komsu_bul(Goruntu_on_isleme[a][b]);
8  a=en_byk_px1_stun+1;//komşuluk ilişkisinden gelen en büyük sütun değerinin 1 fazlası
9  b=0;
10 goto i;
11 }b++;
12 }a++;

```

tum_komsu_bul() /*ilk siyah renk piksel değeri bulunduğundan sonra komşuluk ilişkilerinde yararlanarak rakama ait tüm "0" değerine sahip piksel değerleri bulunur ve yeni matrise atanır. Atanan değerlerin tamamının ön işlemdeki yeni değerleri "255" olur. */

Şekil 5. Dilimleme İşlemi Kaba Kodu.

Figure 5. Pseudo code of slicing process.



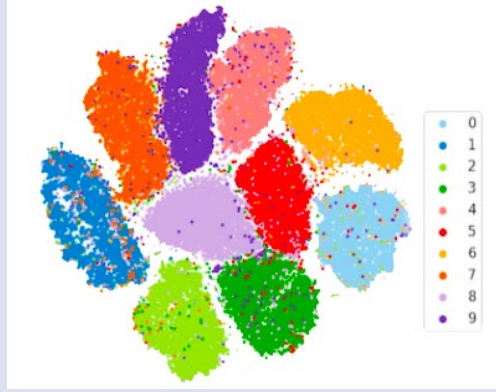
Şekil 6. Görüntü Dilimleme İşlemi.

Figure 6. Image slicing process.

Tablo 1. Geliştirilen dilimleme yöntemi performans değerleri.

Table 1. Performance values of developed slicing method

	Bütün ve Ayrık Rakamlar	Birleşik Rakamlar	İç içe Geçmiş Rakamlar
Örnek Sayısı	600	200	200
Doğru Dilimleme Sayısı	592	160	5
Yanlış Dilimleme Sayısı	2	40	195
Performans	%99,67	%80	%2,5



Şekil 7. MNIST verilerinin K-NN algoritmasına göre sınıflandırılması [15].

Figure 7. Classification of MNIST data according to the K-NN algorithm [15].

Tablo 1'e bakıldığında bütün ve ayrık rakamlardan oluşan görüntülerde %99,67 oranında başarımlar elde edilmiştir. Birleşik rakamlarda %80 başarımlar elde edilmiştir. İç içe geçmiş görüntülerde %2,5 performans elde edilmiştir. Geliştirilen bu yöntem bütün ve ayrık rakamlar ve birleşik rakamların dilimlenmesi için başarılı sonuçlar elde edilirken iç içe geçmiş rakamlar için başarılı sonuçlar elde edilememiştir.

Sınıflandırma

K-En Yakın Komşu Algoritması (K-NN - K-Nearest Neighbor) ile Uygulama

K-en yakın komşu (K-NN) algoritması belirli bir veri seti içinde yeni bir noktanın hangi en yakın gruba ait olacağını belirleyen en temel makine öğrenmesi algoritmalarından birisidir. Algoritmadaki "K" değeri en yakın kaç adet grup sayısının kontrol edileceği değerdir. K-NN algoritmalarında bir noktanın hangi sınıfa ait olacağını belirlemek için kullanılan veri setine ait verilerin koordinat sistemi üzerindeki konumlarının sınıflama için kullanılan noktaya ait uzaklıkları tespit edilir. Bu uzaklıklardan en yakın "K" adet komşu üyeleri seçilir. Genelde komşu üyesi sayıları eşit çıkmaması için "K" değeri tek sayı seçilir. Seçilen en yakın "K" adet komşudan en fazla gruba ait olan sınıfa yeni nokta dahil edilir.

K-NN algoritmasını kullanarak Python programlama dili ile sınıflandırma işlemi gerçekleştirilmiştir. K-NN uygulamasında K değeri "5" olarak alınmıştır. Mesafe algoritması olarak "Öklid mesafe" algoritması kullanılmıştır. Öklid mesafe algoritması kullanmak için Minkowski yönteminden yararlanılmıştır ve "p" değeri 2 olarak kabul edilmiştir. MNIST verilerinin K-NN algoritması ile kümeleneceği Şekil 7'de gösterilmiştir.

"K" değeri için farklı değerler denenmiştir fakat hem zaman hem de performans açısından en iyi sonuç "5" değerinde elde edilerek, %86 oranında bir performans sağlanmıştır. K-NN algoritması hesaplama ve sınıflama işlemini aynı anda yaptığından büyük verilerle çalışması biraz zaman alabilmektedir. MNIST veri setinde, 60000 eğitim 10000 test verisi olmak üzere toplam 70000 veri olduğundan hesaplama süresi 15,28 dakika sürmüştür.

Yapay Sinir Ağları (YSA-Artificial Neural Networks (ANN)) ile Uygulama

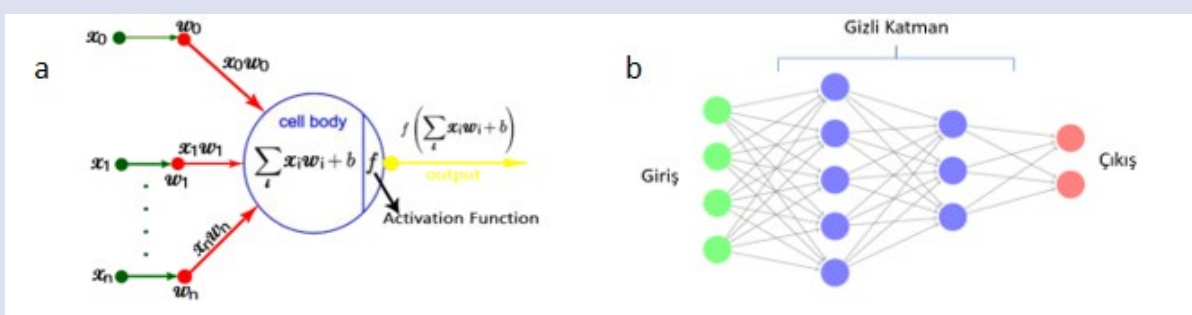
Yapay Sinir Ağları (YSA) beyin temel yapı taşı olan sinir hücrelerinin çalışma prensibinden örnek alınarak geliştirilen bir yöntemdir. Biyolojik sinir hücresi yapısına benzetim yöntemi ile matematiksel sinir hücresi oluşturulmuştur.

Yapay sinir hücresi (Şekil 8. (a)) üzerinden giriş yapan veri sinir hücresinin ağırlık değeri ile çarpılır. Yapay sinir hücresinin çekirdek yapısında bir toplama fonksiyonu bulunur. Bu toplama fonksiyonu yapay sinir hücresine giriş yapan bütün değerlerin ağırlıkları ile çarpımlarını toplar ve bu toplam değerine yapay sinir hücresinin bias değerini ekler. Elde edilen değer lineer bir değerdir. Bu değer direkt çıkışa verilmesi durumunda reel olmayan sonuçlar elde edilir. Bu durumun engellenmesi için aktivasyon fonksiyonları kullanılır. YSA'larda aktivasyon fonksiyonu kullanılmazsa YSA sınırlı öğrenme gücüne sahip bir doğrusal bağlantı (linear regression) gibi davranacaktır. Bu durum gerçek uygulamalar için istenmeyen durumdur ve yanlış sonuçlar elde edilir. Böylelikle yapay sinir hücresinin matematiksel modeli oluşturulmuş olur. Elde edilen sonuç bir sınıflandırma değeri olabileceği gibi başka bir sinir hücresinin giriş değeri de olabilir.

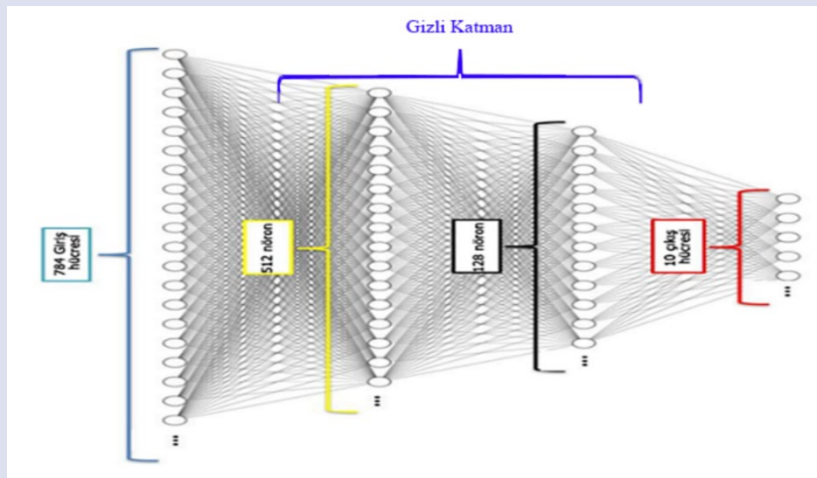
Yapay sinir hücreleri kullanılarak YSA'lar oluşturulur. YSA'lar tek katmanlı ve çok katmanlı olarak kullanılabilir. Çok katmanlı YSA'lar (Şekil 8. (b)) birden fazla gizli katmana sahip olabilir.

YSA'lar kullanarak dilimleme işleminden gelen görüntüler python üzerinden sınıflandırma işlemine tabi tutulmuştur. MNIST veri seti 28x28 boyutunda görüntülere sahiptir. Dilimleme işleminden gelen her bir görüntü de 28x28 boyutundadır. Görüntülerden gelen verilerin tamamı sinir ağına modeline uygulanır. Giriş verileri 28x28 boyutunda olduğu için giriş nöronları 784 adet olmalıdır. Sinir ağı modeli giriş katmanı, gizli (hidden) katman ve çıkış katmanı olmak üzere üç katmandan oluşturulmuştur. Gizli

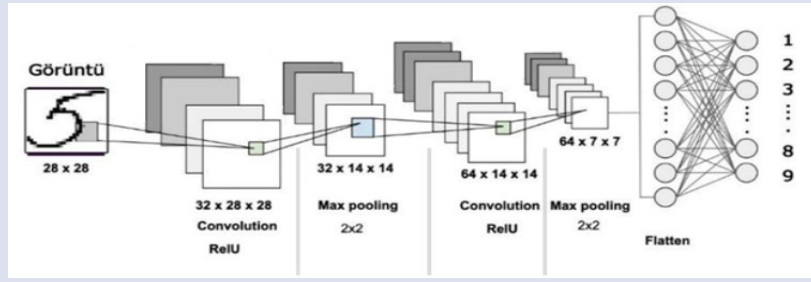
katman iki aşamalıdır. Giriş katmanında 784 adet nöronun, gizli katman ise sırasıyla 512 ve 128 nöronun oluşmaktadır. Hem giriş hem de gizli katmanda aktivasyon fonksiyonu olarak "ReLU" fonksiyonu kullanılmıştır. Çıkış katmanında sınıflandırma işlemi sıfır ile dokuz arasındaki rakamları sınıflanacağı için 10 adet nöron bulunur ve aktivasyon fonksiyonu olarak "softmax" fonksiyonu uygulanmıştır. YSA modeline MNIST veri setinden gelen 60000 adet veri eğitim için 10000 adet veri ise test için kullanılmıştır. Modelimize dahil edilen verilerin sonucunda sistemin doğruluğu %98 olarak hesaplanmıştır. YSA modelinin eğitimi için kullanılan süre 11,85 dakikadır. Kullanılan YSA modeli Şekil 9'de gösterilmiştir.



Şekil 8. (a) Yapay sinir hücresi; (b) Çok katmanlı YSA.
Figure 8. (a) Artificial neuron; (b) Multilayer ANN.



Şekil 9. Kullanılan Yapay Sinir Ağları Modeli.
Figure 9. Proposed artificial neural network model.



Şekil 10. Uygulamada kullanılan CNN modeli.
Figure 10. CNN model used in the application.

Tablo 2. Kullanılan sınıflandırıcıların performans değerleri
Table.2. Performance values of the used classifiers.

Performans	KNN	YSA	CNN
Doğruluk	%86	%98	%99,4
Eğitim Süresi(dk)	9,4	11,85	15,28

Evrişimsel Sinir Ağları (Convolutional Neural Networks – CNN) ile Uygulama

Evrişimsel sinir ağları (CNN) (Şekil 10) son yıllarda görüntü işlemede sıklıkla kullanılan derin öğrenme yöntemlerinden birisidir. CNN görüntü işlemede sınıflandırılacak görüntünün çeşitli filtreleme yöntemleri kullanarak özellik çıkarımı yapar ve bu çıkarımlar üzerinden YSA'ları kullanarak bir sınıflandırma gerçekleştirir.

CNN beş katmandan oluşur. Birinci ve en önemli katman konvolüsyon katmanıdır. Bu katmanda görüntü üzerinde belirli filtreleme yöntemi kullanılarak özellik çıkarımı gerçekleştirilir. Filtreleme yapılan görüntülerin tamamı özellik (feature) matrisi denilen matriste saklanır. İkinci katman doğrusal olmayan (Non-Linearity) katmandır. Bu katman aktivasyon katmanı (Activation Layer) olarak adlandırılır çünkü aktivasyon fonksiyonlarından birisi bu katmanda kullanılır. Üçüncü katman havuzlama (pooling) katmanıdır burada pooling işlemleri gerçekleştirilir. Bu sayede özelliklerin ağırlıkları azaltılır ve uygunluğu denetlenir. Dördüncü katman düzleme (Flattening) katmanıdır. Bu katman son ve en önemli katman olan Tam Bağlantılı (Fully Connected) katmanının girişindeki verileri hazırlar. Sinir ağları üzerinde giriş verileri tek boyutlu bir dizi üzerinden alır. Sinir ağlarında kullanılan giriş verileri ise konvolüsyon ve Pooling katmanından gelen matrislerin tek boyutlu diziyeye çevrilmiş halidir. Beşinci ve son katman Tam Bağlantılı (Fully Connected) katmandır. Verileri düzleme katmanından alır ve sinir ağı yoluyla öğrenme işlemini gerçekleştirir.

CNN kullanılarak dilimleme işlemlerinden gelen veriler sınıflandırma işlemine tabi tutulur. Dilimleme işleminden gelen görüntü 28x28 boyutunda bir matris şeklindedir. Bu görüntüleri eğitim için sırasıyla CNN'e tabi tutulur. CNN modeli (Şekil 10) oluştururken iki tane konvolüsyon katmanı kullanılmıştır. Her konvolüsyon katmanından sonra havuzlama (pooling) katmanı da olacağından iki tane de havuzlama (pooling) katmanı kullanılmıştır. Evrişimsel sinir ağlarının ilk katmanı olan konvolüsyon katmanında ilk olarak görüntülerin 32'li özellik haritaları çıkarılmıştır İlk konvolüsyon katmanında özellikleri çıkarılan görüntüleri havuzlama katmanında 2x2 max pooling (havuzlama) işlemine tabi tutulmuştur. İkinci

konvolüsyon katmanında 64'lü özellik haritası çıkarılmış ve havuzlama katmanında 2x2'li max pooling işlemi uygulanmıştır. Konvolüsyon katmanlarında aktivasyon fonksiyonu olarak "ReLU" aktivasyon fonksiyonu kullanılmıştır. Düzleme katmanında 586 tane giriş verisi tek bir dizi şeklinde tam bağlantılı katmana sınıflandırma için gönderilmiştir. Tam bağlantı katmanında 586 tane giriş 10 tane çıkış nöronları vardır. Giriş nöronlarına "ReLU" aktivasyon fonksiyonu, çıkış nöronlarına "softmax" aktivasyon fonksiyonu uygulanmıştır. CNN modeli şekil 10'da belirtilmiştir. Modelin eğitimi için MNIST veri setinden 60000, testi için 10000 adet veri kullanılmıştır. Oluşturulan modelin doğruluk oranı %99,4 olarak gözlemlenmiştir. Verilerin eğitimi için geçen süre 15,8 dakika olarak hesaplanmıştır.

Performansların Değerlendirilmesi

Sınıflandırma işlemlerinin sonucunda hesaplanan tüm değerler Tablo 2'de gösterilmiştir. CNN yönteminde eğitim süresi 15,28 dakika, doğruluk oranı %99,4 olarak ölçülmüştür. YSA'da modelin eğitim süresi 11,85 dakika, doğruluk oranı %98 olarak ölçülmüştür. K-NN algoritmasında ise eğitim ve hesaplama süresi 9,4 dakika doğruluk oranı %86 olarak ölçülmüştür. Eğitim için harcanan süreler karşılaştırıldığında CNN modeli 15,28, YSA modeli 11,85 ve K-NN uygulaması 9,4 dakika olarak hesaplanmıştır. Bu süreler 3.2 GHZ 32 işlemcili ve 512 GB RAM'e sahip server bilgisayar üzerinde hesaplanmıştır kullanılan donanımlara göre değişkenlik gösterebilir. Burada modellerin eğitim hızları karşılaştırılmasında en hızlı K-NN, onu takip eden YSA ve CNN sınıflandırma yöntemleri gelir. Ancak performans yönünden değerlendirildiğinde CNN sınıflandırıcının en yüksek performansı gösterdiği, onu takip eden YSA ve K-NN modellerinin olduğu gözlemlenmektedir.

YSA ve CNN yöntemlerinde genel bir eğitim modeli oluşturulur ve bu model her sınıflandırma işlemde kullanılır. Yani sistem bir kere eğitilir ve eğitim sonuçlarında çıkan model her sınıflandırma işlemleri için kullanılacak genel model olur. Bu sayede tekrar model oluşturmaya gerek kalmadan gerçekleştirilecek her sınıflandırma için genel eğitim modeli kullanılacaktır. Bu sayede model eğitildikten

sonra gerçekleştirilecek sınıflandırmalar çok daha kısa sürelerde olacaktır. Ancak K-NN sınıflandırma yönteminde her sınıflandırma için K-NN algoritması tekrar yeni hesaplamalar yapmak zorundadır.

Sonuçlar

Literatürde genel olarak el yazısı rakamlarının dilimlenmesinde histogram analizi, kontur analizi, yazı şekilleri vb. yöntemler kullanılmaktadır. Bu çalışma kapsamında sınav kağıtlarında el yazısıyla yazılan başarı notları rakamlarının yeni bir dilimleme yöntemi geliştirilerek bütün ve ayırık rakamlar ve birleşik rakamlar başarılı bir şekilde dilimlenmiş iç içe geçen rakam görüntüleri için dilimleme yöntemi yetersiz kalmıştır. Geliştirilen bu yöntem bütün ve ayırık rakamlar ve birleşik rakamlar için başarılı olarak çalışmaktadır.

Başarılı bir şekilde dilimleme de ayrıştırılan tüm rakamlar CNN modeli, YSA modeli ve K-NN algoritmasına tâbi tutularak performans değerlerinin tablo halinde karşılaştırılması yapılmıştır. MNIST veri tabanı kullanılarak yapılan sınıflandırma işlemlerinin performansları kıyaslandığında CNN modeli %99.4, YSA modeli %98 ve K-NN uygulaması %86 olarak tespit edilmiştir. YSA ve CNN modelinde eğitim işlemi tamamlandıktan sonra model kaydedilip eğitilmiş model yeni durumlar için kullanılabilir. Bu durum da bize yeni veri geldiğinde, sistemi tekrar eğitmeden kullanım olanağı sağlar. Ancak K-NN uygulamalarında yeni durumlar için tekrar eğitim işlemi gerçekleştirilmesi gerekmektedir.

Kaynaklar

- [1] Makkar T., Kumar Y., Dubey A.K., Rocha Á., Goyal A., Analogizing time complexity of KNN and CNN in recognizing handwritten digits, 2017 Fourth International Conference on Image Information Processing (ICIIP), (2017) 1-6.
- [2] Ghadekar P., Ingole S., Sonone D., Handwritten Digit and Letter Recognition Using Hybrid DWT-DCT with KNN and SVM Classifier, 2018 Fourth International Conference on Computing Communication Control and Automation (ICCUBEA), (2018) 1-6.
- [3] E. Lejeune, Mechanical MNIST: A benchmark dataset for mechanical metamodels, *Extreme Mechanics Letters*, 36 (2020) (100659) 1-7.
- [4] Kaziha O., Bonny T., A Comparison of Quantized Convolutional and LSTM Recurrent Neural Network Models Using MNIST, 2019 International Conference on Electrical and Computing Technologies and Applications (ICECTA), (2019) 1-5.
- [5] Palvanov A, Cho Y.I. Comparisons of Deep Learning Algorithms for MNIST in Real-Time Environment, *IJFIS*, 18 (2018) 126-134.
- [6] Alvear-Sandoval R.F., Sancho-Gómez J.L., Figueiras-Vidal A.R., On improving CNNs performance: The case of MNIST, *Information Fusion*, 52 (2019)106-109.
- [7] Gati E.S., Nimo B.D., Asiamah E.K., Kannada-Mnist Classification Using Skip CNN, 16th International Computer Conference on Wavelet Active Media Technology and Information Processing, (2019) 245-248.
- [8] Beohar D., Rasool A., Handwritten Digit Recognition of MNIST dataset using Deep Learning state-of-the-art Artificial Neural Network (ANN) and Convolutional Neural Network (CNN), 2021 International Conference on Emerging Smart Computing and Informatics (ESCI), (2021) 542-548.
- [9] Zhang K., Su H., Dou Y., Shen S., Evaluation of the Influences of Hyper-Parameters and L2-Norm Regularization on ANN Model for MNIST Recognition, 2019 International Conference on Intelligent Computing Automation and Systems (ICICAS), (2019) 379-386.
- [10] Garin A., Tauzin G., A Topological "Reading" Lesson: Classification of MNIST using TDA, 2019 18th IEEE International Conference On Machine Learning And Applications (ICMLA), (2019) 1551-1556.
- [11] Ge D.-y., Yao X.-f., Xiang W.-j., Wen X.-j., Liu E.-c., Design of High Accuracy Detector for MNIST Handwritten Digit Recognition Based on Convolutional Neural Network, 2019 12th International Conference on Intelligent Computation Technology and Automation (ICICTA), (2019) 658-662.
- [12] Gope B., Pande S., Karale N., Dharmale S., Umekar P., Handwritten Digits Identification Using Mnist Database Via Machine Learning Models, *IOP Conference Series: Materials Science and Engineering*, 1022 (2021) 1-11.
- [13] KARAKAYA K., Handwriting Recognition Using Machine Learning, Master Thesis, Sakarya Üniversitesi, Institute of Natural Sciences, 2020.
- [14] GitHub, Mahanteshambi/Clustering-MNIST page, 2020, NOS. Available at: <https://github.com/Mahanteshambi/Clustering-MNIST>, Retrieved August 8, 2023.
- [15] Pythonawesome, A 1D analogue of the MNIST dataset for measuring spatial biases page, NOS. Available at: <https://pythonawesome.com/a-1d-analogue-of-the-mnist-dataset-for-measuring-spatial-biases>. Retrieved August 8, 2023.
- [16] Hochuli A.G., Oliveira L.S., Britto Jr A.S., Sabourin R., Handwritten Digit Segmentation: Is it Still Necessary?, *Pattern Recognition*, 78 (2018) 1-11.
- [17] Gattal A., Chibani Y., Hadjadji B., Segmentation and Recognition System for Unknown-length Handwritten Digit Strings, *Pattern Analysis and Applications*, 20 (2017) 307-323.
- [18] Elkhayati M., Elkettani Y., Mourchid M., Segmentation of Handwritten Arabic Graphemes Using a Directed Convolutional Neural Network and Mathematical Morphology Operations, *Pattern Recognition*, 122 (2022) (108288) 1-15.
- [19] Renton G., Soullard Y., Chatelain C., Adam S., Kermorvant C., Paquet T., S Fully Convolutional Network With Dilated Convolutions for Handwritten Text Line Segmentation, *International Journal on Document Analysis and Recognition (IJ DAR)*, 21 (2018) 177-186.
- [20] Sharma M. K., Dhaka V. S., Segmentation of Handwritten Words Using Structured Support Vector Machine, *Pattern Analysis and Applications*, 23 (2020) 1355-1367.
- [21] P. Jindal, B. Jindal, Line and Word Segmentation of Handwritten Text Documents Written in Gurmukhi Script Using Mid Point Detection Technique, 2015 2nd International Conference on Recent Advances in Engineering & Computational Sciences (RAECS), (2015) 1-6.